Towards a biological profile for South African perinatal remains: osteological and genetic perspectives

Submitted in fulfilment of the requirements for the degree of

Doctor in Philosophy

In

Biochemistry

By Roxanne Thornton

Rhodes University

Grahamstown

June 2018

Abstract

Forensic identification of abandoned and suspected infanticide cases admitted to the South African Forensic Pathology Services is often impossible due to decomposition of the remains. In these cases, investigation of suspected criminal activity is almost never pursued. Ancillary tests in the form of anthropological and molecular analyses can assist with the forensic identification of perinatal remains. To provide fundamental information about bone development of perinatal skeleton, osteological and genetic techniques focusing on the pars basilaris, pars lateralis, sternal rib and left femur were used. Samples were obtained from unidentified and unclaimed remains originating from the Johannesburg Forensic Pathology Service (JFPS). To provide a biological age to individuals in the collection, dental aging was used to categorize remains for comparisons with anthropological and molecular data. A molecular protocol was designed to sex individuals using the X-linked G6PD and Y-linked SRY genes. Bone development was studied using osteometric and morphological data of dry bone remains coupled with bone mineral density analysis (Micro-CT). The methylation levels of CpG rich sites within the promoter region of selected bone-associated genes were incorporated to examine silencing of genes during development. Osteological results support the use of the pars basilaris, pars lateralis and femur for age-at-death estimations as well as provide the foundation for dry bone aging criteria for South African individuals. Data compared with established skeletal aging standards indicated developmental differences between populations. Through the use of animal models and the perinatal sternal rib tissue, insights and precautions into the use of post mortem bone derived RNA for forensic applications is communicated. The methylation status of CpG rich sites within the promoter regions support the hypothesis for interdependent machinery involving selected genes during early bone development.

Declaration

I declare that this dissertation is my own unaided work, except where acknowledged, submitted for the degree of Doctor of Philosophy in Biochemistry of Rhodes University in the Faculty of Science. It has not been submitted for any degree for examination in any other university.

……

Ms Roxanne Thornton

Table of contents

Acknowledgements

Gratitude and thanks to the Sandiswa Imbewu grant for the assistance and funding of this project. The completion of this project would not be possible without the assistance, support and guidance of my supervisors Professor Adrienne Edkins and Dr Erin Hutchinson. Your guidance and encouragement is greatly appreciated.

Special mention of the Biomedical Biotechnology Research Unit lab members is necessary as their friendship and constructive feedback has been incredibly helpful to the completion of assays designed for the molecular component of the project.

To Professor Martin Villet of Rhodes Zoology, thank you for the donation of animal remains and your insights and direction with respect to Forensic Entomology.

The access, processing and collection of individuals for the study was aided by Professor Jeanine Vellema, Ms Ina Botes, Mrs Ildi Fenyvesi Wainer, Mr. Somana and the other service and academic staff members of the University of Witwatersrand, Division of Forensic Medicine and Johannesburg Forensic Pathology Service.

To the NECSA scientists – Mr Jakobus Hoffman and Mr Lunga Bam, thank you for your training in VG studio Max software and Micro-CT 3D image reconstruction. Your patience and attention to detail helped through the long hours of analysis.

Sincere thanks to Mrs Dorothea Paice, for your constant help with data management and consolidation. Photographic credit is due to Tracy Reindorp (Johannesburg Forensic Pathology Service).

List of abbreviations

AC	abdominal circumference
AMEL	amelogenin
cDNA	complementary deoxyribonucleic acid
CHL	crown heel length
CRL	crown rump length
Cq	cycle threshold (quantitative PCR)
DW	distal width
FGFR3	fibroblast growth factor receptor 3
FL	foot length
FN	fibronectin
GW	gestational weeks
gDNA	genomic deoxyribonucleic acid
HC	head circumference
JFPC	Johannesburg forensic paediatric collection
JFPS	Johannesburg forensic pathology service
Micro-CT	micro -computed tomography
ML	maximum length
MW	maximum width
PCR	polymerase chain reaction
PMI	post mortem interval
SAPS	South African police service
SL	sagittal length
SRY	sex determining region y
RT-PCR	reverse transcription-polymerase chain reaction
RT-qPCR	real time – quantitative polymerase chain reaction
RUNX2	runt regulated transcription factor 2

ZF	zinc finger protein

List of figures

List of tables

CHAPTER 1: LITERATURE REVIEW

1.1 Introduction: Forensic Identification of juvenile remains in South Africa

The dumping of fetal, stillborn and suspected infanticide cases within the Johannesburg jurisdiction and across the provinces in South Africa has indicated a possible problem in the delivery of public health and social service (Jacobs *et al.,* 2014; Lamprecht, pers. comm., 2014, du Toit-Prinsloo *et al.,* 2016). The reason for a medico-legal autopsy on a deceased fetus or stillborn, in addition to determining the cause of death, is to identify the individual in terms of maturity and sex. In cases of suspected infanticide, separate existence needs to be estimated. Separate existence can be defined as an 'infant that had issued forth from its mother irrespective of its gestational age, and who breathed or showed any other signs of life after being completely expelled from the maternal passages' (Knight and Saukko, 2004, p 442). Soft tissue age estimation is performed by the pathologist by taking a series of measurements. These include but aren't limited to the weight, crown-heel length, crown-rump length and head circumference of the perinate (Knight and Saukko, 2004). Developmental charts which serve as a reference for this assessment can be found in Wigglesworth and Singer (1991).

Age estimation is important to the legal context especially if the fetus is full term or viable Births and Deaths Registration Act (Act 51 of 1992), Criminal Procedure Act (Section 239(1) of Act 51 of 1977) and the Inquests Act (Act 58 of 1959), as this encompasses the questions of "personhood" and whether the death was due to criminal activity. In South Africa, legal viability is a fetus that has experienced at least 24 gestational weeks intrauterine life before expulsion. Practically, age assessments at autopsy of fetal or perinatal remains are often difficult due to the stage of decomposition (Knight & Saukko, 2004; Nel, pers. comm., 2015). As age is a variable of identification and this cannot be estimated with accuracy using soft

tissue age estimation standards, perinatal individuals are often unidentified and thus, ancillary anthropological assessments are employed. However, without accurate methods and identification, decedents are often released for state burial without any inquest.

Approaches which could assist ancillary assessments include molecular osteology and histomorphology. These approaches are contributing to age estimation modalities (Franklin, 2010). With fibronectin (FN), fibroblast growth factor 3 (FGFR3) and runt-related transcription factor 2 (RUNX2) being considered as important bone-specific transcription and growth-related genes (Ornitz and Marie, 2002; Singh and Schwarzbauer, 2012; McGee-Lawrence *et al.*, 2014), an association to skeletal aging might be possible. The literature on bone development and the modalities used in forensic identification of perinatal remains indicates a dearth of knowledge concerning the South African population. Population specific aging standards are necessary in forensic settings as the current methods employed are not applicable for use on a modern population group of non-European descent (Ubelaker, 2005; Cunha *et al.*, 2009; Sanders, 2009; Franklin, 2010). An evaluation of traditional dry bone measurements using bones of forensic value (pars basilaris and femur) and the understudied pars lateralis bone of South African unidentified perinatal descents would aid in profiling the perinatal skeleton from the current socio-economic and historical context.

The broad aim of this study was to provide a foundation towards a profile of features of South African perinatal remains using radiological, osteological and genetic approaches. Dental aging criteria (Alqahtani *et al.,* 2010) was used a proxy for biological age. It was hypothesized that the degree of mineralization is influenced by the surrounding soft and skeletal anatomy as the fetus grows and develops. The biomechanical force from corresponding anatomy was thought to influence the mineralization at specific regions of the bone as the fetal and perinatal

locomotion increases with age. This is due to the biomechanical force on the regions of the bone where articulation with soft tissue anatomy and bone are influenced by movement and development of anatomical features associated with fetal maturity (Frost, 1987; Rauch and Schoenau, 2001). By combining traditional measurement criteria based on perinatal remains (Fazekas and Kosa, 1978) and new imaging modalities such as micro – computed tomography (Micro-CT) which measures bone mineral density, information regarding growth, such as changes in dimension, size and bone mineral density of perinatal skeleton, can be collected and analysed. As a complement to the osteological data, the levels of mRNA transcripts of Fibronectin, FGFR3 and RUNX2 were assessed for their applicability as biomarkers for age estimation. The literature indicates that sex typing of skeletal remains at this developmental stage is improbable (Weaver, 1998; Ubelaker and Degaglia, 2017). However, some reports have indicated a difference between the sexes (Cope and Murdoch, 1958; Choi and Trotter, 1970; Bagnall *et al.,* 1977, 1982). Therefore, development of a molecular protocol to accurately sex unknown individuals, would aid in the identification process, and would facilitate the comparison of osteological and molecular data within the categories of male and female.

As an added objective to the research, the potential for routine use of postmortem RNA was explored. The use of RNA in forensic sciences has been suggested, but multiple factors influence the integrity and stability of postmortem RNA (Opitz *et al.*, 2010; Koppelkamm *et al.*, 2011; Sampaio-Silva *et al.*, 2013). The biochemistry of postmortem RNA is largely unknown (Van Doorn *et al.*, 2011; Fordyce *et al.*, 2013). Therefore, the use of postmortem RNA in gene expression analyses is questionable. An inquiry into the use of postmortem RNA derived from bone would answer the question of whether RNA could be used in routine assays for forensic identification. Methylation level analysis has been reported as important to aging of individuals

(Hannum *et al.*, 2013; Yi *et al.*, 2014; Jones *et al.,* 2015; Jung and Pfeifer, 2015). However, the methylation status of RUNX2, Fibronectin and FGFR3 transcripts hasn't been linked to skeletal, dental or biological age at this developmental stage. An analysis of methylation status of the promoter region of these genes could provide information and possibly biomarkers for accurate aging of postmortem remains.

The introductory chapter will review the existing knowledge of the age and sex estimation of perinatal individuals. In addition, it will also highlight the current challenges of accurately estimating age and sex within the South African forensic context.

1.2 Modalities for forensic Identification

Techniques have been developed for the estimation of age and sex within a forensic setting. These methods of identification include radiological, linear measurements or digitising of landmarks from dental and skeletal information, and have been designed in order to develop population specific standards (Oxnard *et al.*, 2013). Methods and techniques which have gained popularity in the field include the application of an array of imaging modalities for example Micro-Computed Tomography (Micro-CT), the scanning and digitising of skeletal landmarks and the application of geometric morphometrics. These approaches have been broadly applied to paleo-anthropological (Cazenave *et al.*, 2017) and forensic (Hutchinson *et al.*, 2017) samples. Methods using Micro-CT are considered non-destructive to fragile (fetal) and archaeological tissue. Booth and colleagues (2016) studied the taphonomic influence on archaeological fetal femora by comparing traditional staining techniques and Micro-CT in order to discriminate between stillborn and short lived Romano-British infants (*n*=10). Therefore, indicating its use in not only for archaeological samples, but forensic ones as well.

Indeed, the application of Micro-CT to the study of skeletogenesis has proven to be complementary, and even advantageous, to traditional histological methods (Guldberg *et al.,* 2004). A large majority of studies incorporating this method have used murine or small mammals as a proxy for human development. Imaging of structural anomalies and the processes of spatial and temporal ossification patterns allows for new insights into osteopathology and development of therapeutic agents (Guldberg *et al.,* 2004; Oest *et al.,* 2008; Winkelmann and Wise, 2009). Studies examining skeletogenesis in human fetuses have examined craniofacial morphology related to growth (Neumann *et al.,* 1997; Zumpano and Richtmeier, 2003) as well as the architecture of trabecular bone in the vertebral column (Nuzzo, 2003). Recently, Franklin and colleagues (2013) demonstrated the application of these techniques on the landmarks of Australian crania with traditional osteometric measurements and Multi-Slice Computed Tomography (MSCT) (2013). The application of computed tomography has aided within the autopsy setting as well. Radiographs and 3D imaging allows for non-invasive examination of perinatal remains as well assisting with radiological aging standards (Lombardi *et al.,* 2014; Gorincour *et al.*, 2015). Therefore, the scope of application for Micro-CT is expansive as it allows for visualization and insights into development and pathology from an *in vivo* and *ex vivo* context.

1.3 Morphometric methods of forensic identification

1.3.1 Dental development and dental age estimation

Biological age is estimated by the maturation of a particular tissue system. Maturation is evaluated by the occurrence or sequence of events in the system (Moorrees *et al.,* 1963a). Dental aging relies on the mineralization of dental tissues and the sequential eruption of root and crown structures. Tooth development encompasses deciduous and permanent maxillary and mandibular dentition sets and comprises the formation and growth of the crown and root structures. The stages of tooth development include initial cusp formation, coalescence of cusps, cusp outline and the degree of crown completion, the formation of the root and the degree of root length as well as the apical closure of the root structure (Moorrees *et al.,* 1963a; 1963b). The morphology of teeth and the arrangement thereof, is as unique as fingerprints (Queiroz *et al.,* 2016). Dental development is a life-long process that begins during embryogenesis and ends after adolescence. Formation of teeth includes the organization of the matrix and the subsequent calcification of the teeth (Smith, 1991). Human teeth consist of four dental tissues. These include the soft tissue of the pulp and the calcified hard tissues of dentine, enamel and cementum. While enamel and dentine contribute significantly to the crown of the tooth, the cementum is the part of the tooth structure associated with the periodontium which supports the teeth within the alveolar bone (Turp and Alt, 1998). The deposition of organic matrix results in the production of dentine and enamel, which is subsequently mineralized (Cunningham *et al.,* 2016). Mineralization is a process that takes place in all calcified structures in the body. It is defined as the deposition of mineral salts in and around the organic matrix to make it a calcified structure (Boskey, 2007). Dental tissues

undergo varying stages of mineralization during development. Ameloblast cells produce enamel and odontoblasts form dentine. The change in the process of ameloblast in the matrix results in the incremental growth lines seen in tooth enamel (striae of Retizius) (Risnes, 1986), which is a consequence of apposition of different layers of crown formation. These striae are produced during the second stage of enamel calcification and are associated with circadian rhythms in the metabolism of enamel matrix secretion (Antoine *et al.,* 2009). Tooth germs calcify and later eruption involves the movement of the tooth crown from the alveolar region to the functional occlusal position (Scheuer and Black, 2004).

It is during this transition from the cusp stage of tooth development to the functional state of eruption, that the tooth undergoes the greatest changes in its morphology and dental age estimations in immature individuals is most accurate (Alqahtani *et al.,* 2010; Cunningham *et al.,* 2016). Teeth tend to survive inhumation more so than skeletal elements and dental aging is less variable than skeletal aging (Lewis and Garn, 1960; Demirjian, 1986; Smith, 1991). Dental development is less affected by environmental and physiological circumstances such as nutrition and disturbances in endocrine function (Garn *et al.,* 1958; 1965a; 1965b). The mineralization status of the deciduous teeth and first permanent molars has been tested against other methods for the estimation of gestational age. Dental aging methods have been shown to be more reliable than anthropometric measurements used for soft tissue age estimation (crown rump length, crown heel length) (Luke *et al.,* 1978). Tooth Mineralization is thought to be genetically determined; whereas eruption is affected by systemic influences such as nutrition (Lewis and Garn, 1960; Fanning, 1961; Tanner, 1962; Haavikko, 1973; Brown, 1978). This distinction is not absolute in nature. There is overlap in terms of influential factors on the mineralization and eruption.

Limited variation has been noted between studies on prenatal teeth examining tooth ring analysis, crown formation at birth and calcification schedule (Kronfeld and Schour, 1939; Kraus and Jordan, 1965; Sunderland *et al.,* 1987). The mineralization sequence has been reported through histological means as central incisor, first molar, lateral incisor, canine and second molar (Sunderland *et al.,* 1987). Maxillary dentition is usually more advanced in development than mandibular (Smith, 1991). Typically, mineralization is detected histologically six months before visualization on radiographs (Hess *et al.,* 1932). Early systems of tooth development examined the degree of mineralization and crown morphology from dissection and histological sections (Logan and Kronfeld, 1933; Kraus and Jordan, 1965). The work of Kraus and Jordan (1965) provided indispensable data and a chronology of intrauterine dental development. A 10 stage system was proposed to discriminate the degree of deciduous dentition including the permanent first molar (Kraus and Jordan, 1965). Histological works are limited in the number of individuals included in samples (Smith, 1991). Dental radiography examines the degree of mineralization coupled with the formation and changing morphology of the crown and root structures. Radiographs provide information on unerupted teeth that is not possible with the naked eye. Enamel is the most radiopaque tissue. On X-ray, the crown is distinguished as the whitest part and dentine will appear greyer (Scheuer and Black, 2000). Radiological studies using a large number of radiographs and statistical values provide a solution for this problem, however, the majority of these studies are based on individuals from European derivation and therefore, don't include data on individuals from different population affinities. The radiographic method is quick, simple and economical compared to biochemical and histological methods which require expensive and advanced laboratory equipment (Panchbhai, 2011).

The disadvantages of dental aging with radiography include the amount of training and experience needed, as well as the ethical dilemma of radiographing young children (Scheuer and Black, 2004). Nonetheless, dental aging has proven to be accurate and universal (Alqahtani *et al.,* 2014). It is especially important as there is a lack of documented age for individuals in archaeological collections. There are few skeletal collections where remains are of documented origin (Cunningham *et al.,* 2016). Therefore, the application of this method to unclaimed and unknown forensic remains with no history provides a measure of chronological age.

There is a wealth of studies which address the subject of dental aging (Schour and Massler, 1941; Demirjian *et al.,* 1973 and Ubelaker, 1978) and highlight the application of classical methods that have been tested for cross population applicability and accuracy. In an archaeological context, the most common used method is that of Moorress and colleagues (1963a, 1963b). The extensive work using panoramic radiographs from individuals ranging in age between 6 months and full maturity, suggested a method of dental age estimation which made use of 14 stages of tooth mineralization for both single and multirooted teeth. Female development was more advanced when compared with that of the male. In addition, root formation showed more variation than that of crown development (Panchbhai, 2011).

A drawback of this method is that the accuracy varies across populations (Liversidge and Molleson, 2004). Nonetheless, Alqahtani and colleagues (2010) recently applied the Moorrees method (1963a, 1963b) to 72 prenatal and 104 postnatal remains of known age from archival collections based in the United Kingdom. This developmental chart has proven to be universal and accurate, which can be applied to the analysis of radiographs of individuals between the

ages of 28 *in utero* weeks to 23 years (Alqahtani *et al.,* 2014*)*. The work by Schour and Massler (1941) was based on the earlier work by Logan and Kronfeld (1933). The development of the deciduous and permanent teeth from 4 months to 21 years of age was categorised into 21 chronological steps and a chart was published which makes it possible to directly compare calcification of teeth from radiographs. However, this survey doesn't account for differences between males and females (Panchbhai, 2011).

The work of Demirjian and colleagues (Demirjian *et al.,* 1973; Demirjian, 1986) investigated dental maturity in French Canadian children of known age using a scoring system based on the degree of the mineralization of hard tissues and the development of crown morphology. Demirjian reported a difference for females and males from age five. The major disadvantage of this rating system is that it doesn't include the 3rd molar in its assessment for maturity (Panchbhai, 2011). Additionally, the method is based on mandibular dentition, as the development of the maxillary dentition was not included in the assessments. Liversidge and colleagues (2003) observed that there is advancement in dental maturity since the original French-Canadian sample. The 8 stages of the left mandibular teeth of Demirjian have been critiqued for showing poor applicability to different populations (Scheuer and Black, 2000).

An adjustment of the Demirjian system was reported by Willems in 2001, which is more accurate than the original method which overestimated dental age in relation to chronological age (Queiroz *et al.,* 2016). In a cross sectional retrospective study of 946 healthy children between the ages of 3 and 16 years, Williems adjusted rating system using the Demirjian method were found to be the most accurate with a 95 % confidence interval (Maber *et al.,* 2006).

Another method which is commonly used is that of Nolla (1960). Here the mineralization of permanent dentition was evaluated from both maxillary and mandibular dentition. Based on a reading system, each tooth is compared with the developmental criteria and a total equates to the chronological age (Nolla, 1960). Melo and Ata-Ali (2017) have found that the combination of the Demirjian and Nolla methods of dental aging equates to 99 % accuracy with chronological age. In a Spanish sample of 2641 living subjects between the ages of 7 and 21 years, the Nolla method under estimated and the Demirjian method over estimated age (Melo and Ata-Ali, 2017). Similarly, a Turkish study of children (aged 7 to 13) tested the most common methods from panoramic radiographs and found that the Demirjian method overestimated age (KirIoglu and Ceyhan, 2012). The suggestion from the literature is that a combination of methods might produce a better accuracy when related to chronological age and that population specific standards are needed.

Databases for population specific standards for children have been developed using orthopantograms in Iceland with a high reliability (Vidisdottir and Richter, 2015). In a Western Australian population, a polynomial regression model has been developed using the Moorees (1963a) and Bengston (1935) models. As with Vidisdottir and Richter (2015), orthopantograms were used to formulate this model. The prediction accuracy has been demonstrated within a two year range (±0.998-2.183) (Karkhanis *et al.,* 2015). In a study of a Thai population group, the Demirjian and Williems adjusted methods were used with panoramic radiographs of 1134 children aged between 6 and 15 years (Duangto *et al.*, 2016). Quadratic regression was used to develop new models. Accuracy for this standard was reported for both sexes (Duangto *et al.*, 2016).

Over all, age estimation accuracy increases in younger age groups. This is the one universal agreement among the discrepancies of sample size, uneven composition and methods employed (Scheuer and Black 2004). Most relevant for the purposes of our study, as no dental aging criteria based on the South African population is available, results proved that variability in aging is minimal in infancy and robust during adolescent years. The London atlas of human tooth development and eruption has proven to be valid and reliable when compared with other widely used dental developmental charts (Alqahtani *et al.,* 2014). However, a recent publication based in New Zealand, assessed the precision and accuracy of commonly used developmental charts. The London atlas was compared to that of Schour and Massler and Blenkin and Taylor (Alqahtani et al., 2014). In this study of 875 children of known chronological age, the Blenkin Taylor chart (Australian population based) performed best (Baylis and Bassed, 2017). This suggests that further evaluation is needed to validate developmental charts and regression formulae in terms of universality of use and application.

1.3.2 Sex estimation from perinatal dental tissues

Sex differences in the timing of deciduous tooth development have been previously reported (Burdi *et al.,* 1970; Garn and Burdi, 1971). Interestingly, boys were found to mature faster than girls. Therefore, study of dental development should include separate categories and assessment for female and male individuals. Any dental aging method developed from the study of mineralization, tooth morphology and eruption needs to have separate criteria for the sexes (Burdi *et al.,* 1970; Garn and Burdi, 1971).

Sex differences in tooth size involving the mesiodistal and buccolingual diameters of the tooth crowns in permanent and deciduous tooth crowns have been previously observed (Moorrees,

et al., 1957; Garn *et al.,* 1967; Margetts *et al.,* 1978; Lysell and Myrberg, 1982; Axelsson and Kiryeskari, 1984; Stroud *et al.,* 1994). However, the use of these diameters for dimorphic criteria is more reliable in adults (Cardoso, 2010; Khanghura *et al.,* 2011). In addition, discriminant functions for sex estimation from deciduous teeth have been developed from American (Black, 1978), Canadian (De Vito and Saunders, 1990) and Polish (Zadzinska *et al.,* 2008) children. These discriminant functions were tested by Cardoso (2010) on 46 Portuguese immature skeletons (birth-10 years) of known sex. Mesiodistal and faciolingual crown dimensions were measured. Results indicated poor accuracy and poor cross validation, which further (Cardoso, 2010) suggests low sexual dimorphism in deciduous crown size and tooth size between samples. Deciduous dentition is less sexually dimorphic when compared to the permanent dentition. Additionally, differences observed are subject to variation within and among populations (Harris and Lease, 2005). In sum, currently there is no reliable and universally accepted method for sex estimation based on the deciduous dentition of infants and children.

Another tissue which is used in forensic identification is that of bone. An overview on skeletal development is subsequently presented and methods pertaining to sex and age estimation are reviewed.

1.3.3 Osteological development

Most osteological age estimations are based on the appearance of ossification centres and the subsequent development of bone from these centres (Pryse-Davies *et al.,* 1974). Connective and cartilaginous tissue serve as a blueprint for the future bone. Osteogenesis commences at

a primary site and expands in size as the blueprint is preplaced by bone. These primary sites of ossification appear during the embryonic and fetal period (Scheuer and Black, 2000).

Two different forms of ossification occur which include intramembranous (ossification by direct apposition on tissue within the embryonic connective tissue membrane) and the more common endochondral (a cartilage model serves as a blueprint for ossification) ossification.

Intramembranous ossification can be further subdivided into two distinct types of mesenchymal ossification. The phylogenetically ancient dermal type (neural crest cells) and perichondral (mesenchymal cells) formed in the perichondrium. Intramembranous bone is dense and compact bone of the calvarium or femur. In contrast, endochondral ossification (mesenchymal cells) results in trabecular or cancellous bone. Therefore, it may be suggested that intramembranous ossification is responsible for the external surface of the bone, while endochondral ossification is found within the internal aspect of some bones (Cunningham *et al.,* 2016).

The endochondral cartilage model is penetrated with blood vessels and growth radiates from this point (*nutrient foramen*). A membrane surrounds the cartilage model (*perichondrium*). Osteoblasts beneath this membrane begin to deposit bone around the cartilage shaft. Following this process, the membrane is now a fibrous connective tissue (*periosteum*) which deposits more bone. As the growing bone increases in size, osteoclasts on the endosteal surface remove bone and osteoblasts in the periosteum deposit bone. In adults, compact bone is periosteal in origin and the medullary cavity in long bones is formed from osteoclast activity. During bone growth, the cartilaginous growth plate (*epiphyseal plate*) is between the primary centre of ossification (*metaphysis*) and the secondary centres of ossification (*epiphysis*).

This plate advances in the opposite direction of the metaphysis. Bone replaces cartilage on the diaphyseal side of the plate. Ossification and growth ceases when cells in the growth plate stop dividing and the *epiphysis* fuses with the *metaphysis* (White and Folkens, 2005).

In general, there are three phases of development of bone. These are the appearance, changes in the morphology and size, and the fusion of ossification centres. Ossification centres have been traditionally studied using histological techniques, manual cleaning with the aid of potassium hydroxide and the most favourable radiological imaging (Scheuer and Black, 2004). Early studies examined the ossification centres are based on embryos and fetuses from abortions and stillbirth circumstances (Noback, 1944; Noback and Robertson, 1951; Noback, 1954; Moss *et al.,* 1956; Redfield, 1970). The chronological age of these fetuses is uncertain and in many circumstances the factors influencing the fetus, such as maternal nutrition and teratogenic factors are unknown (Scheuer and Black, 2000).

1.3.4 Age-at-death estimation from perinatal osteology

The study of ossification centre appearance, growth and morphology forms the basis of age-at-death estimations. Skeletal aging is not as reliable and accurate as dental aging. Skeletal and dental tissues have a strong genetic basis in development. However, skeletal tissues are more exposed to environmental factors such as nutrition, socio-economic status and possibly climate (Scheuer, 2002). During juvenile age range, skeletal aging is the most accurate and precise. This is due to extensive changes the skeleton experiences over a relatively short period of time. The distinctive changes in bone size, morphology and fusion of epiphyses aid in the formation of chronologies for skeletal age (Scheuer and Black, 2000). Morphology and the size of ossification centres have mostly been studied on European populations and there is a deficit

data from the rest of the world (Cunningham *et al.,* 2016). Age-at-death estimations involve specialized evaluations that include anthropometric measurements at autopsy and analysis in cases of skeletonised remains (Fazekas and Kosas 1978; Knight and Saukko, 2004).

Current methods of ageing in juvenile osteology are limited to the variable of age (Weaver 1998; Baker *et al.,* 2005). A comparison of the relevance and efficiency of dry bone measurement (Fazekas and Kosa, 1978), ultrasound and radiographic (Sherwood *et al.*, 2000) methods were tested on a historic and forensic fetal remains of known age by Sanders (2009). The methods correlated strongly with known age of the historical individuals but not for the modern forensic fetuses. The regression formula derived from dry bone measurements (Fazekas and Kosa, 1978) was to be the most accurate when compared with known age (Sanders, 2009). In the studies by Fazekas and Kosas (1978), the chronological age of fetuses was unknown. Individuals were grouped by crown heel length (CHL) and age was assigned in lunar month intervals. The formulae were developed by plotting the body length as an independent variable against the bone length as a dependent variable (Fazekas and Kosa, 1978). The contribution of the Fazekas and Kosas (1978) sample to the field is invaluable. However, because they are based on the fetal skeletal elements of mid-20th century European remains, these methods tend to over-age modern samples given the trend of increasing fetal body length during the 20th century (Scheuer and Black, 2000). This criterion is problematic as one cannot avoid the question of its reliability to assess remains from the 21st century and across different races. Despite this, criminal cases are still being evaluated using this criterion which is based on Hungarian remains (Ubelaker, 2005; Cunha *et al.*, 2009; Sanders, 2009; Franklin, 2010).

While there have been multiple studies on osteometric data, there is a limited amount of knowledge available concerning morphological changes in the immature skeleton. Early studies on the morphological changes of bones and appearance of ossification centres *in utero* resulted in stages of development being communicated in combination with anatomical features which could be related to aging (Noback, 1944; Noback and Robertson, 1951; Noback, 1954; Moss *et al.,* 1956; Redfield, 1970). Thus, there is a need for detailed accounts of the bony anatomy of primary and secondary ossification sites (Scheuer and Black, 2000).

It has been demonstrated from ultrasound based studies that population affinity variation exists between populations in terms of fetal growth and development (Scheuer and Black 2000;2004; Patel *et al.,* 2004; Unterscheider *et al.,* 2013; Sletner *et al.,* 2015). Indeed, Lim and colleagues (2000) found differences within different Asian populations when examining the correlation of femur diaphyseal length and CHL. Unterscheider and colleagues (2013) found that Caucasian Irish babies are bigger than infants from African, Caribbean, Bangladeshi, Indian and Pakistani descent in terms of birth weight (Unterscheider *et al.*, 2013). In terms of gestational length and fetal maturation, African and Asian babies mature earlier compared to European babies, but were shorter in length (Patel *et al.*, 2004). Sletner and colleagues (2015) found that head circumference (HC), abdominal circumference (AC) and femur length (FL) vary between European, Asian and African fetuses as early as 24 gestational weeks. From a demographic perspective, 70 % of the South African population is derived from African (black) ancestry (Ngyende, 2012). The numbers of 'stillborn' cases admitted to the Johannesburg Forensic Pathology Services (JFPS) are predominately of African (black) descent. Therefore, evaluating prenatal skeletal remains based on the non-specific standards of Fazekas and Kosas (1978) is potentially unreliable and inappropriate in application to a forensically based dataset

of non-European descent. The consensus on reliability of age estimation at the prenatal stage of development is further limited by influences of sexual dimorphism, asymmetry and ancestry (Sanders, 2009).

In archaeological studies examining infant deaths and burials, the most common set of standards used for age-at-death estimations include the work of several authorities in the field (Fazekas and Kosas, 1978; Scheuer *et al.,* 1980; Scheuer and Black, 2000; Sherwood *et al.*, 2000; Gowland and Chamberlain, 2002; Irish *et al.*, 2008; Kinaston *et al.*, 2009; Mays and Eyers, 2011) Historically, age estimation has been reliant on the diaphysis of long bones or teeth (Scheuer and Black, 2000). The femur has been used to estimate anthropological age both in adult and sub adult remains. Through a longitudinal study of five documented osteological collections, Rissech and colleagues (2008) used a polynomial regression for the four variables of diaphyseal and distal length and maximum length and vertical diameter of the head of the femur to prove that any one of these variables can be used for age assessment and sexing. This can be done from age 15 onwards and is estimated from the maximum length and vertical diameter of the head of the femur. A recent fetal radiological study of long bones by Carneiro and colleagues (2016) further illustrates the use of the femur bone for age-at-death assessment. The study examined long bone lengths for gestational age in a Portuguese sample. Measurements were taken from radiographic images of 257 fetuses of known gestational age and tested the accuracy of findings with known age and then compared measurements to traditional regression formulae of Fazekas and Kosas (1978). This retrospective study critiqued the method of converting bone length to body size and then gestational age as in the femoral study by Scheuer (1980). Conventional least squares regression equations (classical and inverse calibration approaches) and quick reference tables were found to be more accurate than

previously reported techniques for gestational age estimation in forensic contexts (Carneiro *et al.,* 2016). A morphometric study on an Indian population examined the rate of fetal femoral growth in non-viable (12-28 gestational weeks) of 45 fetuses. The medial and lateral growth rates were reported as 2.3 mm per week. It has been noted that fetal growth is more dependent on the increase of femoral length than the soft tissue crown rump length (CRL) after 20 gestational weeks (Dhawan *et al.*, 2014).

Despite the use of the femur in age estimations, this bone is often damaged or absent within a forensic and archaeological setting (Nagaoka *et al.,* 2012). Therefore, the use of the occipital components and more specifically the basilar part is favourable (Scheuer and Black, 2000).

This is due to the robust nature of the bone against decomposition and post mortem artefacts (Scheuer and Maclaughlin-Black, 1994). Several studies have stressed the pars basilaris importance during early embryological development as well as the correlation of morphometric occipital elements and reliable aging criterion for forensic remains (Scheuer and Maclaughlin-Black, 1994; Scheuer and Black, 2000; Nagaoka *et al.,* 2012; Cardoso *et al.*, 2013).

The archaeological study on 117 Yugoslavian individuals (dated 1400-1475 AD) study by Redfield describes the development and growth of the pars basilaris and pars lateralis components comprehensively. Redfield proposed measurement criteria and morphological features which were later compared to German, Egyptian and Inuit skulls. Redfield described that the pars lateralis margin expands rapidly between the 3rd and 8th month *in utero* and the bone increases in rate of growth postpartum. Positive correlations suggested reliability of these stages of development (Redfield, 1970). The dimensions and reliability of using the pars basilaris bone for aging was assessed by evaluating 62 individuals between the ages of 26

gestational weeks and 4 years. The majority of the sample was archaeological and 'known' age was estimated from femoral length (Redfield, 1970). Maximum width, length and sagittal length was recorded based on Fazekas and Kosas (1978) and Redfield (1970) directives.

The authors' findings corroborate that of Redfield's stages of development. In addition, the degree of variation for the width of the pars basilaris in relation to sagittal length indicates nonviability or postpartum survival (Scheuer and Maclaughlin-Black, 1994).

The Japanese study by Nagaoka & Kawakubo examined the dry bones of individuals from the early to middle twentieth century. A total of 272 perinates were examined using the criteria by Fazekas and Kosas (1978). No sex differences were found between skeletons but when the values and morphological observations were compared with previous findings, population differences were evident. The authors propose new standards for the Japanese population using the pars basilaris but caution using these criteria with individuals of another population affinity (Nagaoka *et al.,* 2012). A study which tested chronological age and skeletal age, utilized both the standards of Fazekas and Kosas (1978) and Scheuer and Black (1994) on a sample of 114 pars basilaris elements from the Granada collection aged between 5 months and 6 years. A new regression formula by classical calibration was devised with confidence intervals at 50 and 97.5 % confidence intervals to express error. When aging standards of Scheuer and Maclaughlin-Black (1994) and Fazekas and Kosas (1978), the Hungarian based standards were found to underestimate age and the findings by Scheuer and Black based on the St Brides Spitalfields collection was found to overestimate it (Olivares and Aguilera, 2016a).

These discrepancies suggest the need for population based skeletal aging criteria that would be based on the current South African perinatal remains as no such criteria or standard exists presently.

1.3.5 Sex estimation from perinatal osteology

In the absence of soft tissues, sex estimation is difficult prior to puberty as sexually dimorphic characteristics are generally amplified and more apparent as a result of a change in hormone levels at puberty (Olivares and Aguilera, 2016b, Ubelaker and Degaglia, 2017). However, one cannot dispute the evidence of dimorphic traits evident from intrauterine existence onwards. For example, male fetuses have been found to be longer and heavier than their female counterparts (Crelin, 1973) and sex differences were observed in hand proportions (Garn *et al.,* 1975). Choi and Trotter's (1970) contribution of discriminant functions from the bone lengths and weights of long bones resulted in a 72 % accuracy for sexing fetuses between 16 and 44 gestational weeks. Based on American white and black skeletons, Choi and Trotter's (1970) equations are considered to be mostly sample specific (Weaver, 1998) The work by Schutkowski (1993) proposed a method for morphognostic diagnosis. Based on the London Spitalfields collection of known age and sex, the study examined traits on the mandible and ilium. The method developed was reported to yield a 70-90 % success rate for sex estimation of skeletal remains aged between birth and five years. Vlak and colleagues (2008) tested Schutkowski's functions for the greater sciatic notch on a portuguese sample and argue that the method cannot be applied across populations.

A geometric morphometric approach was applied to the Spitalfields collection of known age and sex. Six metric criteria based on the ilium were examined and proposed as sexually dimorphic for infants and young children. Not surprisingly, these criterion increased in accuracy with age (Wilson *et al.,* 2008). When the Schutkowski method was applied to the Granada osteological collection in Spain, questions about method accuracy and its applicablity to forensic anthropology were raised. The method was appled to the sample of 5 gestational months to 6 years of age. The best results were found for male indivduals and based on the angle and depth of the sciatic notch (73 – 80 % accuracy). Therefore, the authors advise the use of the sciatic notch as a foundation for future method development for sex estimation from juvenile remains.

As with sex estimation from dental tissues, challenges facing researchers is the limted number of documented skeletal collections and application of methods to differing populations. Further research is needed to validate sex estimation from the perinatal skeleton.

1.4 Molecular techniques of forensic Identification

In cases such as juvenile remains, or when severe trauma or deterioration to the skeleton has distorted key sexually dimorphic features, molecular techniques assist in forming a profile of the deceased. The drawbacks of utilizing molecular techniques include the potential contamination of samples during processing. Knowledge and control over the level of nucleic acid preservation in individuals for molecular protocols is often out of researchers' scope due to the environmental factors which induce molecular degradation. This is seen in South African forensic cases where the circumstance of death is unknown. Despite these drawbacks, strict

laboratory sterilization protocols can ensure that contamination is reduced (Bidmos *et al.,* 2010).

From a molecular perspective, the analysis of regions of short tandem repeats found in genomic DNA form the hallmark of forensic identification and individualisation (Jeffreys *et al.,* 1985). As molecular biology has advanced, techniques involving genomic DNA and RNA have been developed for application in a forensic setting. However, these developments pose new problems which require further investigation. Firstly, the use of post mortem RNA has formulated protocols which assist in body fluid identification, post mortem interval estimation and cause of death (Bauer, 2007) which assist in the investigation process. The use of RNA in forensic application is potentially problematic due to the fragility of RNA to enzymatic degradation (Fordyce *et al.*, 2013) but contributory to identification of body fluids, and cause of death assessment if extracted and processed within the guidelines of an optimized assay. Secondly, methylation patterning of selected regions of the DNA genome for the purposes of aging has been documented in the literature (Hannum *et al.*, 2013; Jones *et al.,* 2015; Jung and Pfeifer, 2015). Many of the studies undertaken have incorporated the use of genome wide approaches, pyrosequencing, and microarray hybridization (Kristensen *et al.*, 2008; Kristensen and Hansen, 2009). Studies have focused on the methylation level of developmental and tissue specific genes within longitudinal broad age categories (Hannum *et al.*, 2013; Jones *et al.,* 2015; Jung and Pfeifer, 2015). Future studies are needed to investigate the methylation level analysis of developmental genes during the fetal and perinatal development.

1.4.1 Molecular sex estimation

In some archaeological and forensic cases, molecular techniques can support and, in some incidences, surpass the value of anthropological analyses (Iscan and Steyn, 2013). The analysis of skeletal remains is currently undergoing a molecular revolution. Advances in genetic fingerprinting and molecular assay development for forensic identification are aiding the disciplines of anatomy and physical anthropology (Cunningham *et al.,* 2016). As previously discussed, traditional morphometric sex estimation from juvenile remains is often not possible due to the lack of distinctive morphological features and markers necessary for these analyses. Developing sex typing protocols aids in the forensic identification of remains. The most common genes used in methodologies for sex estimation are sex determining region y (SRY), Zinc finger protein (ZF) and amelogenin (AMEL) genes. In South Africa, only the ZF and AMEL genes have been used for sex identification. The amelogenin structure and properties makes it a good candidate to use in numerous studies for sex estimation, and is the standard used in forensic profiling STR tests. Amelogenin genes are mostly used with juvenile remains where anthropological methods are limited due to the lack of sexually dimorphic bone landmarks and by the South African police service (SAPS) through the silica extraction method (Bidmos, *et al.,* 2010).

Two molecular methods of sex identification were developed from The Raymond Dart collection (University of Witwatersrand) utilizing miscellaneous archaeological skeletal material. These methods provided means for sexing of ancient DNA (aDNA) by sex specific single nucleotide polymorphisms (SNPs) and an addition of an indel (6 bp) (Gibbon *et al.*, 2009). DNA was extracted from the cancellous bone from the intercondylar fossa. As with previously

reported protocols, targeting the amelogenin gene, the quality of DNA and the taphonomic conditions that the sample was exposed to impact the outcome of assays. The dependability of the amelogenin gene has been communicated before (Mannucci *et al.,* 1994 and Stone *et al.,* 1996). Sex has been estimated by Faerman and colleagues (1998) in infanticide victims from the late Roman era and more recently by Lassen and colleagues (2015) who extracted aDNA from long bones in Aegerten stillborn and neonatal remains. Ancient DNA was extracted from long bones through an automated phenol/chloroform method and polymerase chain reaction (PCR) amplified with a primer system targeting a part of the amelogenin gene located on the sex chromosomes. Molecular results were compared to the morphometric data.

Here the molecular sexing confirmed findings of a high prevalence of male infant mortality from the burial site. The sex determining region Y (SRY) has also been extensively used with anthropological remains to ascertain sex and confirm morphometric observations. Researchers compared the anatomical method results found on the diameter of the femoral head and femoral mid-shaft circumference of 20 modern Egyptian adults. A multiplex method for DNA sex estimation using the SRY gene was performed and results compared to anatomical data. The SRY data confirmed deductions made through osteological means (Gaballah *et al.,* 2014).

1.4.2 Bone-related developmental factors as biomarkers for perinatal aging

As introduced in the osteology section of this review, bone growth arises from a combination of bone formation (apposition) and removal (resorption) that relies on nutrients from blood vessels (vascularization) (Baker *et al.,* 2005). These apposition and resorption activities are dependent on two types of cells. These cells, osteoblasts (osteoid depositing cells) and

osteoclasts (bone removing cells), rely on an intricate network of transcription, growth and signalling factors indispensable to the development of the human architecture (St Jacques and Helms, 2003). Factors which have been identified as key to osteoblast and osteoclast formation, control and differentiation are reiterated in the literature by several authors within the field of molecular and human genetics (Ducy et al. 1997; Ducy et al. 1999; Wagner & Karsenty 2001; Karsenty & Wagner 2002; St Jacques & Helms 2003; Thamamongood 2012). The majority of the studies use chick and murine models as proxy for human development.

In more recent publications, the bovine skeletal system has been used as a model. The factors described in the text are summarized in Table 1.

A review on how cartilage is replaced by bone by endochondral ossification was published Mackie and colleagues (2008). The review outlines how the embryonic cartilaginous model serves as a foundation for longitudinal growth. In sum, chondrocytes proliferate and under hypertrophy die. The extracellular matrix is invaded by blood vessels, osteoclasts, bone marrow cells and osteoblasts. The authors describe that systemic factor include hormones whereas local factors would encompass Indian hedgehog (IIh), Parathyroid Receptor (PTHrp) and Fibroblast growth factors (FGFs). Transcription factors which are instrumental to development include RUNX2 and SRY-box 9 (Sox9) (Mackie *et al.*, 2008).

Olsen and colleagues (2000) outline skeletal morphogenesis within the craniofacial, axial and appendicular skeleton. Numerous genes and their constituents are described within this review, however, Sonic hedgehog, (Shh),Ihh, Bone Morphogenetic Proteins (BMPs), FGFs, Vascular Endothelial Growth Factor (VEGF) and the distal-less (Dlx) family of genes, were prevalent and indicate importance to bone development. The Runt family gene of Cbfa1 is highly evident in the literature on osteoblast formation. This gene is expressed exclusively in

fetal development. Disruption of this gene in mice leads to the complete lack of bone formation and osteoblasts (Komori *et al.*, 1997). The homeobox genes (DLX5 and DLX6) reviewed by Olsen and colleagues (2000), were further investigated and reported as critical regulators of not only craniofacial development but axial and appendicular skeletogenesis as well. Deactivation of these genes in murine systems resulted in perinatal lethality (Robledo *et al.*, 2002). Yang and colleagues reviewed the hedgehog signalling pathway in bone formation. As mentioned before, Indian hedgehog is involved in both endochondral and intramembranous ossification and osteoblast differentiation in the perichondrium (Yang *et al.*, 2015). A strong interaction with the Wnt signalling regulates this process. A disruption of this signalling pathway results in multiple bone diseases (Yang *et al.*, 2015). Osteoblast specific genes are further highlighted by Thamamongood and colleagues, in addition to the above, and include Osterix, type 1 collagen and osteocalcin (Thamomongood *et al.*, 2012).

These important factors were found imperative in studies by Kim and colleagues (1998) on signal regulation of cranial morphogenesis and in further reviews of FGF signalling in endochondral and intramembranous ossification (Ornitz and Marie, 2002). Brouwers and colleagues (2006) examination of growth factor regulation in the human fetal femur found that factors PTHrp, Ihh and VEGF, which are imperative to the regulation of endochondral ossification and could also potentially control bone growth rates. The parathyroid hormone is an inducer to new bone formation. Mice lacking in this hormone died from dyschondroplasia, presented with diminished matrix mineralization and neovascularization and reduced metaphyseal osteoblasts and trabecular bone (Miao *et al.*, 2002).

Not only is VEGF important to the regulation of ossification. In general, VEGF is also essential to angiogenesis and osteogenesis. Through the use of immunohistochemistry,

immunofluorescence, real time-quantitative polymerase chain reaction (RT-qPCR) and western blot analysis, it was found that the expression of VEGF is higher in the fetal samples (10-12 gestational weeks) versus adult comparative samples as well as differential between the mandibular and femoral regions (Marini *et al.*, 2012).

Mutations in the Transforming Growth Factor Beta Receptor (TGFβR1 and TGFβR2) genes were identified in children from the John Hopkins University Hospital with cardiovascular, craniofacial, neurocognitive and skeletal development abnormalities following informed consent. This indicates the master regulatory role in development by the TGFβ family (Loeys *et al.*, 2005). Bone morphogenetic proteins interact with the TGFβ superfamily during embryogenesis and development.

Table 1 Bone –related Developmental Factors

Gene		Function
Bone Morphogenetic Proteins	BMPs	Growth factor (bone and cartilage)
Collagen (Type 1)	Col1a1	Bone, skin and tendon extracellular matrices.
Fibroblast Growth Factors	FGFs	Embryonic development, cell growth, morphogenesis, tissue repair, tumor growth and invasion.
Fibroblast Growth Factor Receptor 3	FGFR3	Bone development and maintenance.
Fibronectin	FN1	Cell adhesion and migration processes including embryogenesis
Indian Hedgehog	IIh	Bone growth and differentiation
Insulin Growth Factors	IGFs	Mediates growth and development
Matrix Metallopeptidase 13	MMP-13	Breakdown of extracellular matrix
Osteocalcin	Ocn	Regulates bone remodeling and energy metabolism.
Osterix	Osx	Osteoblast differentiation
Parathyroid Receptor	PTHrp	Endochondral ossification
Runt Regulated transcription Receptor 2 (Cbfa1)	RUNX2	Osteoblastic differentiation and skeletal morphogenesis
Sonic Hedgehog	Shh	Embryonic ventral neural tube, the anterior-posterior limb axis and the ventral somites patterning.
SRY-box 9	Sox 9	Chondrocyte differentiation
Transforming Growth Factor Beta Receptors	TGFβR1 and TGFβR2	Physiological and pathological processes including cell cycle arrest in epithelial and hematopoietic cells, control of mesenchymal cell proliferation and differentiation, wound healing, extracellular matrix production, immunosuppression and carcinogenesis.
Vascular Endothelial Growth Factor	VEGF	Physiological and pathological angiogenesis

Information adapted from www.ncbi.nlm.nih.gov

Mouse knockouts have resulted in embryonic lethality and marked defects. Not only are BMPs critical during bone development but human tooth development is also dependent on high expression levels (Dong *et al.*, 2014; Wang *et al.*, 2014).

Additional factors related to ossification include that of Matrix Metallopeptidase 13 (MMP-13), for endochondral and intramembranous ossification during the early prenatal period (Johansson *et al.*, 1997), and Insulin-like Growth Factors (IGFs) for intrauterine growth. Baker (1993) reported complete growth deficiency in murine models where IGF was silenced (Baker *et al.*, 1993). Moore found that IGF2 is significantly correlated to crown rump length and birthweight when reviewing human fetal growth (Moore *et al.*, 2015).

Based on the above review, a vast amount of data and information about bone formation and the networks associated with the apposition and resorption is available. Considering their importance to bone development, three factors were selected for assay development with respects to gene expression analysis and methylation level analysis. Patterns in expression and methylation percentage have the potential to be linked to biological age of perinatal and postnatal were not included in the study. Details regarding the role and importance of RUNX2, FGFR3 and Fibronectin will follow.

RUNX2

The Runt regulator family has been linked to fetal bone development in various studies. A review on the similarities of mammalian RUNX genes highlighted RUNX2 as particularly involved in osteogenesis (Levanon and Groner, 2004). The tissue specific transcription control of RUNX2 has been demonstrated in in vitro studies. RUNX2 Promoters (P1 and P2) have been identified as osteoblast specific enhancers. Studies in transgenic mice have lead researchers to believe that the expression of RUNX2 is affected by changes in the expression of HOXA-2, MSX2, Twist and PPARy2. All three runt related transcription factors

are expressed in cartilage but RUNX2 is especially evident in hypertrophic chondrocytes (Levanon and Groner, 2004). Therefore, RUNX2 can be classified as a master transcription factor for osteogenesis. This is based on its structural integrity. RUNX genes are tightly regulated and this leads to a regulated spatio-temporal expression pattern. During osteogenesis, the gene is initially down regulated during the proliferation phase induce the maturation process. RUNX2 is responsible for the activation of osteoblast differentiation marker genes. It is also involved in the vascular invasion of developing skeletons and the metastasis of breast cancer and bone pathologies (Vimalraj *et al.*, 2015).

The RUNX2 P1 promoter and its specificity to bone development were investigated in terms of organization by Barutcu and colleagues (2014). SupT3h is a ubiquitously expressed gene located within the first intron of RUNX2. They identified the SupT3h promoter as a regulator of RUNX2 (Barutcu *et al.*, 2014). Osterix is an osteoblast-specific transcription factor which operates during differentiation of preosteoblasts into osteoblasts and osteocytes (Sinha and Zhou, 2013). A genome wide DNA methylation study on the epigenetic changes in osteoarthritic cartilage found 550 differentially methylated sites in arthritic cartilage from 485, 000 sites. Patients (n=24) with eroded and intact cartilage which were undergoing hip arthroplasty were included in the study. RUNX2 was one of the differentially methylated genes, supporting the importance of RUNX2 in bone regeneration (Jeffries *et al.*, 2014). The methylation status of synovium-derived mesenchymal stem cells during chondrogenesis was investigated by bisulfite sequencing analysis. Promoter regions of 10 candidate genes (including RUNX2 and FGFR3) were assessed by RT-qPCR. Sites were targeted 1000 bp upstream of the transcriptional start site (TSS) for both RUNX2 and FGFR3. Methylation levels were consistently low in RUNX2 and FGFR3 transcripts.

This suggests that at a mesenchymal stage of development, RUNX2 and FGFR3 are active during chondrogenesis (Ezura *et al.*, 2009). RUNX2 and Osterix act downstream of BMP2 pathway. RUNX2 and Osterix in double heterozygous embryos displayed reduced bone length in the humeri and femora elements. Hypoplastic or complete absence of maxillary and palatine shelf, presphenoid bone, zygomatic bone and tympanic ring were also observed. During histological analyses, an expanded region of hypertrophic chondrocytes was evident with a reduced area of mineralized tissue. This study illustrated how instrumental Osterix and RUNX2 are during endochondral ossification (Baek *et al.,* 2014).

The essential nature of this master regulator can be observed in bone pathology studies. The association and collaboration of RUNX2 and Axin2 was studied in a murine model which focused on skeletal defects attributed to improper endochondral bone formation. Axin2 deficiency exacerbated calvaria components of the cleidocranial dysphasia phenotype in RUNX2 +/-mice (McGee-Lawrence *et al.*, 2014). The suggestion from this research is that Axin2 operates as a modulator of terminal stages of endochondral bone formation. Core binding factor beta (Cbfβ) is a protein complex that binds to one of the three RUNX proteins to assist in the activation and expression of these genes. Qin and colleagues (2015) experimented with Cbfβ deficient mice using skeletal, histological and radiographic analyses. *In situ* hybridization, RT-qPCR and western blotting techniques were incorporated to examine the phenotype and consequences of RUNX2 knock out in the murine model. Researchers observed a delay in both intramembranous and endochondral ossification, a general deceleration in endochondral ossification, Ihh, Col10a1 and inhibited chondrocyte differentiation in primary Cbfβ mice. A significant inhibition of osteoblast differentiation was also observed in the mice (Qin *et al.*, 2015).

FGFR3

Fibroblast Growth Factor Receptor 3 (FGFR3) has been linked to the regulation of cell growth and division, the estimation of cell type, the formation of blood vessels, wound healing and embryonic development (Ornitz and Marie, 2002). The role of this growth factor in bone development and disease has been reported from mouse models, knock in and knock out and transgenic technologies. Congenital bone diseases have been attributed to a lack of FGFR3 activity in missense mutation studies (Su *et al.,* 2014). Knockout mice studies have shown that FGFR3 regulates growth and a lack thereof results in skeletal overgrowth (Pannier *et al.,* 2010). The K644M knock in mutation leads to severe dwarfism and the K644E knock in mutation equates in an Achondroplasia-like dwarfism (Pannier *et al.*, 2010). Gene expression analysis and immunohistochemistry results have indicated that FGFR3 is active in the centre of mesenchyme condensation, in cartilage proliferation, chondrocytes of the growth plate as well as in osteocytes and osteoblasts. Therefore, one can surmise that FGFR3 is expressed throughout bone development (Ornitz and Marie, 2002). FGFR3 mutations in mice have resulted in a smaller body size and shortened long bone length (Su *et al.,* 2014).

Achondroplasia is a common form of human dwarfism. It is caused by a mutation in FGFR3 (Y367C), which results in a disruption in endochondral ossification (Pannier *et al.*, 2010). FGFR3 is also considered a negative regulator of bone growth. Pannier and colleagues (2010) examined the radiographs of 148 children with achondroplasia. The Greulich and Pyle method was used to estimate bone age. Chronological age was compared to bone age. Radiographical results were compared to the histological and immunological analyses of FGFR3+ mice which ubiquitously expressed the Y367C mutation. Analyses from the mice studies showed a delay in bone growth and secondary ossification centre formation, a delay

in chondrocyte proliferation and a disruption of genes and protein expression (Col II, VEGF, CD34 and MMP13) during secondary centre formation, which was compared to the Achondroplasia patient results. Bone age delay was observed in both datasets for human and murine subjects (Pannier *et al.*, 2010).

The expression pattern of all three FGFR1 ,2 and 3 genes in human embryos and fetuses was studied by excising cartilage and cranial bones from voluntary and spontaneous abortion individuals. The embryos were aged using the Carnegie classification (stage 10-20) and the gestational age of the fetuses were between 8 and 35 weeks (Delezoide *et al.,* 1998). High expression of FGFR3 was found in the mature chondrocytes of the cartilage plate, indicating activity in cartilage development. Membranous ossification of the skull vault was characterized by the co-expression of all three variants by presence in pre-osteoblasts and osteoblasts. This suggests importance in cranial bone development (Delezoide *et al.*, 1998). This has been demonstrated in a murine study on craniosynostosis mutations in the homeobox gene Msx2 as well as the FGF receptors cause human craniosynostosis syndromes. Mutations of the FGFR3 transcript in murine models results in calvaria morphological differences of the sagittal suture between embryonic and postnatal stages (Kim *et al.*, 1998).

The expression of the two FGFR3 isoforms (IIIc and IIIb) in the bovine fetal rib growth plate was examined to estimate if levels are zone-related. Both isoform transcripts are expressed in the rib plate, primarily in the hypertrophic region. Western blot analysis confirmed that full length FGFR3 is present in the reserve zone. Immunostaining localized FGFR3 to the pericellular region of reserve chondrocytes and the extracellular matrix in the hypertrophic zone. The authors suggest that a transmembrane form of FGFR3 undergoes proteolytic cleavage towards the hypertrophic zone (Pandit *et al.*, 2002).

Fibronectin

Weiss and Reddi (1981) found that Fibronectin, an extracellular matrix protein, was expressed ubiquitously throughout the development of endochondral bone and bone marrow (Weiss and Reddi, 1981). Demineralized bone matrix was prepped from rat diaphyses and implanted into 28-31-day old rats. Bone plagues were used for protein labelling. An Enzyme Linked Immunoabsorbent Assay (ELISA) and immunofluorescence staining was conducted. Fibronectin was present in developing bone and synthesized by mesenchymal cells, chondrocytes and osteoblasts. Fibronectin appears to be a ubiquitous component of the developing skeletal matrix (Weiss and Reddi, 1981). A review on how Fibronectin operates during chondrogenesis, describes how changes in extracellular matrix composition and mechanical properties can affect cell shape and stem cell differentiation. Singh and Schwarzbauer (2012) used chronogenic differentiation as a model which examined the changes that occur before and after mesenchymal differentiation by Fibronectin. The possibility that the Fibronectin matrix has an instructive role in directing cells through condensation, proliferation and differentiation of cartilage development was suggested. The reasoning behind this hypothesis is based on the presence of Fibronectin before and after chondrogenesis, where the protein is found in the matrices of cartilage and has been shown to support deposit of collagens (Singh and Schwarzbauer, 2012). Collagen (COL27AI) is expressed in cartilaginous tissues and plays a role in the calcification of cartilage and the transition to bone. Hjorten and colleagues (2007) investigated the gene expression and protein product of this factor in a fetus (20 gestational weeks of age). Immunohistochemistry revealed that collagen is mostly in hypertrophic cartilage as is expected during mid-fetal life (Hjorten *et al.*, 2007).

Due to its properties of adhesion and involvement in collagen and cartilage development within the extracellular matrix, Fibronectin is known as the "extracellular glue" in developmental biology. It is unregulated and necessary in a number of developmental contexts and is present during periods of change, pathological progression and wound healing (Zollinger and Smith, 2017). The cell adhesion properties of Fibronectin were tested by Kawashita and colleagues (2016) when examining the effect of Fibronectin absorption on osteoblastic cellular responses to hydroxyapatite and alumina. Fibronectin coating of MC3T3-E1 osteoblastic cells lead to better adhesion and spreading. The authors hypothesize that Fibronectin stimulates preosteoclast cell proliferation and therefore, is a facilitator for the initial ossification process (Kawashita *et al.*, 2016).

In summary, a multitude of factors and regulators are responsible for cartilage and bone development. Several reviews and experimental studies emphasize the involvement of these factors in bone generation. Studies such as the above provide grounds for the investigation into molecular control of bone growth and especially with consideration into the control, differentiation and proliferation of osteoblasts and osteoclasts.

1.4.3 Post mortem RNA

Bone is a highly-mineralized tissue with a low number of cells embedded in it. This makes extraction of nucleic acids especially challenging and difficult (Carter *et al.*, 2012). Methods for nucleic acid extraction from bone are destructive to skeletal remains and consequently there is a need to sample from a skeletal element not used in anthropometric analyses or through a non-invasive method. The processes of sample sites, homogenization and purification are not the only obstacles facing researchers interested in RNA. Despite the affirmations that post mortem RNA has forensic applications (Bauer, 2007; Fordyce *et al.*,

2013), many factors influence the rate of RNA degradation. The use of DNA in the applications of forensic science has dominated the field.

The utilization of RNA in this discipline has been hindered by the widely held perception that RNA is unstable due to its structure and is degraded by RNAses in deceased tissues (Kuliwaba *et al.,* 2005). Endogenous (nature of bases, sugars and phosphate residues) and exogenous (pH, presence of cations, ultraviolet light and presence of oxygen and water) factors affect the stability and possibility of extracting pure and intact RNA (Fordyce *et al.*, 2013). The rate of degradation is variable across the different post mortem scenarios. Fordyce and colleagues (2013) review the structure of RNA and its long-term survival in post mortem circumstances. They surmise that RNA is more resistant than DNA in terms of depurination and depyrimidation processes, which provides a level of resilience to degradation post mortem. The authors stress that in order for RNA to be preserved, a macromolecular barrier needs to be in place between the environment and the nucleic acid. For archival and archaeological tissue, FFPE acts as barrier against RNA degradation (Fordyce *et al.*, 2013).

The rate or level of RNA degradation seems to be gene dependent. In a study on the impact of degradation, total RNA was isolated from human rectal tumour biopsies (Opitz *et al.,* 2010). RNA was subjected to heat induced degradation at time dependent points. Degradation was shown to be highly affected by biological differences between patients. Researchers discovered that genes with short mRNAs and probe positions near the 5' end were the most affected by heat degradation (Opitz *et al.*, 2010). A Portuguese study attempted to characterize the RNA degradation in different post mortem tissues to develop a mathematical model for accurate post mortem interval (PMI) estimation (Sampaio-Silva *et al.*, 2013). As noted by the researchers, reliable PMI estimation by physically observable

signs at autopsy (*algor*, *rigor* or *livor mortis)* are not dependable assessment measures. Sampaio -Silva and colleagues (2013) examined expression levels of reference genes (ACTB, GAPDH, HPRT, CYP2E1 and PPIA) from murine post mortem tissues by quantitative Real Time Polymerase Chain Reaction (qRT-PCR). Eight murine tissues, heart, lung, spleen, femoral quadriceps, liver, stomach, pancreas and skin were removed and maintained at room temperature in aseptic conditions for up to 24 hours prior to RNA isolation. Results highlighted that the loss of RNA integrity during PMI is tissue specific. Here organs of the abdominal cavity had the fastest degradation rate, whereas organs of the thoracic region displayed the highest stability. Through this enquiry, the authors were able to identify four quadriceps muscle genes (ACTB, GAPDH, and PPIA AND SRP72) which correlate with PMI (Sampaio-Silva *et al.*, 2013).

The PMI of deceased tissue affects the integrity of RNA (Koppelkamm *et al.*, 2011). The successful RNA extraction from human post mortem tissues was found in six tissues from decedents varying between 15 and 118 hours PMI. In this investigation, sampling was subject to no macroscopic visible signs of putrefaction at area of excision. Samples were snap frozen in liquid nitrogen or immersed in RNA*later* when liquid nitrogen was not available. Storage at -80 °C was followed until isolation. The expression levels of the GAPDH housekeeping transcript was quantified by quantitative polymerase chain reaction (qPCR). Signalling from all tissues was evident through screening by agarose gel electrophoresis and qPCR Ct values; however, the highest level of gene expression was found in RNA originating from skeletal muscle, brain and heart tissue (Heinrich *et al.*, 2007). In evaluating the stability of RNA isolated from human trabecular bone at post mortem and surgery, researchers obtained samples during autopsy from the proximal femur and iliac crest bone of adult individuals (Kuliwaba *et al.,* 2005). To assess the effect of a longer PMI, one case

sample with a PMI of 24 hours was divided into 250 mg equivalents and isolated at 24-hour intervals up to 96 hours. Samples were stored at 4 °C until RNA isolation. Surgical samples were obtained from proximal femur and tibia from patients undergoing hip arthroplasty. Kuliwaba and colleagues (2005) surmise that for gene expression studies in bone and post mortem cases, a PMI of less than 48 hours needs to be selected based band detection and intensity of RT-qPCR products visualized following agarose gel electrophoresis. In addition, the authors advise that samples need to be stored at 4 °C as soon as possible following retrieval at autopsy (Kuliwaba *et al.,* 2005).

Studies by Bahar *et al.,* (2007) and Van Doorn *et al.,* (2011) highlight that it is possible to extract RNA from post mortem tissues at time points beyond those described in the studies mentioned before. Authors aimed to qualitatively and quantitatively assess the integrity of total and messenger RNA extracted from bovine skeletal muscle, subcutaneous adipose tissue and liver stored at 4 °C for 3 weeks. Housekeeping genes (GAPDH and ACTB) and two diet-related genes (RBP5 and SCD) RNA from skeletal muscle was detectable up to 22 days post mortem (Bahar *et al.*, 2007). The integrity of bone and bone marrow RNA for reverse transcription-polymerase chain reaction (RT-PCR) derived from controlled conditions was studied by Van Doorn and colleagues (2011) by extracting RNA from the compact bone and bone marrow tissue of six skeletally mature rabbits. These individuals were placed in room temperature glass tanks 24 hours after death. The researchers allowed for aerobic decomposition but used a fine mesh to cover tanks and avoid oviposition by blowflies and other insects. Therefore, air temperature was kept constant and influence of insect activity within the decomposition process eliminated. Bone and bone marrow samples were collected at 0, 4, 7, 15, 21 and 31 days. Assays included the assessment of RNA by absorbance, the RT-qPCR of extracted RNA (targeting sequences of HRB, HPRT and 18S

rRNA) and the visualization of 28s and 18s bands for detection of intact ribosomal RNA. Bone marrow RNA presented with intact rRNA bands up to 21 days' post mortem (Van Doorn *et al.*, 2011).

Different methods of tissue storage prior to RNA isolation and subsequent gene expression analysis are an important consideration in RNA stability. This was shown by Mutter and colleagues (2004) by comparing quantitative RNA expression profiles of uterine myometrial tissue individuals stored in replicate aliquots for immediate homogenization (fresh), flash frozen in liquid nitrogen and then stored at either at -80°C, a 24-hour immersion in RNAlater at room temperature or a 72-hour immersion in RNAlater at room temperature. The results indicated that tissue storage within commercially available preservation agents (RNAlater) did not lead to any differences in levels of specific RNA transcripts, when compared to tissues stored by traditional flash frozen/-80 °C methods (Mutter *et al.*, 2004). These results are certainly in agreement with Michaud and Foran, who claim that solution based storage (DMSO/NaCl/EDTA), is one of the most effective, practical and economical of options (Michaud and Foran, 2011).

The stability of RNA derived from post mortem tissues and its use in the field of medicolegal investigation is promising. The current challenge for researchers in this field is firstly that casework conditions haven't been incorporated into study designs for forensic RNA investigations. Many studies were carried out within controlled conditions and samples. This warrants the question of whether techniques and protocols optimized in controlled experimental designs can be applied to case work from medicolegal environments for mRNA derived from post mortem tissues. Secondly, caution has been communicated by researchers to not place post mortem RNA degradation under the same biochemical mechanisms as *in vivo* mRNA. Studies need to be designed to evaluate enzymatic turnover

in post mortem tissues as very little is known about the biochemistry of post mortem RNA decay mechanisms (Yasojima *et al.,* 2001; Van Doorn *et al.*, 2011; Fordyce *et al.*, 2013).

1.4.4 Methylation analysis of gene promoters

As an alternative method of studying gene expression, the methylation of specific CpG islands within the promoter regions of genes can be studied. Methylation analysis has been applied to aid in the identification of biological tissues and fluids. Within the realm of forensic application, new techniques are being developed to estimate sex and provide a phenotype of donors (Kader and Ghai, 2015).

Methylation of CpG islands and sites is a dynamic form of regulation of gene expression during development. Generally, methylation of promoter regions leads to reductions in gene transcription. Methylation occurs on cytosine residues and is catalysed by DNA methyltransferases (DNMTs) which occur in high levels in all vertebrates. Methylation is targeted to important developmental genes and is involved in tissue specific gene regulation. Indeed, tissue specific gene expression signatures have been found to be present as early as 9 gestational weeks in amnion, muscle, adrenal and pancreatic fetal tissue (Slieker *et al.*, 2015). DNA methylation is heritable during somatic differentiation and suggested to be inherited through generations (Guibert *et al.,* 2009; Tost, 2010; Lalruatfela, 2013).

DNA methylation is an epigenetic mechanism which changes throughout the life cycle. This makes it an attractive avenue to study aging dynamics and recently new techniques and methods have developed in application to the field of forensic identification. Methylation patterning has been found to differ between adult and fetal tissues. By comparing the profiles of human fetal and adult red blood cell progenitors, dynamic changes in

methylation were found to occur during human erythropoiesis (Lessard *et al.*, 2015). Fetal femur development was studied through this epigenetic programming by de Andres and colleagues (2013). Methylation levels were studied using pyrosequencing in human embryonic stem cells, fetal bone cells and adult chondrocytes. Methylation inversely correlated with the expression of genes including INOS and COL9A1 (de Andrés *et al.*, 2013). Methylation of DNA has been shown to be necessary for proper development and function of bone cells (Bocheva and Boyadjieva, 2011; Reppe *et al.,* 2015). Fetal brain development has been studied by evaluating the CpG site methylation for indication of autism and neural tube defects (Schneider *et al.*, 2016; Wang *et al.*, 2017). The majority of studies have focused on genome wide approaches using pyrosequencing and Illumina 450k methylation array assays. However, methylation specific PCR based approaches are also incorporated in study designs to investigate single locus DNA methylation (Kristensen *et al.*, 2008; Kristensen and Hansen, 2009).

With respect to aging, longitudinal projects have been designed and undertaken using DNA methylation and its correlation to chronological age. Aging using this technique has been applied to forensic identification for aging using blood as a sample base (Yi *et al.*, 2014; Zubakov *et al.*, 2016). Genome wide approaches have been applied here to produce linear correlations with age. The majority of these studies and prediction models are based on young children or adolescents, to individuals in advanced age groups (75 years +) (Hannum *et al.*, 2013; Jones *et al.,* 2015; Jung and Pfeifer, 2015). A common trend among these is a standard error of a few years. Accuracy is more reliable in younger age categories, although within the larger population group, this error is minimal. However, no studies have been published detailing aging of perinatal or fetal individuals using DNA methylation.

1.5 Research Questions

In light of the literature reviewed and the knowledge gaps identified, answers to the following questions will be addressed by the techniques in the subsequent chapters. Firstly, can European juvenile osteology standards be used to age South African populations? Secondly, can the gene expression levels and methylation status of RUNX2, FGFR3 and Fibronectin be linked to bone development be used to age South African perinates? Thirdly, is there a relationship between perinatal osteological anatomy observed in a South African population and methylation of selected genes during the fetal and postnatal stages of development?

1.6 Aim

Estimation of sex and age of forensic fetal, perinatal and postnatal remains using osteological and molecular methods from a South African population.

1.7 Objectives

Dental

1. Use dental aging of perinatal individuals using Nomad portable scanner digital images and the standards of the London atlas of human tooth development and eruption (Alqahtani *et al.,* 2010) in order to establish biological age.

Use of postmortem RNA

2. Evaluate the routine applicability of postmortem RNA from bone for the purposes of forensic identification and investigation.

Sex estimation

3. Molecular estimation of sex of unknown perinatal samples from individuals with no sex recorded at autopsy.

Age estimation

4. Evaluation of the morphometric features from the occipital pars basilaris and pars lateralis and the femoral skeletal elements within the dental age categories and sexes using traditional osteological analyses and bone mineral density from Micro-CT analysis.
5. Formulation of population specific dry bone measurement criteria for the application of skeletal aging.
6. Analysis of the expression levels (mRNA) and promoter methylation status of RUNX2, FGFR3 and Fibronectin within sex groups and dental age groups and investigate any correlations with the osteological data for age estimation.

CHAPTER 2: MATERIALS AND METHODS

2.1 The perinatal sample

To estimate the sex and age of forensic fetal, perinatal and postnatal remains using osteological and molecular methods from a South African population, individuals originated from the JFPS and the Johannesburg forensic paediatric collection (JFPC) and were housed at the University of the Witwatersrand. Individuals associated with the JFPC, were donated for research by the School of Anatomical Sciences. In accordance with chapter 8 of the National Health Act 61 of 2003, human tissues may be donated with permission by relevant authority for the purposes of health research. Under the National Health Act, 2003 (Act No. 61 of 2003), the core function of the Forensic Pathology Service in the Department of Health (DOH) within South Africa is the medico-legal investigation of unnatural death. Fetal and perinatal remains are admitted to the services in accordance with the Births and Deaths Registration Act no.51 of 1992, section 12, and the Criminal Procedure Act, section 239. The main reasoning of a medico legal autopsy of these remains is to ascertain the viability of the fetus (by gestational age) as well as to estimate if there is evidence of life or separate existence. In South Africa, the medical and legal gestational age of viability is 26 weeks I.U.

Therefore, individuals were processed and collected for osteological and genetic analyses at the discretion of the forensic pathology services. Following the legal requisites cited in the regulations of Forensic Pathology Services regarding unidentified remains, unclaimed fetal or perinatal remains were included in the study and processed after 30 days of custody at the service within the jurisdictional area (Regulations Regarding the Rendering of Forensic Pathology Services, 2007). Identified and claimed fetal and perinatal remains were excluded from the study.

Under these parameters, 80 individuals were initially collected in the study. Perinatal individuals included fetal (9-40 gestational weeks) and postnatal remains (birth-7.5 months). Documentation accompanying each individual was recorded in the post mortem report, whereby (if possible) demographic details are reported (gestational age, sex and race) as well as cause of death. Data were also collected from the police report, which provided information regarding the circumstance of death and particulars of the scene.

In many circumstances, this case information was unavailable or not reported. Individuals included in this collection were admitted as dumped fetal remains (n=20), abandoned or concealment of birth babies (n=2) and stillborn (n=6). The remaining circumstance of death was not available. Cause of death (as per the autopsy report) was recorded as nonviable fetal remains (n=10), stillborn (n=14), unascertained (n=9), blunt force head trauma (n=2) and sharp force head trauma (n=1). The remaining cause of death was not available.

Due to the forensic nature of the cases included, post mortem damage or missing bones were evident. Individuals were excluded from analyses if post mortem damage or the incomplete skeletal remains made ascertaining a biological age (see Dental aging section) difficult. Thus, a total of 74 individuals were included in the sample as biological age was estimated. Of these, 44 originated from the Johannesburg Forensic Pathology Service. All individuals here were at a stage of advanced decomposition at dissection. The remaining 30 fetal and neonatal remains were from the Johannesburg Forensic Paediatric Collection and were formalin fixed and therefore stage of decomposition was unknown at dissection. All individuals were of a black (African) ancestry except for one white and one mixed race perinate, based on the police documentation or autopsy report findings.

2.2 Materials

Animal models were used to optimize develop methods and assays which were applied to the human skeletal tissue. For the animal studies, rib samples were obtained from *Gallus Gallus* (chicken) remains (commercially bought), while *Cercopithecus pygerythrus* (Vervet monkey) remains obtained from the Department of Zoology, Rhodes University were utilized.

Human studies used skeletal elements (pars basilaris, pars lateralis, left femur and sternal rib) from 80 perinatal (<30 gestational weeks – 7.5 months postpartum) unidentified individuals, obtained on site at the JFPS and the JFPC, University of the Witwatersrand. Ethical approval was granted through the Rhodes University Ethical Standards committee (RU-HSD-15-05-0004) and the University of Witwatersrand Human Ethics committee (Medical) (M160280). (Appendix B)

2.3 Methods

Method optimisation and development for assays including individuals from the perinatal sample is detailed in appendix A. This includes a list of reagents for experiments, the description of primers used for sex typing, gene expression analysis and methylation levels for the promoter regions of genes under investigation. In addition, development of plasmid controls and the optimization of the sex typing protocol are described.

The pars basilaris, pars lateralis, femur and bilateral sternal rib samples of individuals (n=74) were incorporated in qualitative and quantitative osteological and molecular analyses. These analyses aimed to develop and/or detect potential forensic identification parameters (age and sex) which are applicable to the South African population.

2.3.1 Dental aging for biological age

At admission to the JFPS, police documentation details the age of individuals. This age is confirmed at the medico-legal autopsy by soft tissue age parameters. These include measurements (Cm) made from CRL, CHL and foot length (FL). Additionally, AC and weight are recorded. These values correspond to growth charts which produce an estimated gestational age. However, the state of these remains is often so decomposed that soft tissue age estimation is difficult during external examination at autopsy. To resolve this issue, individuals included in the study were subjected to dental aging through the use of criteria by Alqahtani *et al.,* (2010). Dental aging is considered more stable and reliable than skeletal aging. Criteria are based on the degree of mineralization and development of the dental hard tissues within the dental crypt. These criteria are widely used for prenatal and perinatal aging in forensic settings and are considered gold standard.

Anterior and lateral digital radiological images of the maxilla and mandible were taken using the Nomad portable X-ray unit (Aribex, Charlotte, NC, USA). This qualitative method was used to evaluate X-rays (lateral and anterior views) and estimate an age of the individuals included in the study. Dental age estimations were based on dental development standards outlined in the London atlas of human tooth development and eruption (Alqahtani *et al.,* 2010). This dental age was subsequently used in place of the soft tissue age previously derived from the measurements. The developing mandibular dentition was used in majority of the cases to ascertain age. In circumstances where the mandible was absent, maxillary dentition was examined. Table 2 outlines the criteria used to estimate dental age based on the findings from radiographic images.

This criterion of dental aging is only applicable to fetuses older than 30 gestational weeks. For this reason, individuals from this collection were categorized as younger than 30

gestational weeks (<30 GW) if Nomad scanning produced an X-ray with no developing dentition evident. Information from the post mortem report supported this categorization as these individuals were categorized as non-viable. A gestational range was estimated based on the criteria in Table 2. The ranges include younger than 30 gestational weeks (<30 GW), 30 – 34 gestational weeks (30-34 GW), 34-38 gestational weeks (34-38 GW), 38 gestational weeks – Birth (38 GW – Birth), Birth – 1.5 months, 1.5 – 4.5 months and 4.5 – 7.5 months.

These categories were used for all subsequent correlations with osteological measurements, bone morphological changes, density ratio analysis, methylation level analysis and RNA expression level.

It should be noted that due to the forensic nature of these remains and the effect of decomposition on the soft tissue, the degree of tooth mineralization within the tooth crypts was often difficult to visualize from X-rays as the dental tissues were at times displaced from the tooth crypts during the decomposition process. In majority of cases, the lateral view of the posterior mandibular dental crypts provided the best view of the developing posterior dentition.

Table 2: Criteria for dental aging of individuals in the collection

		Prenatal				Postnatal		
Dentition	**FDI nomenclature (Left/Right)**	**30 GW**	**34 GW**	**38 GW**	**Birth**	**1.5 mths**	**4.5 mths**	**7.5 mths**
Maxillary								
Central Incisor	(51/61)	Cr ½	Cr ¾	Crc	Crc	Crc	Ri ¼	Ri ½
Lateral Incisor	(52/62)	Coc	Cr ½	Cr ½	Cr ¾	Cr ¾	Cr ¾	Ri ¼
Canine	(53/63)	Cco	Cco	Cco	Coc	Coc	Cr ½	Cr ¾
Deciduous Molar 1	(54/64)	Cco	Cco	Cco	Coc	Coc	Cr ½	Ri
Deciduous Molar 2	(55/65)	Ci	Ci	Ci	Cco	Cco	Cr ½	Cr ¾
Mandibular								
Central Incisor	(71/81)	Cr ½	Cr ¾	Crc	Crc	Crc	Ri	Ri ½
Lateral Incisor	(72/82)	Coc	Cr ½	Cr ½	Cr ¾	Crc	Ri	Ri ½
Canine	(73/83)	Cco	Cco	Cco	Coc	Coc	Cr ½	Cr ½
Deciduous Molar 1	(74/84)	Cco	Cco	Cco	Coc	Coc	Cr ½	Cr ¾
Deciduous Molar 2	(75/85)	Ci	Ci	Ci	Cco	Cco	Cr ½	Cr ½

Table adapted from The London Atlas of Tooth Development and Eruption, Alqahtani *et al.,* 2010. Ci – Initial cusp formation, Cco – coalescence of cusps, Coc – cusp outline complete, Cr ½ - Crown half completed with dentine formation, Cr ¾ - Crown ¾ completed, Crc – Crown complete with defined pulp roof, Ri – Initial root formation with diverse edges, Ri ¼ - Root length less than crown length with visible bifurcation area, Ri ½ - Root equals crown length. GW =-gestational weeks, mths – postnatal month

2.3.2 Osteological data collection

The skeletal elements of the individuals, corresponding with specific dental age categories in the sample, were subject to morphological (qualitative) analysis. Osteometric (quantitative) analysis using traditional dry bone measurements (mm) were taken between specific landmarks and recorded at each dental age category. Osteological elements from the cranial and postcranial regions of the body were selected for osteological analysis. The pars basilaris, pars lateralis (left and right sides) and the left femur of each individual were selected for osteological assessments. These bones were selected for evaluation due to their application to forensic identification of juvenile remains. Osteometric (quantitative) and morphological (qualitative) data were categorized within each dental age category for comparative purposes.

In preparation for the osteological analysis, the pars basilaris, pars lateralis and left femur were excised manually, cleaned with cold water and air dried for 24 hours prior to assessment. Qualitative morphological landmark observations and quantitative anthropometric dry bone measurements were conducted. The laboratory and field manual for Juvenile Osteology was utilized as a directive for reference landmark information for measurements and morphological summaries (Schaefer *et al.,* 2009).

Figure 1 illustrates the measurement landmarks transposed on photographs of an individual included in the study. Measurements were taken with a digital calliper (mm) in the inferior view for the pars basilaris, the intracranial for the pars lateralis bones and the anterior view for femora. For the pars basilaris bone, maximum width (1) was measured by the greatest width in line of the lateral angles. Midline distance between the foramen

magnum and spheno-occipital synchondrosis was measured for the sagittal length (2) of the pars basilaris.

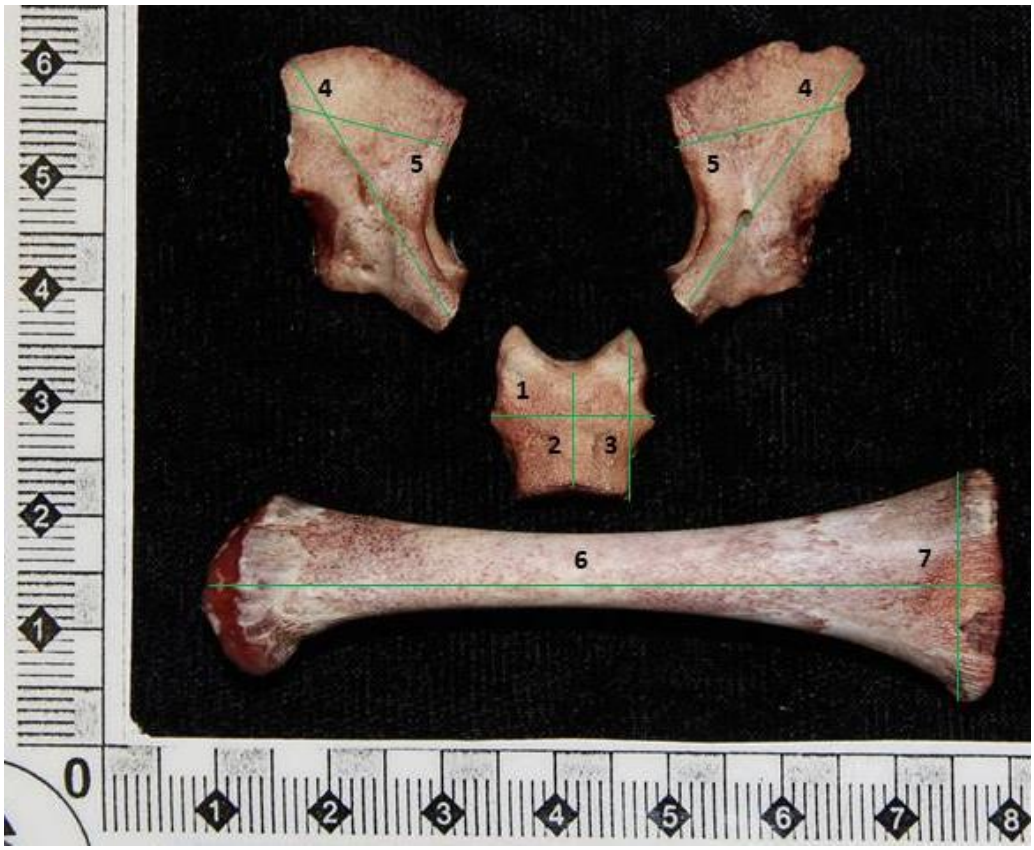

Figure 1: Anthropometric landmarks for the pars basilaris, pars lateralis and femur. Anterior view of the pars basilaris; maximum width (1): greatest width in line of the lateral angles; sagittal length (2): Midline distance between the foramen magnum and spheno-occipital synchondrosis; maximum length (3): maximum distance between the posterior edge of the lateral condyle and the spheno-occipital synchondrosis. Intracranial view of the pars Lateralis: maximum length (4): greatest distance between the anterior and posterior interoccipital synchondrosis; maximum width (5): The greatest distance between the medial and lateral margins of the pars lateralis posterior interoccipital synchondrosis. Anterior view of the left femur: maximum length (6): greatest distance between the proximal and distal articular surfaces; distal width (7): the greatest distance across the distal metaphyseal articular surface was measured. Landmarks adapted from Schaefer M., Black S. & Scheuer L. (2009).

The maximum distance between the posterior edge of the pars basilaris lateral condyle and the spheno-occipital synchondrosis was measured for maximum length (3).

For the pars lateralis, the greatest distance between the pars lateralis anterior and posterior interoccipital synchondrosis was measured for maximum length (4) of the left and right pars lateralis bones. The greatest distance between the medial and lateral

margins of the pars lateralis posterior interoccipital synchondrosis was measured for maximum width (5) of the left and right pars lateralis bones.

With respects to the left femur, the greatest distance between the proximal and distal articular surfaces was measured for maximum length (6) of the femur. For distal width (7) of the femur, the greatest distance across the distal metaphyseal articular surface was measured.

Table 3 details the morphological features which were included for qualitative analysis and recorded as either present, absent or developing for each individual included in the study. Individuals were excluded if bones were missing at dissection or if there was any ante/post mortem damage to a morphological feature.

Table 3: Morphological features for the occipital and femur skeletal elements

OCCIPITAL	**Prenatal age**
Pars basilaris develops lateral angle	7 months
Pars lateralis longer than pars basilaris	8 months
Pars basilaris anterior border of foramen magnum rounded	Older perinates
Articular surfaces of the pars basilaris for the condylar limb and jugular limb well developed	Older perinates
Articular surfaces of the pars basilaris for the pars lateralis and occipital condyle well developed	Older perinates
'Fan appearance' of posterior and mastoid-temporal border surface of the pars lateralis	Older perinates. In younger perinates' borders are straightened and more uniform.
Pars lateralis posterior condylar canal well developed	Older perinates
Pars lateralis jugular tubercle rounded	Older perinates
Pars lateralis jugular limb pointed	Older perinates
Pars lateralis condylar limb articular surface	Older perinates
Pars lateralis occipital condylar articular surface	More pronounced in older
Pars lateralis immature jugular process and border of jugular foramen	Still cartilaginous in younger perinates
Foramen magnum medial borders	90° angle in older perinates. Younger perinates present with a straighter morphology
FEMUR	
Rounded upper anterior surface of shaft	Older perinates. Straighter in younger perinates
Flattened lower anterior surface of shaft	Older perinates
Lateral supracondylar line present on posterior surface	More pronounced in older
Nutrient foramen (multiple) on posterior surface	Older perinates
Linea aspera on posterior surface	More pronounced in older
Lesser trochanteric articular surface	Developed in older perinates
Metaphyseal surface for distal epiphysis	Evident in older perinates

Table adapted from Schaefer M., Black S. & Scheuer L. (2009).

2.3.4 Bone mineral density (Micro-CT) data collection

To assess bone mineral density in fetal and perinatal individuals, the occipital complex and femur skeletal elements were scanned using a Nikon XTH 225L micro-focus CT X-ray unit (Nikon Metrology, Leuven, Belgium), located at the MIXRAD laboratory at the South African Nuclear Energy Corporation (NECSA), Pelindaba.

To ascertain if there were changes in bone mineral density during development, 3D images of the bones were scanned by Micro-Computed Tomography (Micro-CT), reconstructed and analysed using VG studio max software. Sixty individuals (38 females and 22 males) from the sample were selected for bone mineral density analysis. The groups consisted of 11 females and 7 males (early prenatal), 11 females and 9 males (prenatal) and 16 females and 6 males (postnatal). In the case of the pars basilaris, there was one less prenatal male. Therefore, 59 individuals were included for bone mineral density analysis on the pars basilaris bone.

Reproducibility in plotting and determining the bone mineral density on various points of the pars basilaris was validated by an inter-observer error range of 81-99.4 %. The pars lateralis bone mineral density method was analyzed. The inter-observer error for the left pars lateralis was estimated between 82.7 – 89.4 %. The inter-observer error for the right pars lateralis averaged between 74 – 98.5 %.

The Lin Concordance Coefficient observer error for the femur bone mineral density method was validated with a range of 74.5 – 95.3%. The only point that deviated from this was the distal medial border. The error here was 51 %. The pars basilaris density point data were compared within sex and dental age groupings.

Scanning parameters were set to 100 kV/100 µA and 100 µm as a means of standardising the scanning conditions across the sample. A 0.1 mm thick aluminium filter was used to approximate a homogeneous X-ray beam spectrum by removing the lower energy photons.

Individuals were securely mounted in oasis foam and orientated in the intracranial anatomical perspective. A material of uniform composition was used as a density reference value across all scans. The mounted individuals were then placed on to a rotating sample manipulator, which facilitated scanning at 360°. One-thousand projection images were obtained resulting in a good-quality scan with optimised time. The scanning setup was optimised for highest spatial resolution by setting the sample with maximum magnification (magnification is a property of a cone beam). A resolution of between 0.023 and 0.050 µm was obtained. The scans were then reconstructed using NIKON CTPRO software (Nikon Metrology, Leuven, Belgium). After three-dimensional reconstruction, all the scans were imported into VGStudio Max V2.2 (Volume Graphics GmbH, Heidelberg, Germany) as volume files for further analysis.

For clear estimation of surface landmarks, all imported volume files were subjected to a surface estimation analysis. The orientation of the Micro-CT slices of the occipital complex and femora elements were then standardised by aligning each slice a pre estimated reference plane. Reference planes were established by selecting a minimum of three reference points along the anterior view of the pars basilaris, intracranial view of the pars lateralis and cross-sectional views of the proximal, midshaft and distal femur (Figure 2 and 3). Points were used to generate reference planes for alignment reasons. These points are outlined in Appendix C.

Three reference planes were generated for the femur bone. Figure 3 depicts the orientation and plotting of these reference planes for the proximal (Figure 3.1A, B & C),

midshaft (Figure 3.2A, B & C) and distal (Figure 3.3A, B & C) regions. The reference planes (red grid lines) for the proximal and distal ends were plotted at the maximum end of the bone where the tissue was still cartilaginous.

The density marker plane (blue) was plotted just above (distal end) or below (proximal) to ensure that bone density was being measured and not cartilage (Figure 3). The midshaft reference and density planes were plotted above the nutrient foramina closest to the proximal end of the femur. These reference planes assisted in standardising the alignment of the Micro-CT slices within the transverse plane. All slices of the occipital and femoral elements were aligned to these reference points. After the Micro-CT slices were aligned with the established transverse plane, the density markers were plotted for the individual bones (Figure. 4, 5, 6). The assessment of each point included a radius of 1.5 mm and thickness of 1.mm.

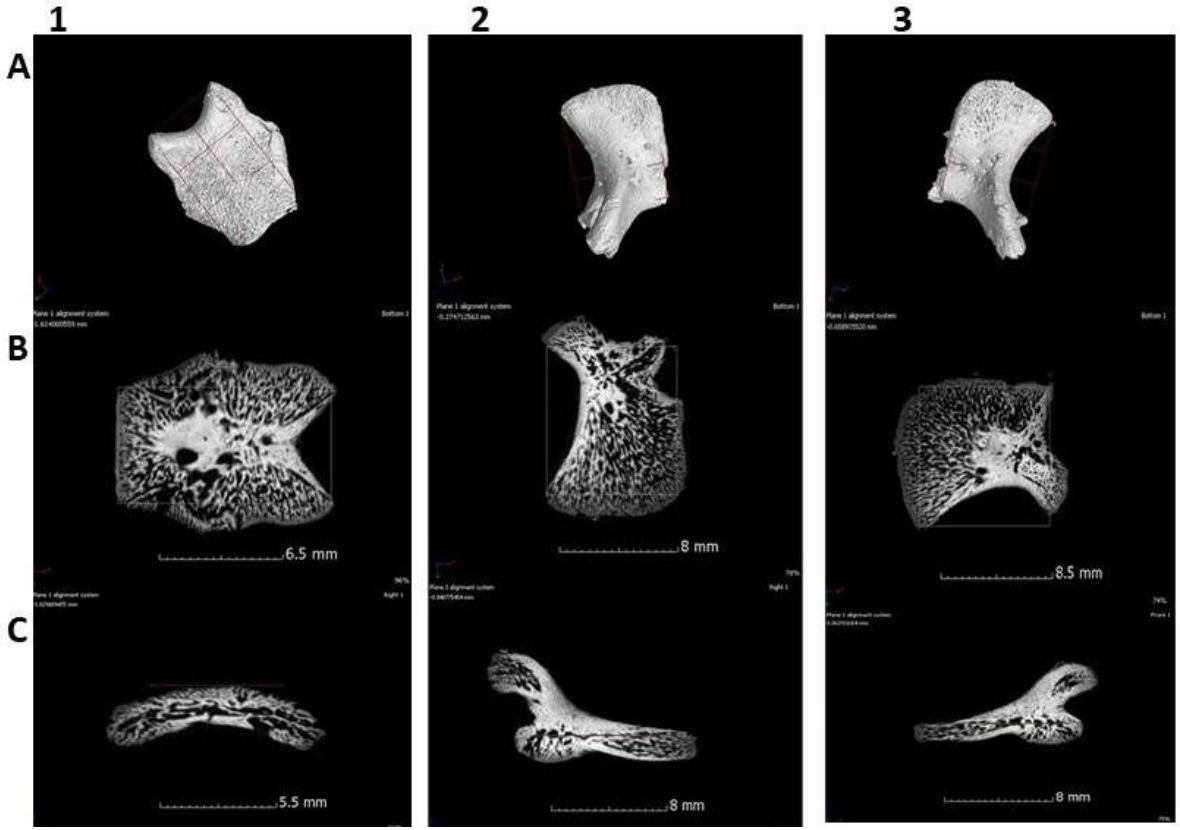

Figure 2: Reference plane images for the occipital bones: 1. pars basilaris images A.) 3D reconstruction of the early prenatal pars basilaris: Red grid represents reference plane B.) Transverse view of the pars basilaris: white border represents reference plane C.) Coronal view of the pars basilaris: Red line represents reference plane. Pars lateralis images: left pars lateralis (2) and right pars lateralis (3). A.) 3D reconstruction of the early prenatal pars lateralis. Red grid represents reference plane B.) Transverse view of the pars basilaris: white border represents reference plane C.) Coronal view of the pars lateralis: Red line represents reference plane. Images generated from VGStudio Max V2.2 software.

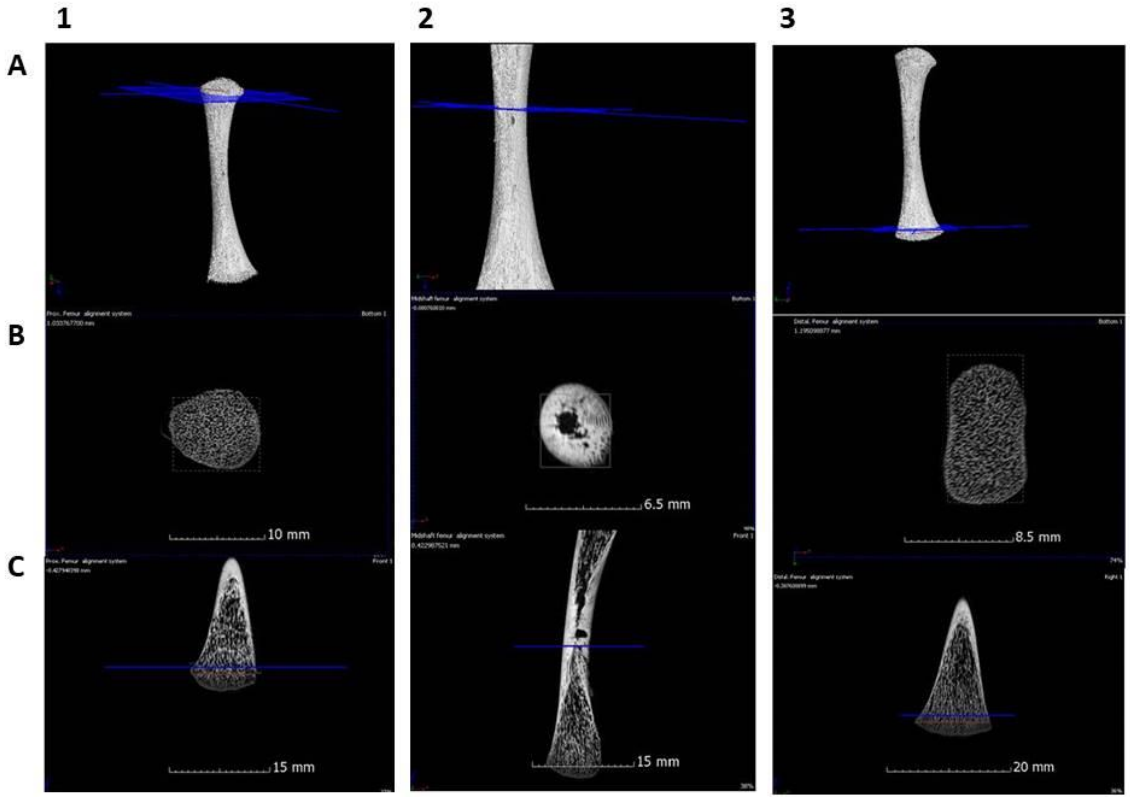

Figure 3: Reference plane for the femur bone. 1A.) 3D reconstruction of the early prenatal proximal femur end 1B.) Transverse view of the proximal femur end 1C.) Sagittal view of the proximal femur end 2A.) 3D reconstruction of early prenatal femur (midshaft) 2B.) Transverse view of the femur (midshaft) 2C.) Sagittal view of the femur (midshaft) 3A.) 3D reconstruction of early prenatal distal femur end 2B.) Transverse view of the distal femur end 3C.) Sagittal view of the distal femur end. Red line represents reference plane. White border represents reference plane. Blue line represents density marker plane. Images generated from VGStudio Max V2.2 software.

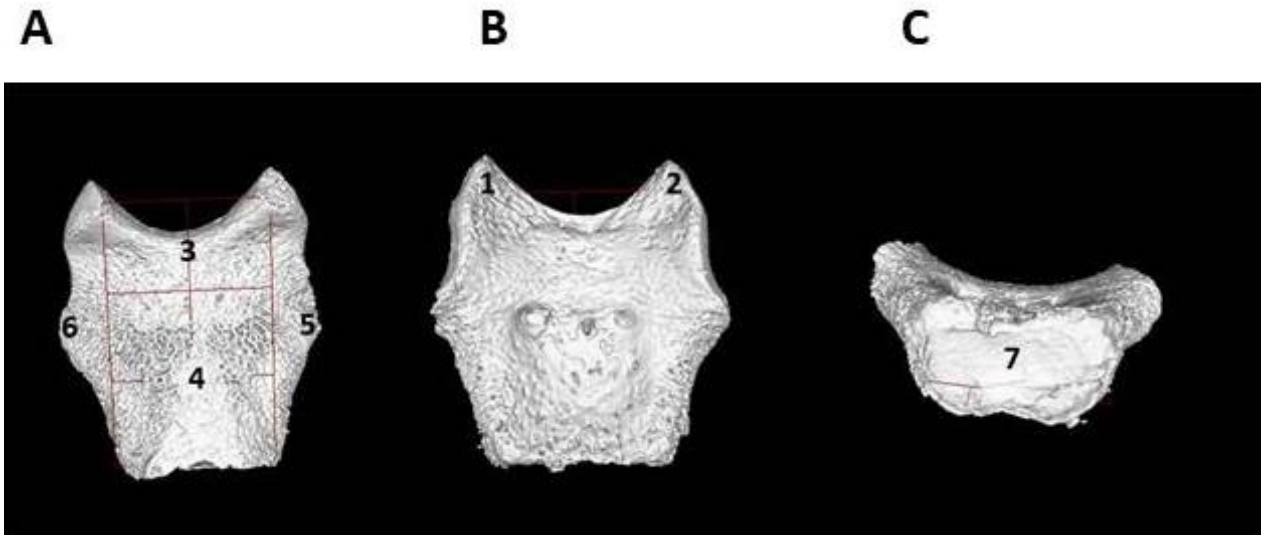

Figure 4: Density marker sites for the pars basilaris bone. A.) inferior view of pars basilaris. B.) Intracranial view of the pars basilaris. C.) Metaphyseal surface of the spheno-occipital synchondrosis. Density marker sites: 1. Right condyle, 2. Left condyle, 3. Anterior border for the foramen magnum, 4. Primary ossification site, 5., Right lateral angle, 6. Left lateral angle, 7. Spheno-occipital synchondrosis.

Anatomical landmarks were selected for the skeletal elements to compare bone mineralization at sites of development relative to primary ossification sites (Figure. 4A (4), 5B (5) and 6B (4.1, 4.2, 4.3)).

Figure 4A, represents the placement of density markers on the intracranial and inferior surfaces of the pars basilaris bone. Seven sites were selected for assessment of bone mineral density. Site 1 and 2 (borders of the occipital condyles) were plotted in the coronal view.

The anterior border of the foramen magnum (site 3) was measured in the coronal view as well. The primary ossification site on the anterior surface of the bone (site 4) was plotted in the transverse view. The density markers for lateral angles of the pars basilaris (site 5 and 6) were plotted in the coronal view. Finally, the metaphyseal surface of the spheno-occipital synchondrosis (site 7) was placed in the sagittal view.

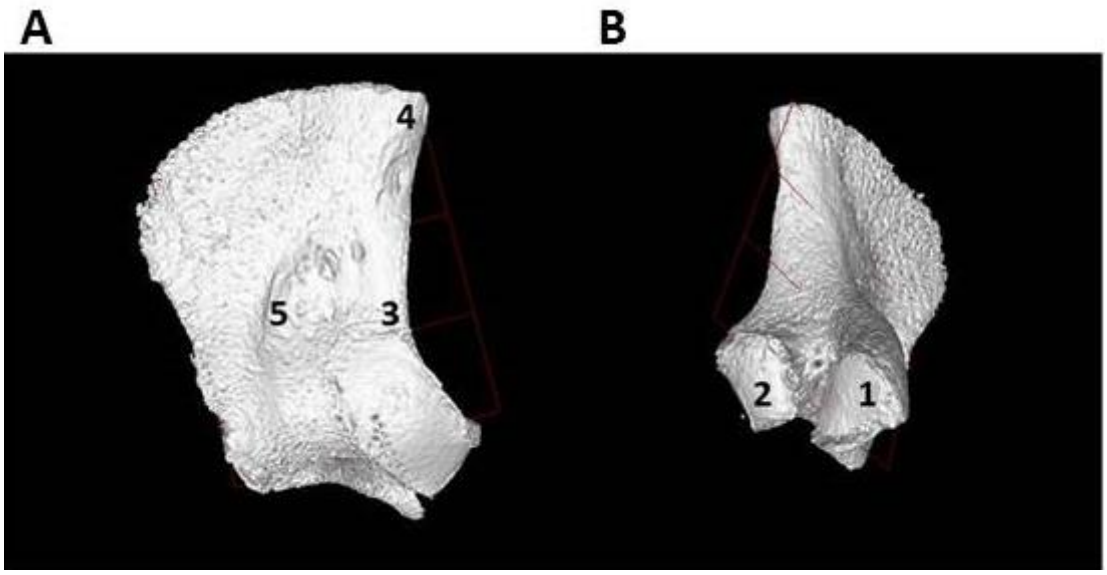

Figure 5: Density marker sites for the pars lateralis bone. A.) Inferior view of the left pars lateralis bone B.) Intracranial metaphyseal view of the left Lateralis bone. Sites repeated for the right pars lateralis bone. Density marker sites: 1. Jugular limb facet, 2. Condylar limb facet, 3. Inferior border of the foramen magnum, 4. Medial edge of the posterior region for the supra occipital (pars squama) of the occipital complex, 5. Primary ossification site.

The pars lateralis bones were assessed with a total of 5 sites (Figure 5). The articular facets of the jugular and condylar limb facets (site 1 and 2) were evaluated in the transverse view. A sagittal view was used to plot site 3 at the inferior border of the foramen magnum. The medial edge of the posterior region for the supra occipital (pars squama) of the occipital complex (site 4) was assessed with a marker plotted in the coronal view. The primary ossification site (5) was plotted with a marker in the sagittal view.

The femur bone primary ossification sites (Figure 6B -4.1, 4.2, 4.3) were placed in a cross-sectional transverse view. This region was selected to assess the difference in bone mineral density in the midshaft region. This region was also selected to evaluate the directionality of growth between the lateral and medial regions. The corresponding proximal and distal sites were also plotted in transverse view. The medial proximal end (site 1), lateral proximal end (site 2) and lesser trochanteric surface at the proximal end (site 3) were assessed by plotting

markers just below the reference plane to ensure accuracy in assessing the level of ossification. Sites 5 (distal lateral border), 6 (distal centre border) and 7 (distal lateral border) were measured in the same method.

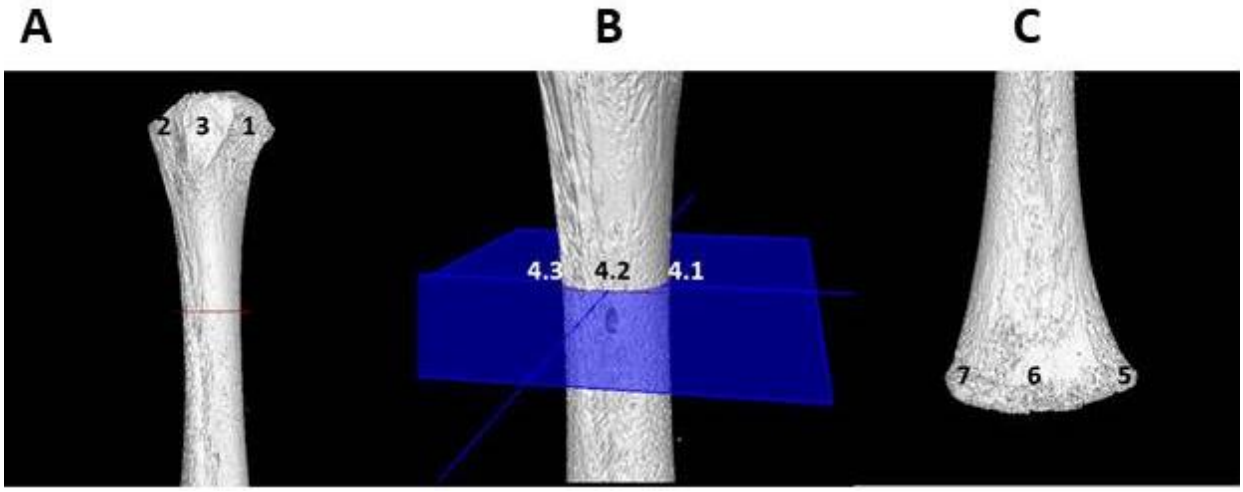

Figure 6: Density marker sites for the left femur bone. A.) Posterior view of the proximal femur. B.) Posterior view of the midshaft femur. C.) Posterior view of the distal femur. Density marker sites: 1. Medial proximal end, 2. Lateral proximal end, 3. Lesser trochanteric surface at the proximal end, 4.1. Medial midshaft, 4.2 Centre midshaft, 4.3 Lateral midshaft, 5. Medial distal end, 6. Centre distal end, 7. Lateral distal end.

2.3.4 Sex estimation of human fetal remains

The sex of the majority (n=65) of individuals was recorded on the documentation accompanying remains to the Johannesburg Forensic Pathology Service. However, in nine cases included in the sample, no sex was noted as per the autopsy report. Therefore, a molecular sex typing protocol was developed and used to estimate sex from sternal bone tissue (Appendix A).

2.3.5 Post mortem nucleic acids for molecular identification and ageing of human perinatal remains.

To determine if there was a relationship between estimated dental age and expression of these genes (table 1), gene expression levels from post mortem bone derived RNA was assessed. As the individuals in the sample were of a forensic nature, and as such in an advanced stage of decomposition, RNA stability and therefore the possibility of RT-qPCR amplification was unknown. To satisfy this aim, the following questions had to be answered. Firstly, can intact RNA be extracted and RT-qPCR amplified from post mortem bone? Secondly, which is the best method of bone preservation prior to RNA isolation? Finally, at what stage of decomposition is RT-qPCR amplification no longer possible? Although some studies have shown that it is possible to isolate nucleic acids from post mortem tissues, there are few studies that have conducted isolations at different stages of decomposition (Bauer *et al.*, 2003; Van Doorn *et al.*, 2011). To address these questions, preliminary investigations and validations were made using animal models (*Gallus Gallus* and *Cercopithecus pygerythrus)* (Appendix A), which were subsequently tested on six sternal bone samples from the perinatal sample.

2.3.5.1 Rib sampling and preservation

Animal models

The perinatal remains included in the study originate from circumstances of death that is unknown. As stated before, case information pertaining to deceased individuals included in the study was missing or unavailable. The majority of individuals were documented as 'dumped' in toilets, street corners and dustbins. To imitate a real world 'dumping' scenario, chicken individuals were placed in a plastic tray at an elevated level within an outside caged

area to avoid predation on remains from domestic animals. This area was subject to sunlight in the mornings and shade in the afternoons. Insect activity and weather conditions (air temperature, humidity) were documented throughout the process. Bilateral sternal bone (≤ 1cm) samples were excised from individuals at the consecutive stages of decomposition. The stages were taken as following: **Stage 1**: Fresh: No physical discolouration of the body. No odours admitted. Rigor mortis is evident. Livor mortis is also present depending on the position of the body. No insect activity. **Stage 2**: Bloat: Green discolouration and bloat of the face and abdomen. Skin slippage may be present. Faint odour. Flies and maggot eggs are present. **Stage 3**: Active decay: Mass decay and destruction of the abdominal organs. Maggot masses and strong odour present. **Stage 4**: Advanced decay: Majority of the body is decomposed due to maggot activity. Cartilage, skin and bone are still present. Beetles will be evident. Maggot pupae will be present. **Stage 5:** Dry bone: No insect activity. Only hair, bone and desiccated skin left. Fresh skin, pectoral muscle and sternal rib ends of commercially bought chicken and monkey cadavers were dissected using a standard dissection kit. Sections of ≤ 1cm were dissected from left and right ribs and then split into microcentrifuge tubes for either -80 °C storage or storage in 1 ml of RNA*later* at room temperature (22 °C) until homogenization 1 week later. Samples were thawed on ice and homogenized by grinding tissue samples in liquid nitrogen with a mortar and pestle or lysing the sample through a nuclease free 20-gauge (0.9mm) needle attached to syringe (Isolate II kit). A total of 500 µl TriReagent was added per ≤ 65 mg of tissue to facilitate the lysis of tissue and extraction of total RNA. The DirectZol miniprep kit (Zymo Research) was used to extract total RNA according to manufacturer's instructions.

Perinatal samples

Human perinatal bilateral rib samples equivalent of 5x10 mm were excised from unclaimed individuals from the Johannesburg Forensic Pathology Service and the School of Anatomical Sciences, University of the Witwatersrand. Individuals were frozen at the medico-legal mortuary prior to thawing and formalin fixed neonates were stored in a tank in the school's mortuary. Isolated rib samples were placed in a microcentrifuge tube with 1 ml of RNAlater and stored at 4 °C for 24 hours prior to -80 °C storage until transportation to BioBRU, Rhodes University for RNA extraction and subsequent RT-qPCR analyses. Formalin fixed rib samples were placed in a microcentrifuge tube without RNAlater and stored directly at -80 °C prior to transportation. The skeletal elements of the occipital (pars basilaris and pars lateralis) and left femur were excised and cleaned with cold water for analysis of morphological landmarks and anthropometric measurements.

2.3.5.2 Nucleic acid isolation

RNA purification using TriReagent and Direct-Zol miniprep kit

Samples stored at either RNAlater and/or -80 °C were processed for RNA isolation. Bone samples were mechanically homogenized on ice with a mortar and pestle by adding liquid nitrogen and TriReagent (500 µl per 50 mg bone). One volume of ethanol (100 %) was added to one volume of the homogenate in TriReagent. The mixtures were loaded into the DirectZol Zymo IIC columns in a collection tube and centrifuged at room temperature at 14 000 x *g* for 30 seconds. The flow through from each collection tube was discarded. An in-column DNase digestion was followed whereby 80 µl of DNase1 Reaction mix was added directly to the column and incubated at room temperature for 15 minutes. A

volume of 400 µl of Direct-Zol RNA prewash was added to the columns and centrifuged at room temperature at 14 000 x *g* for 30 seconds. The flow through was discarded and this step repeated. A RNA wash buffer of 700 µl was added to the columns and centrifuged at room temperature at 14 000 x *g* for 2 minutes. The columns were transferred to RNAse free tubes and 50 µl of nuclease free water was added directly to the matrix of the columns. Microcentrifuge tubes were centrifuged at room temperature at 14 000 x *g* for 1 minute to elute the RNA. The RNA was stored at -80 °C until use.

Isolation of DNA and RNA using the Isolate II DNA/RNA/Protein kit

A total of 300 µl of Lysis buffer TX was added to the tissue sample and was transferred to 1.5 ml RNAse-free microcentrifuge tube. The lysates were centrifuged for 2 minutes at 14 000 x *g* to pellet any cell debris and the supernatant was transferred into another 1.5 ml RNAse-free micro-centrifuge tube. The ISOLATE II DNA column was assembled and 600 µl of lysate was added to column. Columns were centrifuged at room temperature for 1 minute at 14 000 x *g*. and the flow through retained for RNA isolation. A genomic wash was completed by adding 500 µl wash buffer W1 to column and centrifuging at room temperature for 1 minute at 14 000 x *g*. Following this, 500 µl of wash buffer W2 was added to the column and centrifuged at room temperature for 1 minute at 14 000 x *g*. The flow through was discarded and the column centrifuged at room temperature for 2 minutes at 14 000 x *g*. DNA was eluted in 100 µl of DNA elution buffer by centrifugation for 2 minutes at 200 x *g* followed by 1 minute at 14 000 x *g*. DNA was stored at -80°C. The ISOLATE II RNA/protein column was assembled and for every 100 µl of flow through, 60 µl of 95 % v/v ethanol was added and mixed by vortexing. The lysate (600 µl) was added to the column and centrifuged for 1 minute at ≥ 3 500 x *g*. Thereafter, the

flow through was discarded. An RNA wash was done with 400 µl of wash buffer W1 added to the column and centrifuged for 1 minute at 14 000 x *g.* The flow through was discarded and column washed a second time by adding 400 µl of wash buffer W1 and centrifuging for 1 minute at 14 000 x *g.* The column was centrifuged for 2 minutes at 14 000 x *g* to dry the column. To elute RNA, RNA elution buffer (50 µl) was added to the column and centrifuged for 2 minutes at 200 x *g* followed by 1 minute at 14 000 x *g*. RNA purity and quality was confirmed via absorbance at 260 nm using the Nanodrop 2000 spectrophotometer and stored at -80 °C until required.

Genomic (g) DNA extraction

Isolation of SW480 cell line, vervet monkey and perinatal genomic DNA (gDNA) was conducted using the Quick-gDNA miniprep kit as per the manufacturer's instructions. The gDNA purity and quality was confirmed via absorbance at 260 nm using the Nanodrop 2000 spectrophotometer and stored at -20 °C until required. For formalin fixed perinatal samples, the Quick-DNA FFPE kit was utilized as per the manufacturer's instructions.

First strand synthesis of cDNA

First strand complementary deoxyribonucleic (cDNA) synthesis was conducted using Revert Aid H minus First strand cDNA synthesis kit per manufacturer's instructions. Template RNA (according to Table 4) was added to 20 µl test reactions of 1 x reaction buffer (250 mM Tris-HCl pH 8.3, 250 mM KCl, 20 mM $MgCl_2$, 50 mM DTT), Ribolock RNase inhibitor (1 µl), 10 mM dNTP mix (2 µl), random hexamer primer (1 µl at 100 µM), and MLV reverse transcriptase (1 µl). Control reactions included all components except that nuclease free water was used

instead of the reverse transcriptase (RT-). The reaction was incubated for 5 minutes at 25 °C, 60 minutes at 42 °C and then terminated by heating at 70 °C for 5 minutes. A volume of 2 µl of the first stand reaction mixture was used as the template for PCR amplification.

Table 4: Amount of RNA added for cDNA synthesis

RNA	Concentration per reaction
SW480 (Sex typing plasmid controls)	1 µg
Chicken skin, muscle and bone	1 µg
Post mortem Chicken RNA from Decomposition study	100 ng
Post mortem Monkey RNA from Decomposition study	100 ng
Perinatal RNA	300 ng

2.3.5.3 PCR and RT-qPCR amplification of post mortem RNA

Animal models

A gradient PCR was set up to establish the optimal annealing temperature for the beta-actin (*Gallus Gallus*) and CD4 (*Cercopithecus pygerythrus*) primers. The cDNA was converted from commercial chicken skin, muscle and bone RNA (1 µg) and monkey RNA and gDNA (100ng) (Table 4) was used for the optimization process. Both +RT and –RT control reactions was used as a template for the 50 µl reactions with GoTaq mastermix (25 µl), forward and reverse beta actin primers (10 µM) and nuclease free water (up to 50 µl). Reactions were subject to an initial denaturation of 2 minutes at 95 °C and 30 cycles of 95 °C denaturing for 30 s, either a gradient annealing for 30 s at 60 °C, 59.5 °C, 58.3 °C and 57.1 °C or a fixed annealing temperature of 58.3 °C for 1 minute (Beta actin primers) or 55.2 °C, 55 °C, 54.6 °C and 54.2 °C or a fixed annealing temperature of 45 °C (CD4 primers), followed by a 1 minute 72 °C extension and a

final extension of 72 °C for 5 minutes, followed by a 72 °C extension for 1 minute with a final extension of 72 °C for 5 minute. Results were visualized by an ethidium bromide (10 µg/ml) stained 0.8 % w/v agarose gel in TAE.

Optimization of the CD4 primers was attempted by adding BSA (0.5mg) to reactions, using gDNA as a template and extending the temperature gradient as well as attempting a gradient of primer concentration. Primer conditions for PCR were optimized with post mortem gDNA from tissue stored in either RNAlater (room temperature) or -80 °C prior to RNA isolation. Parameters included 40 cycles of 95 °C for 30 s, 10 s at 45 °C annealing, a 20 s 72 °C extension and final extension at 72 °C for 5 minutes. Reactions were set up with a concentration of 50 µM for CD4 primers. The optimized primers and PCR parameters (beta actin and CD4) were used in PCR reactions with template cDNA from RNA (100 ng) (Table 4) extracted from the *Gallus gallus* and *Cercopithecus pygerythrus* biological replicates incorporated in the decomposition study.

Results were visualized by an ethidium bromide (10 µg/ml) stained 0.8 % w/v agarose gel in TAE. Based on the gel results, the first biological replicate samples from the decomposition study were selected for qPCR amplification to ascertain the abundance of the beta actin and CD4 gene during the decomposition process.

Serial dilutions (10 fold) starting with cDNA prepared from 1 µg of RNA was prepared for amplification of the beta actin gene in PCR assays with chicken skin and bone. In these assays, RNA was extracted with the DirectZol miniprep kit. Results were visualized by an ethidium bromide (10 µg/ml) stained 0.8 % w/v agarose gel in TAE. Following this, a qPCR assay was set up with 6 different 10-fold dilutions in 20 µl test and control reactions with 1x Kapa SYBR Fast

qPCR mastermix, 10 µM primers and 2 µl template cDNA. Parameters were 95 °C for a 3-minute activation, 95 °C for 3 s denaturing, 58.3 °C for 20 s annealing, and 60 °C for 20 s extension for a total of 40 cycles.

RT-qPCR assays was set up in triplicate 20 µl test and control reactions with 1x Kapa SYBR Fast qPCR mastermix (10 µl), 50 µM CD4 primers *(Cercopithecus pygerythrus*), 10µM beta actin primers (*Gallus gallus)* and cDNA from 100 ng of RNA derived from the 1st biological replicate bone samples. Beta Actin transcript RT-qPCR parameters were set up as 40 cycles of 95 °C for 30 s, 20 s at 58.3 °C annealing, 60 °C for 20 s extension. CD4 transcript RT-qPCR parameters were set up as 40 cycles of 95 °C for 30 s, 10 s at 45 °C annealing, a 20 s 72 °C extension and final extension at 72 °C for 5 minutes.

Perinatal samples

Assays were set up to evaluate the gene expression for Fibronectin (FN1), RUNX2, and FGFR3 mRNA in the study samples. Serial dilutions (8x 10-fold starting at 10 ng) of plasmid DNA containing the target sequence were prepared as standards to allow for absolute quantitation of transcript concentration present in unknown samples included. Triplicate test reactions and one control were prepared for each sample included. Reactions (20 µl) for qPCR included 1x Kapa SYBR Fast qPCR mastermix, 10 µM primers and 2 µl template unknown cDNA or plasmid DNA. Parameters for assays were 95 °C 3-minute activation, 95 °C 3 s denaturing, 55 °C (for Fibronectin) or 50 °C (for RUNX2 and FGFR3) 20 s anneal, and 60 °C 20 s extension for a total of 40 cycles.

2.3.5.4 Region specific methylation of genomic DNA

Enzyme digestions and controls were set up with 1X CutSmart® Buffer (2µl) in a 100 µl reaction with 200 ng of genomic DNA, enzymes (0.5 µl of Hpych4IV, *Hpa*II, *Scrf*I, *Aci*I) (5 units) and nuclease free water. A control or reference reaction was set up without enzymes. Each reaction was incubated at 37 °C for 3 hours and stopped by incubating at 65 °C for 20 minutes. Test and control reactions (20 µl) were set up in triplicate with 2 µl of restriction digest mixture included 1x Kapa SYBR Fast qPCR mastermix and 50 µM primers. Annealing temperatures for Fibronectin_1, FGFR3_1 and the RUNX2 sites were at 50 °C., RT-qPCR.

Parameters included 95 °C for a 3-minute activation, 95 °C for 3 s denaturing, 20 s annealing, and 60 °C for 20 s extension for a total of 40 cycles.

2.4 Data Analysis

Dental age categories and sub categories were used for biological age and a reference point when comparing osteological and molecular data. Dry bone measurements were taken three times with a digital calliper (mm) for each individual and thereafter an average was calculated. The bone mineral density ratio analysis method from Micro-CT application of fetal and postnatal mandibular growth was used as reference for this portion of the study (Hutchinson *et al.*, 2017). The grey value assessed at each point was used as an estimate of bone mineral density. This value was standardised using the grey value of the reference material included in each scan, i.e. the grey value of each assessment point was subdivided by the grey value of reference. This resulted in the data for each assessment point being presented as ratios or

absolute values, which allowed for further statistical analysis and comparisons of the bone mineral density distribution values across the sample.

For the osteological component of the project, method repeatability and validation for dry bone measurements and bone mineral density methodologies was conducted by Lin Concordance coefficient Analysis. This was used to assess the degree of agreement between two variables. The measurement values (mm and density points) taken by one observer (variable 1) was compared to another observer's findings. This produced an inter-observer error for each landmark measurement and density point plotted for the four bones examined. Inter- and intra-observer errors were evaluated using 8 individuals (osteometric) and 6 individuals (Micro-CT). Additional observations were made regarding the morphology of skeletal elements. The percentage of morphological features present, immature and absent in the different dental age groups was estimated using Microsoft Excel formulae.

Methylation percentage data were analysed by averaging the test Ct values and dividing this by the average of reference values. The following equation was followed to calculate the level of methylation: Percent Methylation = $100 \times 2^{-\Delta C}$.

Descriptive statistics, including means and standard deviations were calculated for the landmark measurement data, bone mineral density ratios associated with skeletal site, stage of decomposition with respect to RNA purity and integrity as well as cycle number means from RT-qPCR data and methylation percentage level data collected within the dental age categories. A pairwise comparison was undertaken to test for differences between left and right pars lateralis bones.

Quantitative osteometric and bone mineral density data from the pars basilaris, pars lateralis and left femur were evaluated by 2-way multivariate analysis of variation (MANOVA) with Scheffe post hoc test to assess the relationship between independent and dependent factors. Molecular data (mRNA purity/abundance and methylation of CpG sites) were assessed with 2-way analysis of variation (ANOVA). A significance level of $p \leq 0.05$ was considered statistically significant. Principle component Analysis (PCA) was used to assess the degree of variation in terms of size and shape within the different dental age groups. Osteological metric data from this study were compared to the metric data of Fazekas and Kosas (1978) and Scheuer and Black (1994). Skeletal Age was assigned based on the mean and range of measurements documented in accordance with Fazekas and Kosas (1978) and Scheuer and Black (1994) cited in Schaefer *et al.,* (2009). Dental and skeletal age ranges were compared. A Lins Concordance Correlation analysis to test the level of agreement between dental and skeletal age ranges. Osteometric data and methylation level percentage means were correlated using Pearson correlations.

CHAPTER 3: RESULTS

3.1 Molecular sex typing of human fetal remains in the sample

Once optimization of the PCR parameters and development of positive controls was complete, the X-linked G6PD and Y-linked SRY primers were tested using the optimized PCR protocol on five samples of perinatal gDNA for which the sex had been recorded. The molecular confirmation of sex is represented in Figure 8, where panel A represents detection of the X chromosome (due to the 191 bp G6PD amplicon) while B represents detection of the Y chromosome (due to the 556 bp amplicon). A single band at 191 bp indicates a female (XX) sex typing, while a band at both 191 bp and 556 bp indicates a male (XY) individual.

Due to the limited amount of sternal tissue and gDNA extracted; the optimization of the sex typing protocol resulted in small amounts of gDNA remaining for the confirmation of sex (Figure 8), therefore only 20 ng of gDNA was used in the PCR reaction for individual 449.

The two faint bands present in panel A for this individual is the result of a low template concentration. When comparing molecular sex with that recorded on the autopsy report, positive correlation was found for four of the individuals. Individual 706 was noted as female at autopsy. However, following this assay and visualization by agarose gel electrophoresis, a faint band was present for the Y-linked primers at 556 bp. Therefore, this individual was re-categorized as male.

The individuals of unknown sex were subsequently tested using the optimized protocol and primers and incorporating the positive plasmid controls generated for the study (Appendix A).

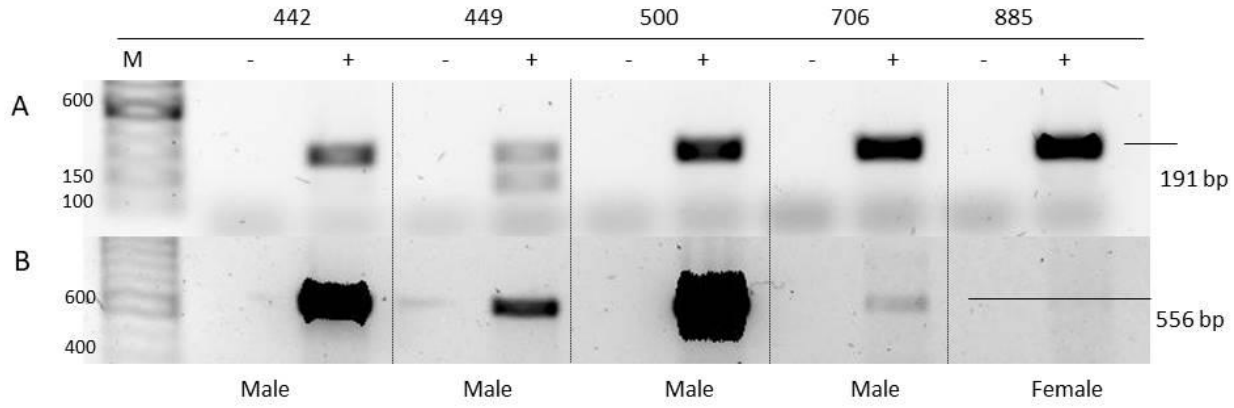

Figure 7: Confirmation of sex in selected individual samples using X-linked G6PD AND Y-linked SRY optimized primers. A.) Ethidium Bromide stained 0.8 % agarose gel of PCR protocol optimized for X-linked G6PD primers targeting perinatal gDNA B.) Ethidium Bromide stained 0.8 % agarose gel of PCR protocol optimized for Y-linked SRY primers targeting perinatal gDNA. +: reactions prepared with template. -: reactions prepared without template. Female = band at 191 bp only. Male = band at 556 bp only.

Figure 9 represents the sexing of unknown perinatal remains using the protocol designed for this project. The gDNA used in these assays derived from three individuals from the JFPS and six formalin fixed individuals from the JFPC. Following PCR, reactions were visualized by agarose gel electrophoresis. The positive control plasmids (G6PD and SRY) are represented by strong bands at 191 bp (X-linked G6PD) and 556 bp (Y-linked SRY) and confirm that the PCR reaction worked correctly. Negative controls reactions were used with the respective primers and no gDNA template.

Each sample of unknown gDNA was added to separate reactions with X-linked primers and Y-linked primers to estimate sex (Figure 9). The positive control plasmids produced strong amplicons at the expected sizes for the X and Y linked primers. These positive signals also confirm that the PCR reaction worked correctly.

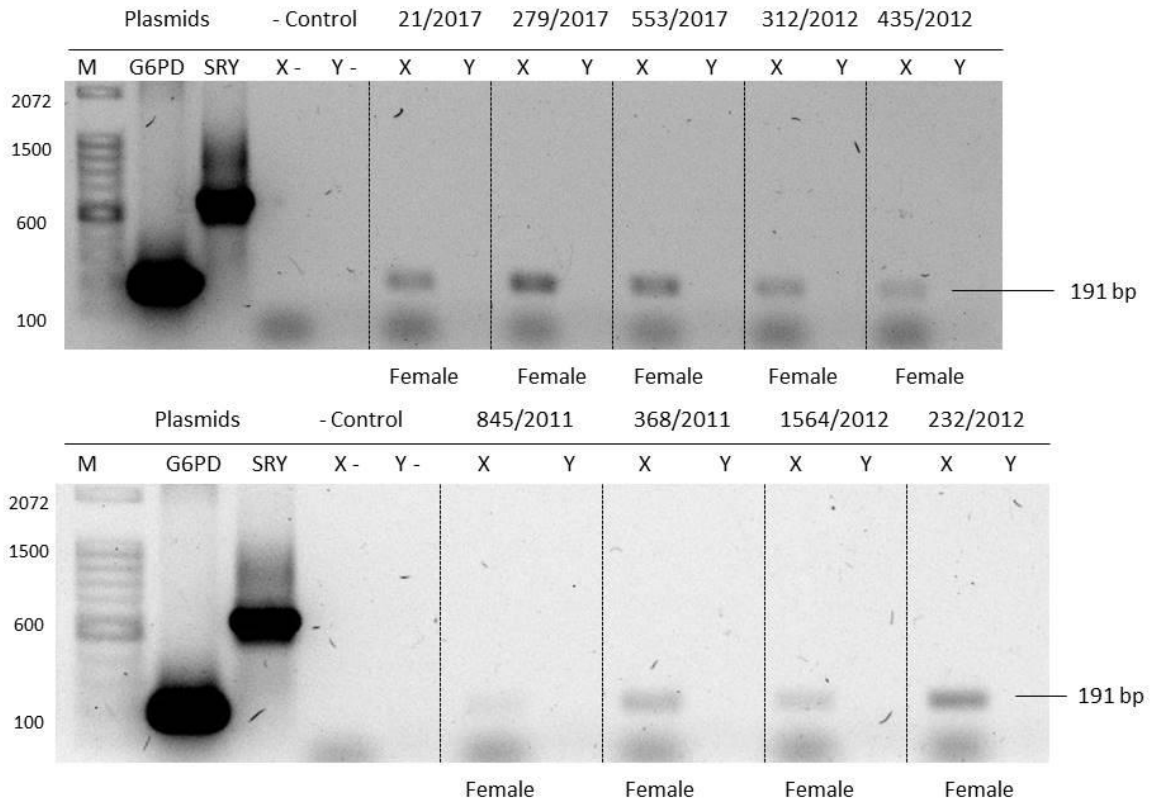

Figure 8: Sex typing of unknown individuals by PCR. Ethidium Bromide stained 0.8 % agarose gel of PCR products indicating sex of unknown perinates included in the study. G6PD and SRY = plasmid controls at 191bp (X-linked) and 556 bp (Y-linked). Control = No template added in PCR reaction. X = X-linked primers only. Y = Y-linked primers only.

Bands were present at only 191 bp and not 556 bp for the nine unknown individuals. There was a minor difference in band intensity between mortuary (21/2017, 279/2017, 553/2017) and formalin preserved individuals (312/2012, 435/2012, 845/2011, 368/2011, 1564/2012 and 232/2012). These individuals were categorized as female and added to the collection database. The individual collection therefore comprised of 45 females and 29 male perinates.

3.2 Morphometric age estimation of perinatal remains

3.2.1 Dental aging of the occipital pars basilaris, pars lateralis and femur elements

The initial cusp formation for the developing dental tissues was not visible in individuals younger than 30 gestational weeks (Figure 7A). At 30 gestational weeks, the central (71) and lateral incisors (72) were present with crown development (half complete) and evidence of dentine formation. The cusp of the canine (73) had commenced with coalescence. The multi-rooted deciduous molars were present with initial cusp formation and coalescence. Deciduous molar 1 (74) presented with coalescence of the molar cusps (Cco) and deciduous molar 2 (75) demonstrates initial cusp development (Ci) (Figure 7B).

Individuals aged at 34 gestational weeks were identified by the development of the central incisor (71) (Cr ¾) and the lateral incisor (72) crowns (Cr ½) respectively. In the X-ray of the deciduous molars, the cusp coalescence of deciduous molar 1(74) (Coc) and the initial cusp formation for the 2nd molar (75) were observed (Ci) (Figure 7C). At 38 gestational weeks, the crown of the central incisor (71) was complete in development. At birth, the lateral incisor (72) crown was partially complete (Cr ¾), while the cusp outline of the canine (73) and deciduous molar 1 (74) was complete. Deciduous molar 2 (75) cusps had united. The coalescence of cusps for both molars and the outline of the canine (Coc) (Figure 7D) indicated an age closer to birth.

At the postnatal stage of development (Birth – 1.5 months), there was a difference in development between the maxillary and mandibular dentition. The maxillary central (51/61) and lateral (52/62) incisors had completed crown development (Crc), while the crown of the lateral (82/72) incisors of the hemi-mandibles were still developing.

The radiological images for the postnatal period (Birth – 1.5 months) were more defined than previous X-rays used as examples of this method (Figure 7E). The anterior view of the left hemi-mandible indicated complete crown formation for the incisors (71; 72) and the outline of the developing canine (Coc) (73) (Figure 7E). The outline of the cusp was also present for the 1st deciduous molar (74) and there was an indication of cusp coalescence for the 2nd deciduous molar (75).

At 4.5 postnatal months, the maxillary central incisor (51/61) was more advanced when compared to its mandibular counterpart. Initial root formation (Ri) of the lateral (82/72) and central incisor (81/71) crowns of the hemi mandibles was evident. In the maxilla, the central incisor (51/61) root formation had advanced (Ri ¼) but to a lesser degree when compared to the crown in length. The lateral incisor (52/62) was delayed at the postnatal stage of development as crown development is still not complete (Crc ¾). The canine (53/63 - 83/73) and molars (54/64; 55/65 – 84/74; 85/75) dentition for both the maxillary and mandibular regions had advanced in terms of crown development (Cr ½) at 4.5 months postpartum. The crown of the canine (83/73) was half completed with definite dentine formation (Figure 7F). The age of the individuals was estimated to be between 1.5 and 4.5 months based on the crown development (Cr ½) of the deciduous molars (84/74 – 85/75) (Figure 7F) and associated dental features.

Finally, at 7.5 months, root length had increased for both the maxillary central and lateral incisors (Ri ½ and Ri ¼), the maxillary canine crown development had advanced (Cr ¾), and the maxillary molar demonstrated root formation (Ri). As seen in earlier stages of growth, the development of the mandibular dentition was delayed during this stage of growth.

Figure 7G represents the advanced crown development of the deciduous molars (74; 75) of an individual aged between 4.5-7.5 months. Based on the dental aging, the individuals in the collection were categorized into groups, namely early prenatal (<30 gestational weeks), prenatal (30-40 gestational weeks) and postnatal (Birth – 7.5 months).

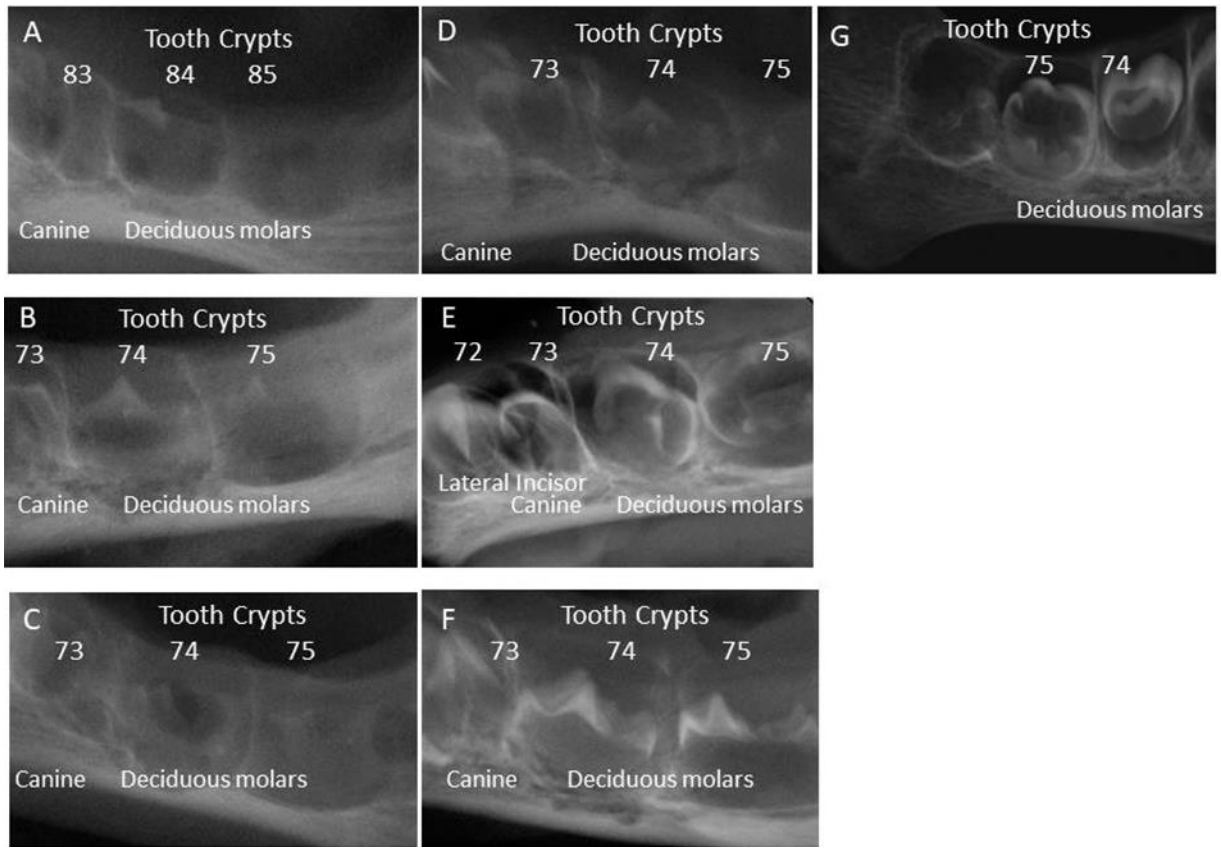

Figure 9: Lateral Nomad X-rays of the perinatal hemi-mandible. A.) Right hemi-mandible, illustrating incisor, canine and deciduous molar dental crypts of an individual younger than 30 gestational weeks. B.) Left hemi-mandible, illustrating initial cusp development of the deciduous molars of an individual aged at 30-34 gestational weeks. C.) Left hemi-mandible illustrating cusp development and coalescence of the deciduous molars of an individual aged 34-38 gestational weeks. D.) Left hemi-mandible illustrating cusp development of the canine and deciduous molars of an individual aged 38 gestational weeks and birth. E.) Left hemi-mandible illustrating the development of the lateral incisor, canine and deciduous molars of an individual aged birth and 1.5 months. F.) Left hemi-mandible illustrating the development of the canine and deciduous molars of an individual aged 1.5-4.5 months. G.) Left hemi-mandible illustrating the development of the deciduous molars of an individual aged 4.5-7.5 months. FDI nomenclature: Right hemi-mandible (81-85); Left hemi-mandible (71-75).

Table 5 indicates the breakdown and numbers of cases in the individual collection according to gestational age, the broad dental age categories and sex (for sex typing: see appendix C: optimization and 3.1 Molecular sex typing). The majority of the sample consisted of individuals in the early prenatal and postnatal categories. Furthermore, there was a preponderance of females within the study sample.

Table 5: Dental age and sex distribution in the sample

Dental Age Range	Gestational Age Range	Categories within Range	Female	Male	N
Early Prenatal	< 30 gestational weeks	< 30 gestational weeks	14	10	24
Prenatal	30-40 gestational weeks	30-40 gestational weeks	11	11	22
		30-34 gestational weeks	2	7	9
		34-38 gestational weeks	5	1	6
		38 gestational weeks –Birth	4	3	7
Postnatal	Birth – 7.5 months		20	8	28
		Birth – 1.5 months	11	3	14
		1.5 – 4.5 months	6	4	10
		4.5-7.5 months	3	1	4

3.2.2 Osteology of the occipital pars basilaris, pars lateralis and femur elements

The osteological features of the occipital complex and femur observed at the three dental age ranges respectively are represented in the radar graphs in Figures 10 - 21. These graphs illustrate the percentage of the sample where associated the feature/s was either present or immature.

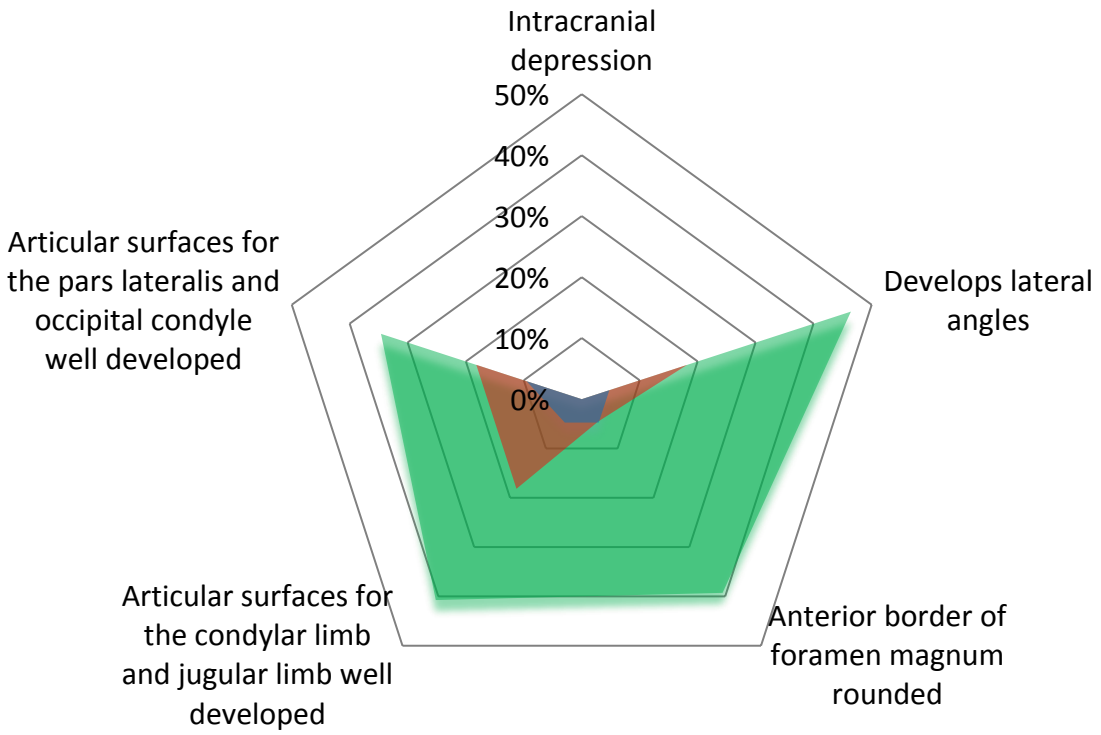

Figure 10: Percentage of present morphological and osteological feature development for the pars basilaris bone. Present features in the dental age categories: Early prenatal: <30 gestational weeks (blue), prenatal: 30-40 gestational weeks (red), postnatal: birth -7.5 months (green).

Figure 10 and 11 details the anatomical features recorded for the pars basilaris bone. In Figure 10, the percentage of the perinatal sample which displayed these features is detailed. In individuals younger than 30 gestational weeks (blue), only 5 % of the collection exhibited the lateral angles of the basilaris bone, the rounded border of the foramen magnum and the articular surfaces for the pars basilaris bone. At the prenatal dental

control (red), 10 % of the individual collection presented with surface development of the articular facets and only 5 % showed definite formation of the rounded border for the foramen magnum. Forty percent of the postnatal (green) individuals in the sample displayed the majority of features for the pars basilaris bone. The intracranial depression was not present across any of these dental age ranges, indicating a gradual development during gestation and infancy.

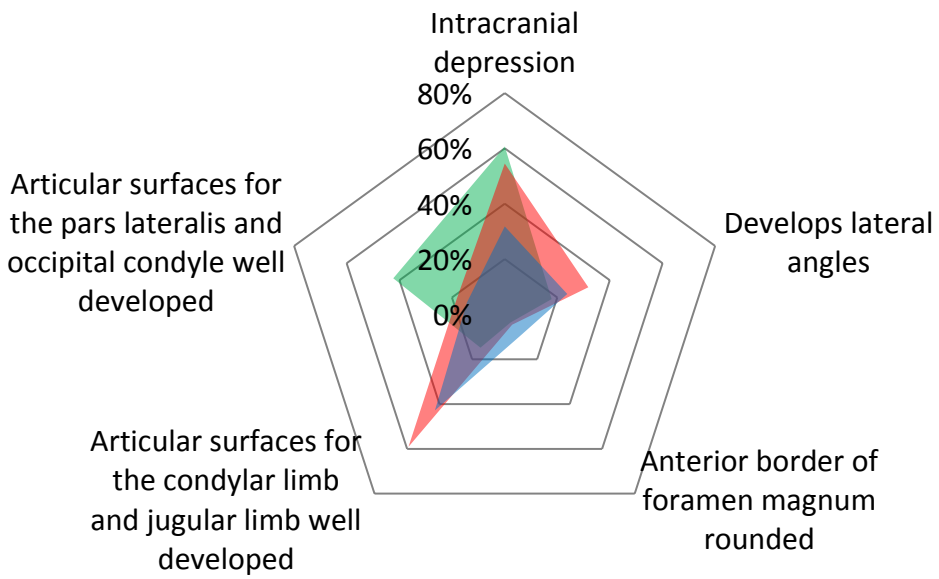

Figure 11: Percentage of immature morphological and osteological feature development for the pars basilaris. Immature features in the dental age categories: Early prenatal: <30 gestational weeks (blue), prenatal: 30-40 gestational weeks (red), postnatal: birth -7.5 months (green).

Immature features are outlined in Figure 11. The intracranial depression was categorised as developing in 30 % of early prenatal (blue), 45 % of prenatal (red) and 60 % of postnatal (green) individuals. In terms of lateral angle development, formation of this anatomy was evident in 20 % of early prenatal (blue) and 35 % of prenatal (red) individuals. The development of the rounded border of the foramen magnum was delayed in terms of ossification and morphology when compared to the lateral angles for the early prenatal

(blue) and prenatal (red) groups. However, the articular surface development of the jugular and condylar limb was more advanced than the lateral angles, as 40 % of early prenatal (blue) and 60 % of prenatal (red) individuals showed signs of development. The articular surfaces for the pars lateralis and occipital condyles were found to be under development in 40 % of the postnatal (green) group.

Figure 12 and 13 represents the anatomical features recorded for the pars lateralis bones. In Figure 12, the percentage of perinates which displayed these features is detailed. In individuals younger than 30 gestational weeks (blue), only 5-15 % exhibited the features assessed. The age related feature of the pars lateralis being longer than the basilaris was not found in any of the early prenatal individuals studied.

At the prenatal dental control (red), the fan appearance for the mastoid temporal part was present in 10 % of individuals; the posterior condylar canal was evident in 30 % of individuals, the articular surfaces for articulation with the pars basilaris was present under 20 % of individuals in the sample. However, when the postnatal individuals were studied, these features increased to 40 percent.

The presence of immature features described above for the pars lateralis bone is represented in the radar graph of Figure 13. The immature articular facet for the mastoid temporal was present in 20 % of early prenatal (blue), 30 % of prenatal (red) and 40 % of postnatal (green) groups, indicating an increase in development over time. The growth of the pars lateralis articular osteology in relation to the pars basilaris was underway in 10 % of early prenatal (blue), 20 % of prenatal (red) and 25 % of postnatal (green) groups. Evidence of the 'fan-like' appearance of the mastoid temporal border was not evident in the early prenatal (blue) group; but developing in 10 % of prenatal (red) and 30 % of postnatal (green) groups.

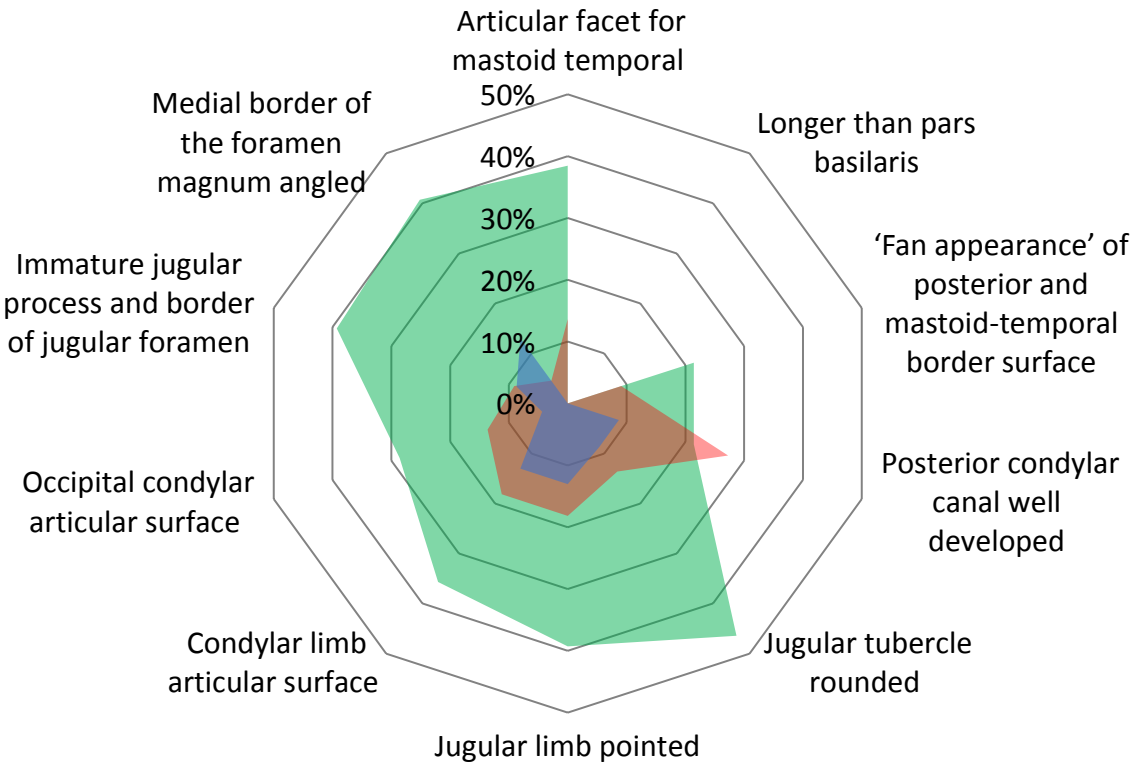

Figure 12: Percentage of present morphological and osteological features for the pars lateralis bone. Present features present in the dental age category. Early prenatal: <30 gestational weeks (blue), prenatal: 30-40 gestational weeks (red), postnatal: birth -7.5 months (green).

The rounding of the jugular tubercle was present in 40 % of early prenatal (blue) group and 30 % of prenatal (red) group. The pointed morphology of the jugular limb followed the same pattern as the jugular tubercle in terms of development.

An increase in articular facet development was represented by the red radar for the prenatal group (40-60 %), while 50 % of the postnatal group exhibited development of the occipital condylar articular surface and condylar limb surface (Figure 13). The pars lateralis osteology for articulation with the pars basilaris and mastoid temporal was mostly present and developing during the prenatal and postnatal stages of development.

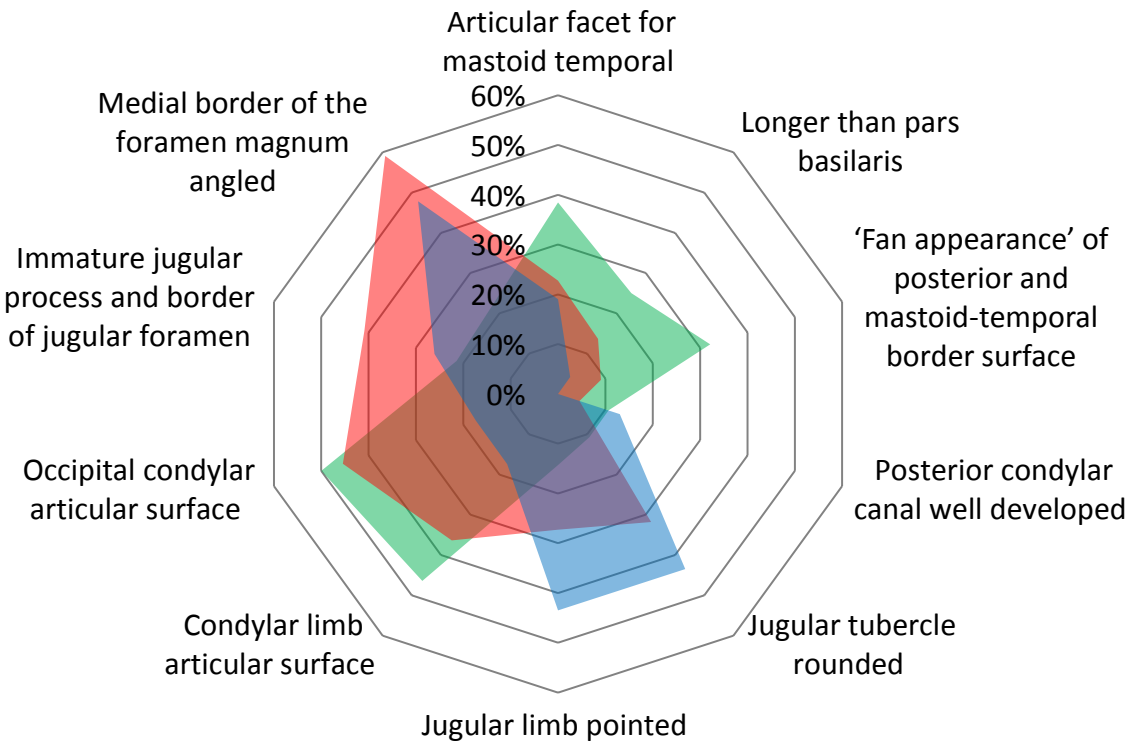

Figure 13: Percentage of immature morphological and osteological features for the pars lateralis bone. Immature features in the dental age categories. Early prenatal: <30 gestational weeks (blue), prenatal: 30-40 gestational weeks (red), postnatal: birth -7.5 months (green).

Figure 14 displays the percentage of individuals with present osteological features of the femur in the three dental age groups. The early prenatal (blue) group exhibited present features of the nutrient foramina (65 %) and linea aspera (60 %). The upper anterior surface of the shaft was rounded in 35 % of early prenatal (blue) individuals. The lower anterior surface of the shaft was flattened in 35 % of early prenatal (blue) individuals.

This percentage was repeated in the prenatal (red) age range for both the upper and lower anterior surfaces. However, more development was evident, as the lateral supracondylar line on the posterior surface as this feature was present in 35 % of prenatal individuals.

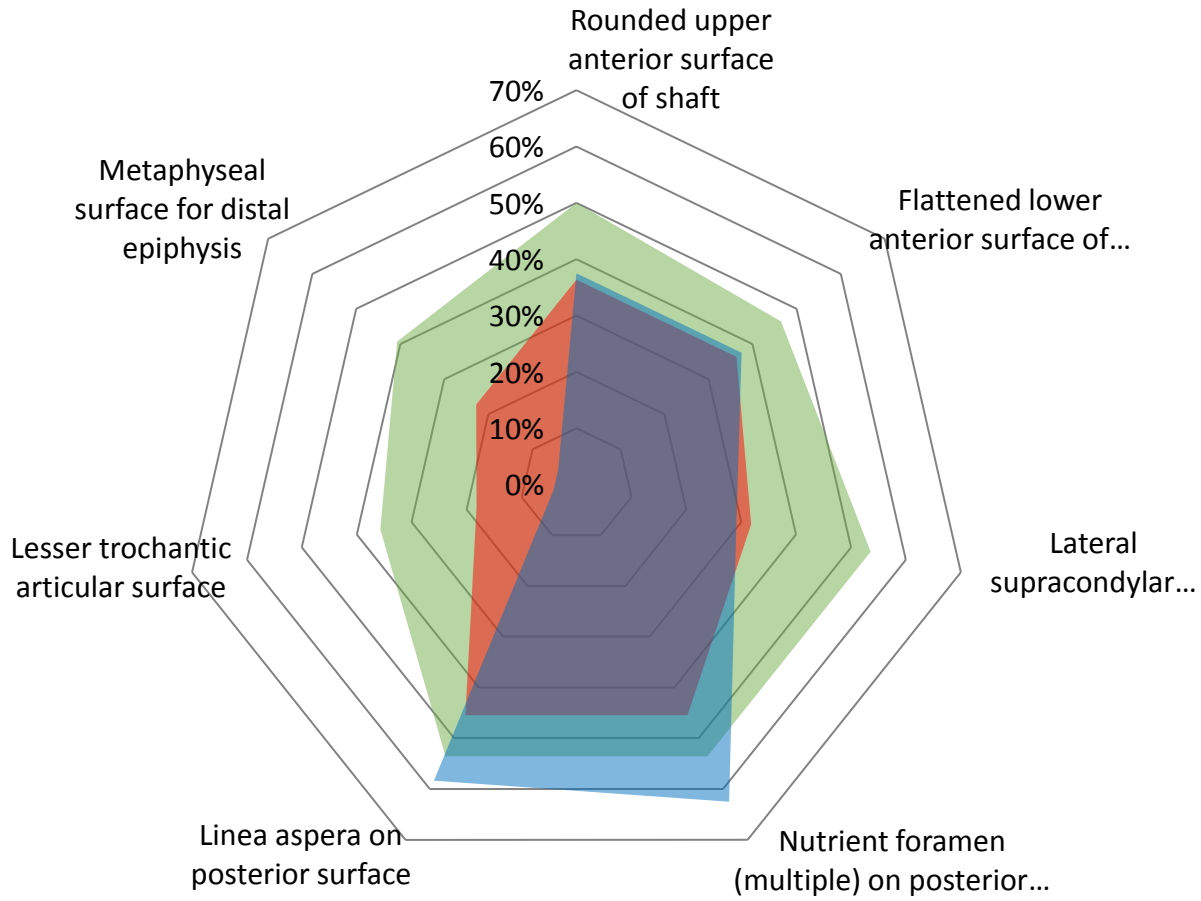

Figure 14: Percentage of present morphological and osteological features for the femur. Present features in the dental age categories: Early prenatal: <30 gestational weeks (blue), prenatal: 30-40 gestational weeks (red), postnatal: birth -7.5 months (green).

The upper and lower shaft morphology was present in 50 % of individuals categorized as postnatal. The lateral supracondylar line on the posterior surface was also present in 50 % of postnatal individuals. The articular facet for the lesser trochanteric surface and the metaphyseal surface of the distal epiphysis was present in 40 % of postnatal (green) individuals. Therefore, the anatomical features of the femur were more observable at the early prenatal (blue) stage of development when compared with that of the cranial bones (Figure 10-13).

In contrast to Figure 14, the developing osteological features of the femur (Figure 15) were in the lower percentile range (10-20 %). In the early prenatal group (blue) in the individual collection, 10 % presented with femoral features which were immature. These included the lateral supracondylar line and linea aspera on the posterior surface, metaphyseal surface of the distal epiphysis and the rounded upper surface and flattened lower surface of the anterior shaft.

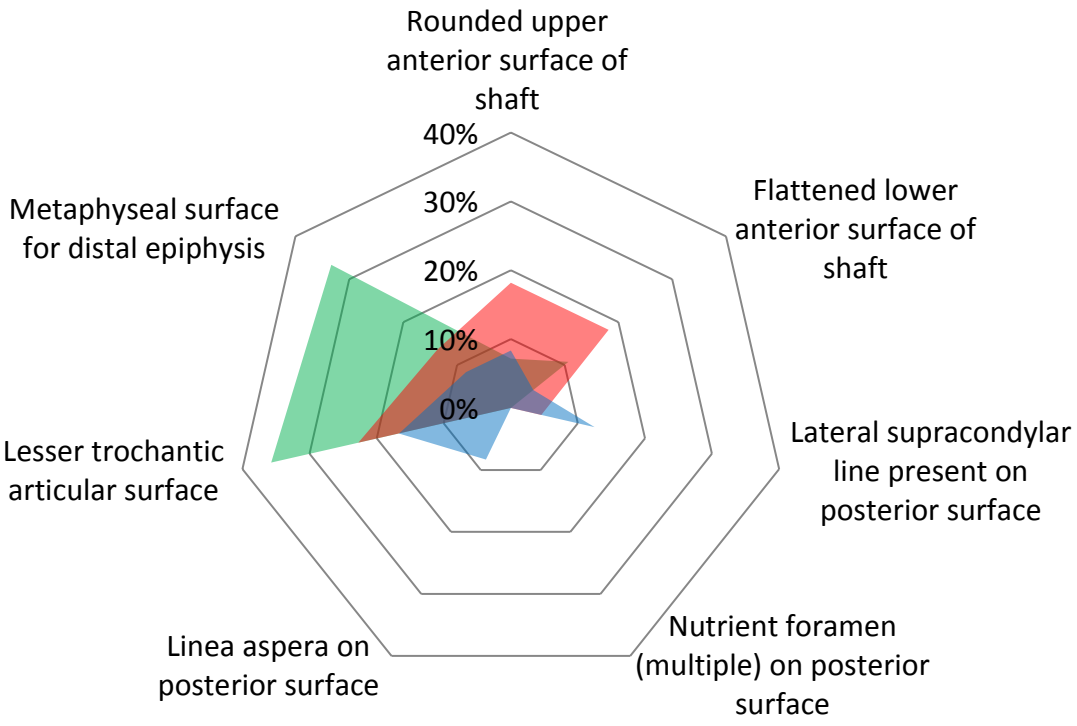

Figure 15: Percentage of immature morphological and osteological feature development for the femur. Immature features in the dental age categories. Dental age categories: Early prenatal: <30 gestational weeks (blue), prenatal: 30-40 gestational weeks (red), postnatal: birth -7.5 months (green.

For the prenatal age group (red), in 20 % of individuals, the rounded upper surface of the anterior shaft and the articular facet for the lesser trochanteric surface was immature.

The lateral supracondylar line on the posterior surface, nutrient foramina and metaphyseal surface for the distal epiphysis was immature in 10 % of prenatal (red) individuals.

The articular surface for the lesser trochanteric surface and the metaphyseal surface of the distal epiphysis were immature in 35 % of postnatal (green) individuals.

To examine the growth and development of the pars basilaris at the perinatal stage of development, measurement values were compared between the dental age categories (Figure 16). The values within these dental age categories were found to be statistically significant for the three landmarks examined within the dental age categories ($p \leq 0.000$) (Figure 16). The maximum width (MW) of the pars basilaris (1) in the prenatal age range was significantly larger when compared with the early prenatal age range ($p \leq 0.002$) and significantly larger in postnatal age range when compared with the prenatal age range ($p \leq 0.000$) and the early prenatal age range ($p \leq 0.000$).

The sagittal length (SL) (2) of the pars basilaris was significantly larger ($p \leq 0.010$) in the prenatal period when compared to the early prenatal period. In addition, the SL of the pars basilaris in postnatal individuals was significantly larger *(*$p \leq 0.000$) when compared to the prenatal and early prenatal individuals. This trend was even more significant when one studies the values for maximum length (ML) (3), as the measurement difference between the prenatal period and early prenatal ($p \leq 0.001$). As with MW and SL, the ML of the pars basilaris in postnatal individuals was significant larger *(*$p \leq 0.000$) when compared to prenatal and early prenatal individuals.

Principle component analysis (PCA) of osteometrics for the pars basilaris was represented by changes in the degree of variation between the age groupings, as observed by the level of separation for the dental age categories (Figure 17). Figure 17 indicated a proportional increase in size for the three landmarks. A small degree of overlap between dental aging groups indicates a high level of variation between age groups with respects to MW, SL and

ML. The high level of variation between dental age groups may be attributed to changes in the MW of the pars basilaris, which was in agreement with the MW results in Figure 16.

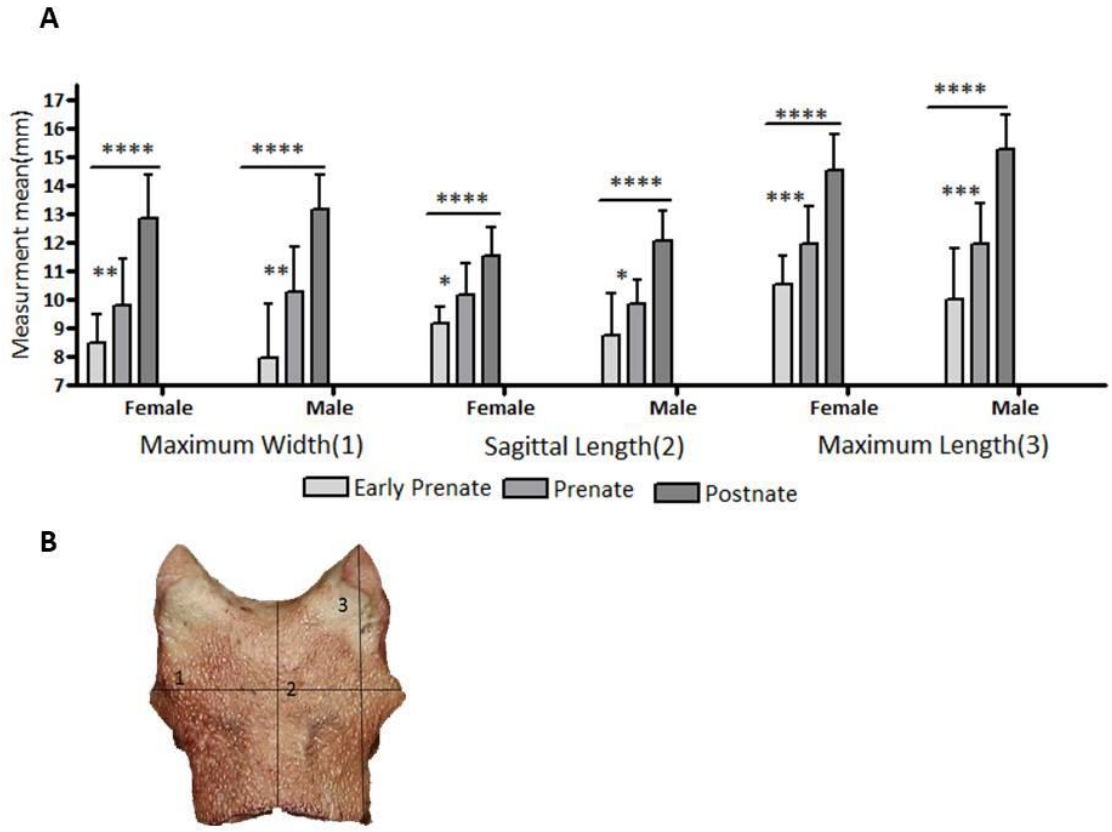

Figure 16: Anthropometric data for the pars basilaris bone. A.) Metric means and standard deviation between female and male individuals in the dental control groups: Female – 12, male – 8 (early prenatal), female – 10, male – 10 (prenatal), female – 19, male – 7(postnatal). Statistical significance measured by 2-way MANOVA (Scheffe post hoc test) for variation between age and sex. Significance: * 0.10, ** .002, ***.001, ****.000. B.) Measurement landmarks: 1= MW, 2= SL, 3= ML.

This was in agreement with the MW results in Figure 16. The pars basilaris MW was significantly larger in the prenatal age range ($p \leq 0.002$), when compared with the early prenatal age range and in the postnatal age range ($p \leq 0.000$) when compared with the prenatal age range. These findings are in agreement with the morphological feature analysis (Figure 10 and 11) and indicate changes in maturity and distinctive feature development over time.

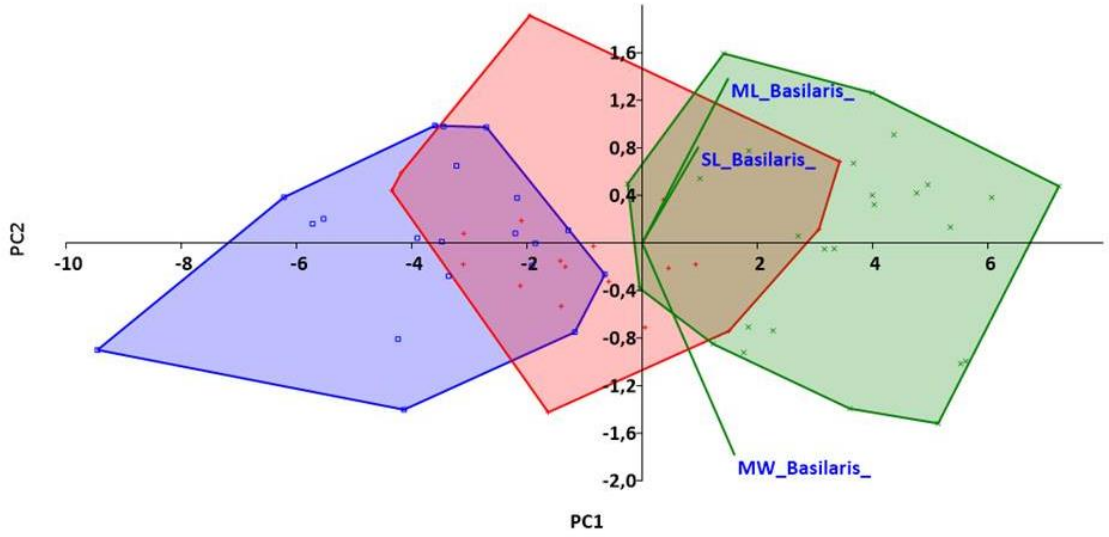

Figure 17: PCA for the pars basilaris bone anthropometrics. Early prenatal (blue), prenatal (red) and postnatal (green) age groupings. PC1: Represents changes in size and shape. PC2: Represents changes in shape only. ML (Maximum length), SL (Sagittal Length), MW (Maximum Width).

There were no statistically significant differences for the pars basilaris anthropometric measurements between male and female individuals (data not shown). Therefore the pars basilaris is not sexually dimorphic at this stage of development.

The left and right pars lateralis were found to be asymmetrical with respects to ML measurement values. The osteometric landmark means were assessed by t-test pairwise comparisons to estimate asymmetry of the sample. The ML measurement was found to be significantly different ($p \leq 0.02$) (data not shown). This suggested a degree of asymmetry.

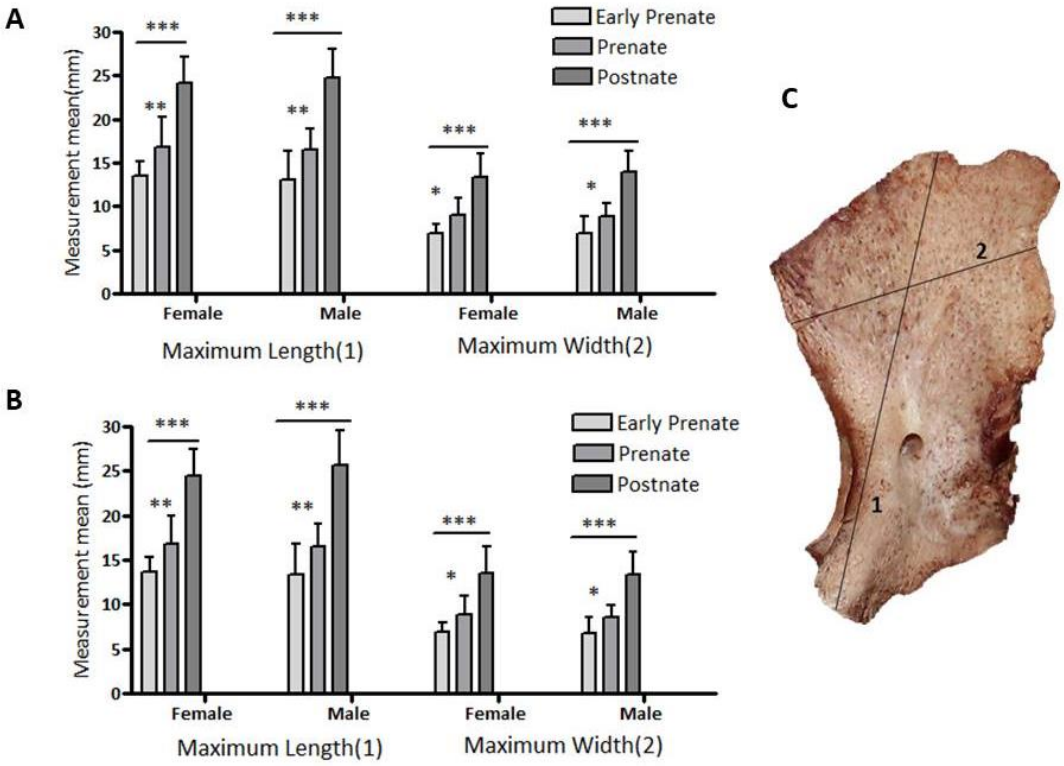

Figure 18: Anthropometric data for the pars lateralis bones. A.) Left pars basilaris metric means and standard deviation between female and male individuals in the dental control groups: female – 12, male – 8 (early prenatal), female – 10, male – 10 (prenatal), female – 19, male – 7(postnatal). Statistical significance measured by 2-way MANOVA (Scheffe post hoc test) for variation between age and sex. Significance: * 0.01, ** .003, ***.000. B.) Right pars basilaris metric means and standard deviation between female and male individuals in the dental control groups: Female – 12, male – 8 (early prenatal), female – 10, male – 10 (prenatal), female – 19, male – 7(postnatal). Statistical significance measured by 2-way MANOVA (Scheffe post hoc test) for variation between age and sex. Significance: * 0.31, ** .005, ***.000. C.) Measurement landmarks: 1= ML, 2= MW.

When comparing the left and right pars lateralis (Figure 18A & B), no difference between left and right components were apparent. However, the level of significance varied between left and right for the MW (2) measurement. In the left pars lateralis, the MW was significantly larger ($p \leq 0.01$) in the prenatal age group compared with the early prenatal age group. The right pars lateralis MW differences between the same age range was less significant ($p \leq 0.31$) (Figure 18A & B). A similar trend was found for the ML (1) between the dental ages of early prenatal to prenatal (left pars lateralis ($p \leq 0.003$) and right pars lateralis ($p \leq 0.005$) (Figure 18A & B). Statistically significant differences were found in the pars

lateralis for the ML (1) means ($p \leq 0.000$) and MW means ($p \leq 0.000$) between the age categories of prenatal to postnatal and early prenatal and postnatal respectively (Figure 18A & B).

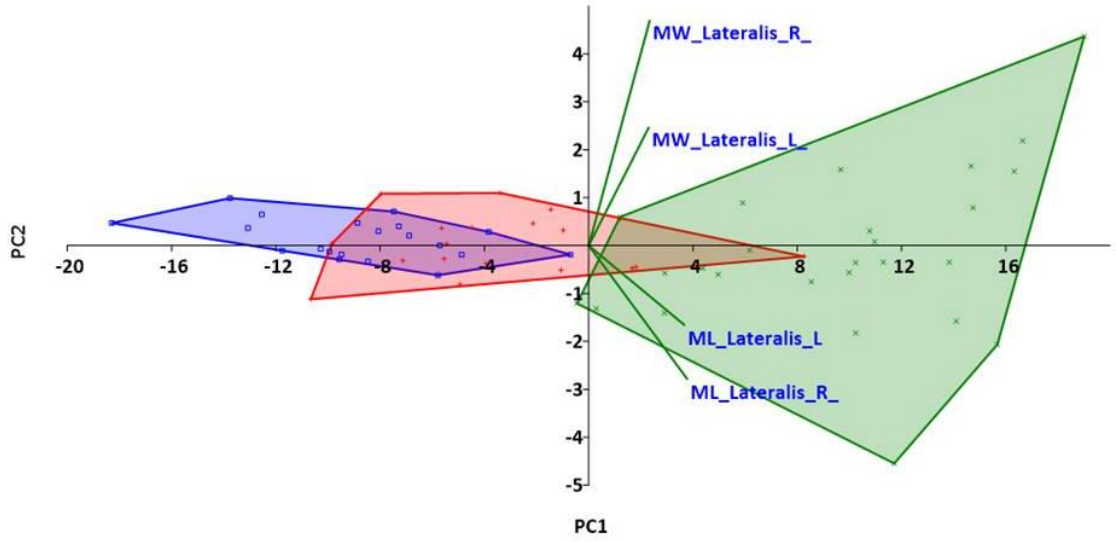

Figure 19: PCA for the pars lateralis anthropometrics. Early prenatal (blue), prenatal (red) and postnatal (green). PC1: Represents changes in size and shape. PC2: Represents changes in shape only. ML = Maximum length, MW= Maximum Width.

The left and right pars lateralis were grouped together for the PCA analysis (Figure 19). Changes in terms of size and shape correlated with that of the osteometric data in Figure 18. The same age related pattern and proportional growth was represented by the depiction of variation. There was adequate separation and minimum overlap between age categories. This supported the data on anthropometric differences of size. The high level of variation between dental age groups may be attributed to changes in the MW of the pars lateralis. This was in agreement with the MW significance ($p \leq 0.000$) in Figure 18.

There were no statistically significant differences for the pars lateralis anthropometric measurements between male and female individuals (data not shown). Therefore, the pars lateralis was not sexually dimorphic at this stage of development.

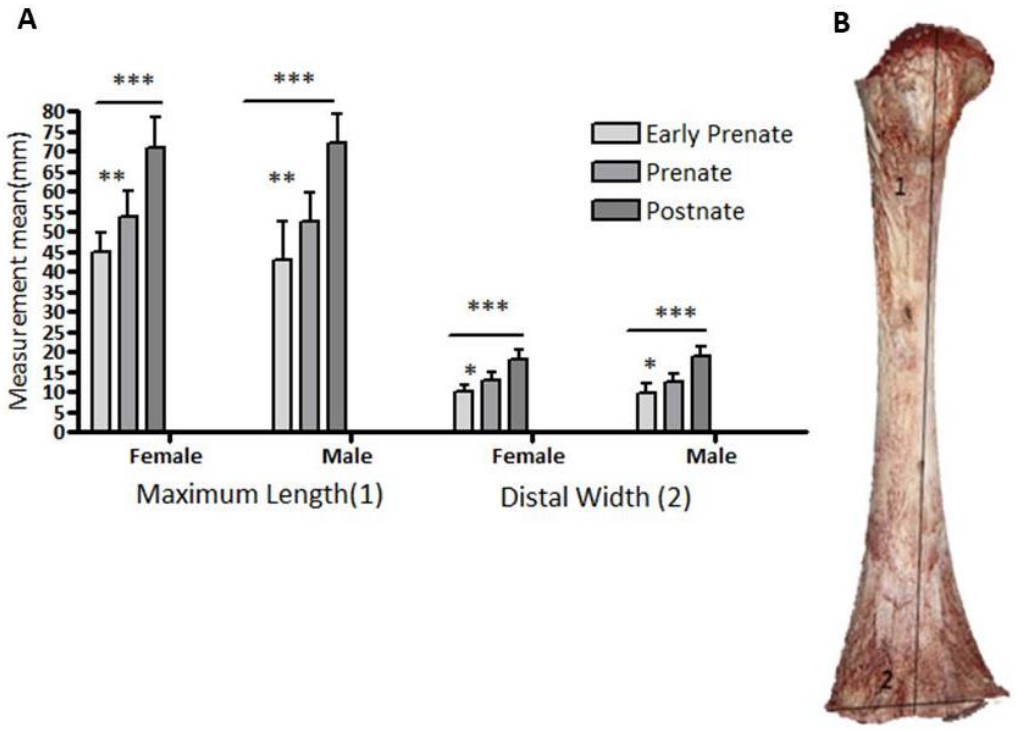

Figure 20: Anthropometric data for the femur. A.) Left pars basilaris metric means and standard deviation between female and male individuals in the dental control groups. Female – 12, male – 8 (early prenatal), Female – 10, male – 10 (prenatal), female – 19, male – 7(postnatal). Statistical significance measured by 2-way MANOVA (Scheffe post hoc test) for variation between age and sex. Significance: * .002, ** .001, ***.000. B.) Measurement landmarks: 1= ML, 2= DW.

The femur osteometric means for the ML (1) and distal width (DW) (2) were found to be statistically significant within each dental age category ($p \leq 0.000$)(Figure 20). Between the periods of early prenatal to prenatal, the ML (1) of the femur was significantly larger ($p \leq 0.001$). This significant difference for the ML (1) was larger during prenatal and postnatal dental age ranges ($p \leq 0.000$). A similar pattern was evident for the DW (2) of the femur ($p \leq 0.002$). When compared to the ML (1), the DW (2) did not increase at the same rate during the gestation. A significant difference ($p \leq 0.000$) was observed for both the ML (1) and DW (2) between the prenatal and postnatal age ranges (30 gestational weeks to 7.5 months) and early prenatal and postnatal stage (<30 gestational weeks to 7.5 months).

The PCA of the femur is represented in Figure 21. The DW was driving the degree of variation for the femur. The maturity of the femur and several age related changes were present before 30 gestational weeks.

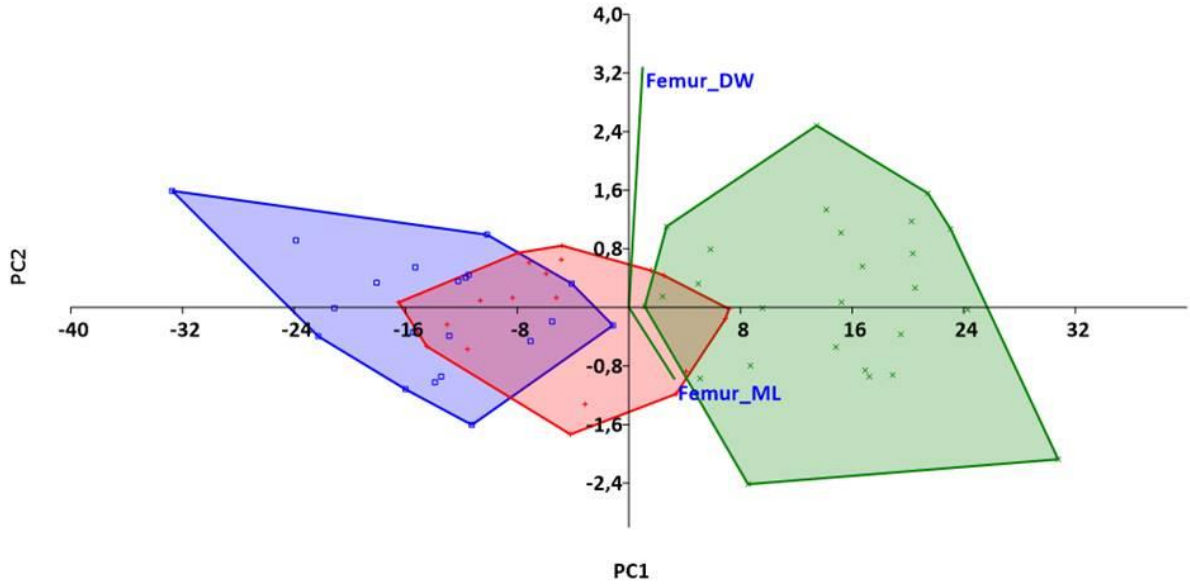

Figure 21: PCA for the femur anthropometrics. Early prenatal (blue), prenatal (red) and postnatal (green). PC1: Represents changes in size and shape. PC2: Represents changes in shape only. Represents changes in shape only. ML = Maximum Length, DW= Distal Width.

There were no statistically significant differences for the femur anthropometric measurements between male and female individuals (data not shown). Therefore the femur was not sexually dimorphic at this stage of development.

3.2.3 Bone mineral density analysis

The mean values of the pars basilaris density points were relatively similar and variability of standard deviation within each density point was uniform (Figure 22). Density mean values were larger in the postnatal age range when compared with the prenatal and early prenatal age ranges respectively at the 7 density points for male individuals.

When compared with the female individuals, the density means were lower during the transition from prenatal to postnatal for the pars basilaris bone. However, no statistically significant differences were found between density points, age ranges and sex.

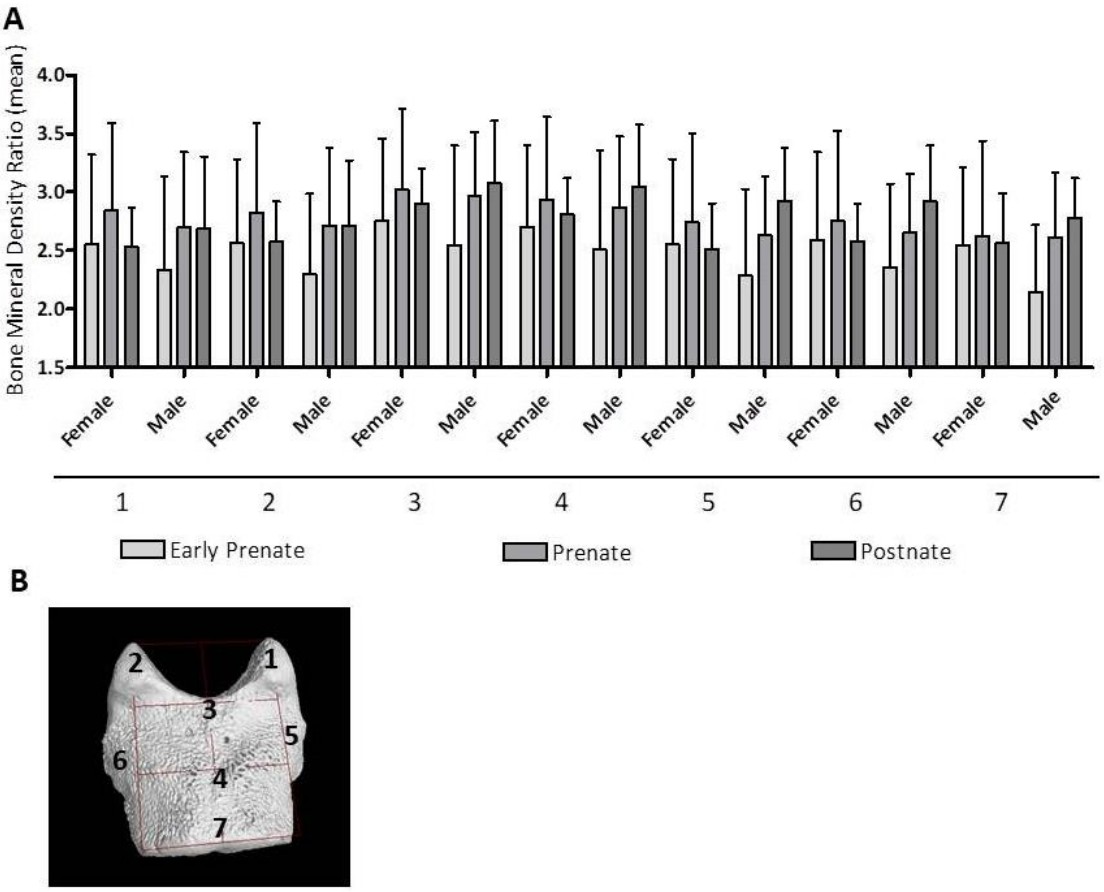

Figure 22: Bone mineral density for the pars basilaris. A.) pars basilaris bone mineral density means and standard deviation within dental control groups. 1: Right condyle, 2: Left condyle, 3: Border for the foramen magnum, 4: Primary ossification site, 5: Right lateral angle, 6: Left lateral angle, 7: Metaphyseal surface of the spheno-occipital synchondrosis. B.) Bone mineral density landmarks for the pars basilaris bone. 1: Right condyle, 2: Left condyle, 3: Anterior border, 4: Primary ossification site, 5: Right lateral angle, 6: Left lateral angle, 7: Metaphyseal surface for the spheno-occipital synchondrosis.

The PCA for the pars basilaris bone density (Figure 23) displays a high level of overlap between the age categories. There was some degree of separation within the prenatal age group. This minor level of variation was being driven by density point 5, 6 and 7.

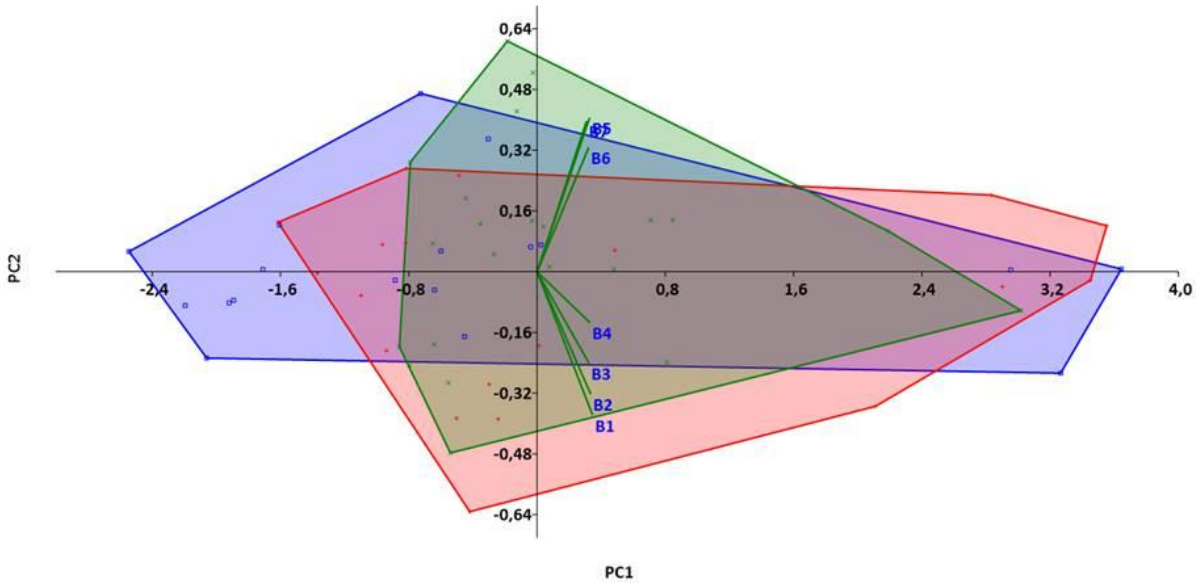

Figure 23: PCA for the pars basilaris bone mineral density. Bone mineral density landmarks for the pars basilaris bone: B1: Right condyle, B2: Left condyle, B3: Anterior border, B4: Primary ossification site, B5: Right lateral angle, B6: Left lateral angle, B7: Metaphyseal surface for the spheno-occipital synchondrosis. PC1: Represents changes in size and shape. PC2: Represents changes in shape only. Early prenatal (blue), prenatal (red) and postnatal (green).

The pairwise correlations for pars lateralis asymmetry resulted in significant differences for the metaphyseal surface of the condylar limb ($p \leq 0.006$), foramen magnum border ($p \leq 0.001$) and the centre of the wing portion for the mastoid temporal ($p \leq 0.003$). The left and right pars lateralis indicated no statistically significant difference in terms of the left and right components (Figure 24A & B).

The pars lateralis density point mean was larger in postnatal when compared with prenatal and early prenatal for male individuals. Density means were smaller between prenatal and postnatal for female individuals. No statistically significant differences were found for the left and right components of the occipital complex when bone mineral density points were compared between age groupings and sex (Figure 24A & B).

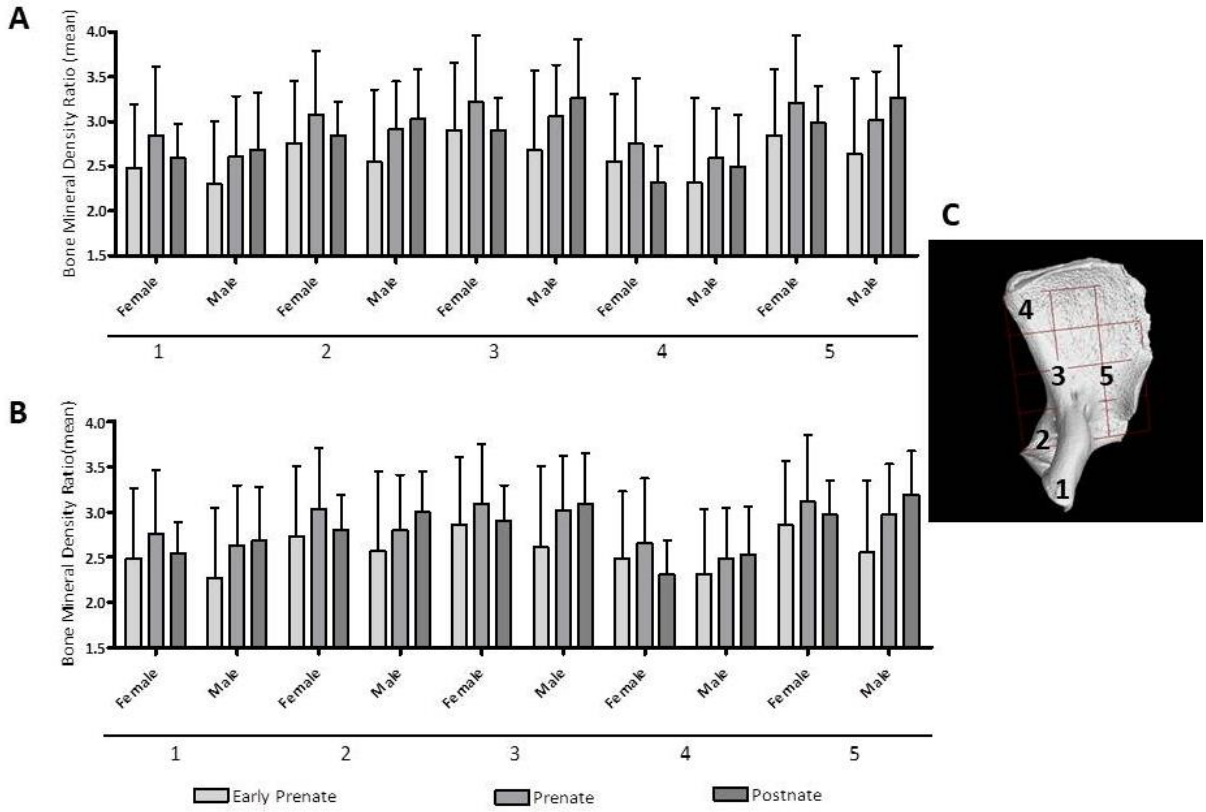

Figure 24: Bone mineral density for the pars lateralis bones. A.) Left pars lateralis bone mineral density means and standard deviation within dental control groups: 1.Tip of jugular condyle, 2: Metaphyseal surface of condylar limb, 3: Inferior border for the foramen magnum, 4: Medial border for the inter-squamous part, 5: Midline of wing aspect. B.)Right pars lateralis bone mineral density means and standard deviation within dental control groups: Tip of jugular condyle, 2: Metaphyseal surface of condylar limb, 3: Inferior border for the foramen magnum, 4: Medial border for the inter-squamous part, 5: Midline of wing aspect. C.) Bone mineral density landmarks for the Right pars lateralis bone. 1: Tip of Jugular condyle, 2: Metaphyseal surface of condylar limb, 3: Inferior border for the foramen magnum, 4: Medial border for the inter-squamous part, 5: Midline of wing aspect.

When considering the PCA for these bones, the left pars lateralis (Figure 25) showed a variation between early prenatal and late prenatal age ranges which was being driven by the medial border for the foramen magnum (LL4 & LR4). The variation between the late prenatal and early postnatal age ranges was being influenced by the tip of the jugular foramen (LL1 & LR1), the border for the foramen magnum (LL3 and LR3), the metaphyseal surface of the condylar limb (LL2 & LR2) and the centre of the wing portion for the mastoid temporal (LL5 and LR5).

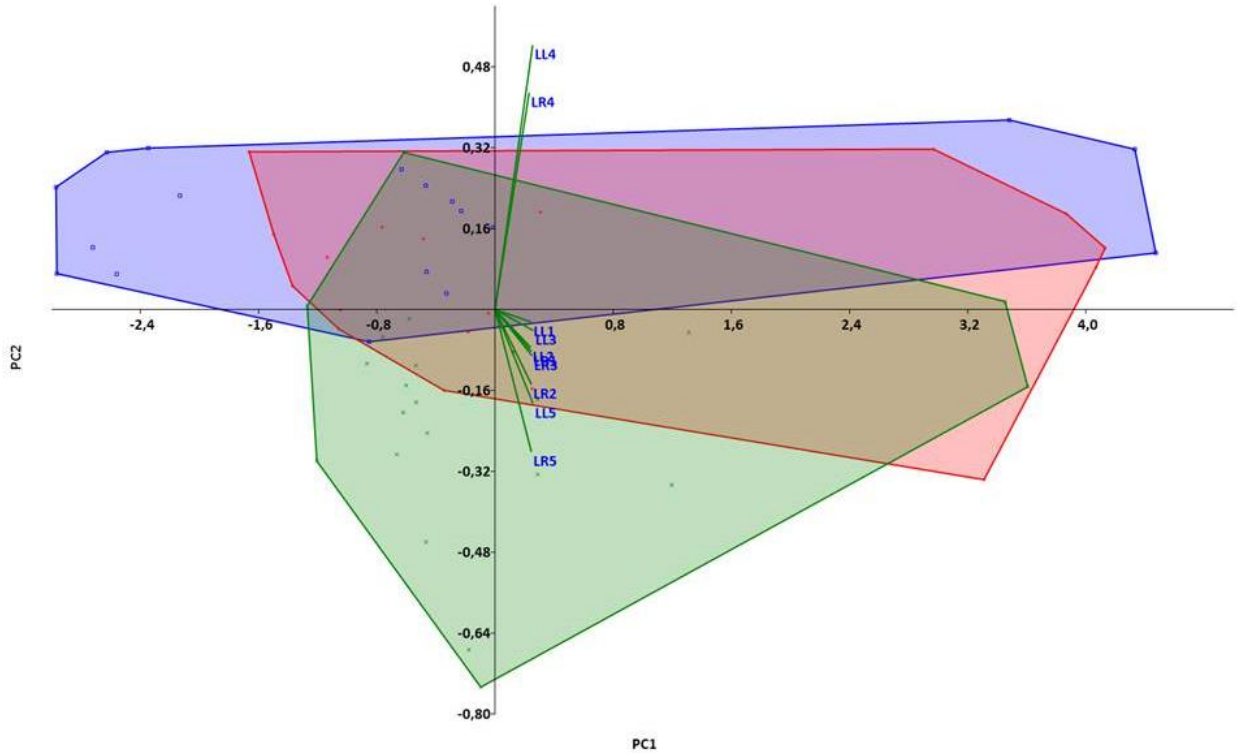

Figure 25: PCA for the pars lateralis bone mineral density. Bone mineral density landmarks for the pars lateralis bone: LL1: Tip of the jugular limb LL2: Metaphyseal surface of the condylar limb, LL3: Inferior border for the foramen magnum, LR4: Medial border of the inter-squamous part, LR5: Midline section of wing aspect. Right pars lateralis: LR1: Tip of the jugular limb LR2: Metaphyseal surface of the condylar limb, LR3: Inferior border for the foramen magnum, LR4: Medial border of the inter-squamous part, LR5: Midline section of wing aspect. PC1: Represents changes in size and shape. PC2: Represents changes in shape only. Early prenatal (blue), prenatal (red) and postnatal (green).

The pars lateralis PCA (Figure 25) displayed a greater separation between the age groups than the pars basilaris PCA (Figure 23) and femur PCA (Figure 27).

The mean density points at the midshaft of the femur – 4.1 (medial midshaft), 4.2 (midshaft centre) and 4.3 (lateral midshaft) were averaged for 2-way MANOVA analysis. As seen with the cranial bones, there was an increase in the density point mean during development for male individuals. Density means decreased between prenatal and postnatal periods for female individuals. The comparison of bone mineral density means for the femur between the different age ranges and sex resulted in no significant differences (Figure 26).

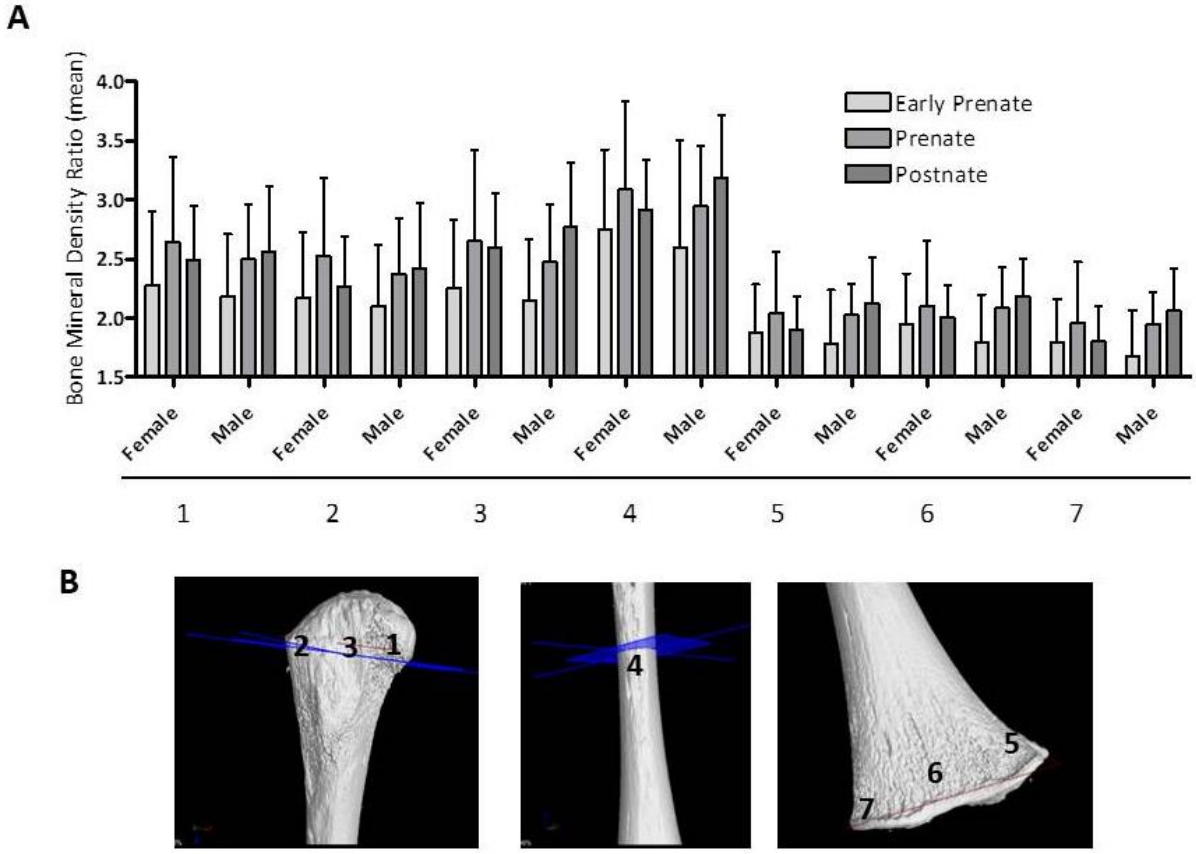

Figure 26: Bone mineral density for the femur. A.) Femur bone mineral density means and standard deviation within dental control groups. 1: Proximal medial border, 2: Proximal lateral border, 3: Metaphyseal surface for the lesser trochanteric facet, 4.1: Medial midshaft, 4.2: Midshaft centre 4.3: Midshaft lateral, 5: Distal medial border, 6: Distal centre, 7: Distal lateral border B.) Femur density points: F1: Proximal medial border, F2: Proximal Lateral border, F3: Metaphyseal surface of the lesser trochanteric facet, 4.1: Medial midshaft, 4.2: Midshaft centre, 4.3: Lateral centre, F5: Distal medial, F6: Distal centre, F7: Distal Lateral.

There was a high level of overlap between the age categories (Figure 27). The proximal and distal ends (Figure 27) were grouped together for the PCA for the femur bone density indicating some variation between the late prenatal and early postnatal age ranges.

The change in density was driven during the early prenatal and prenatal stages of development by the midshaft density points (4.1, 4.2, and 4.3).

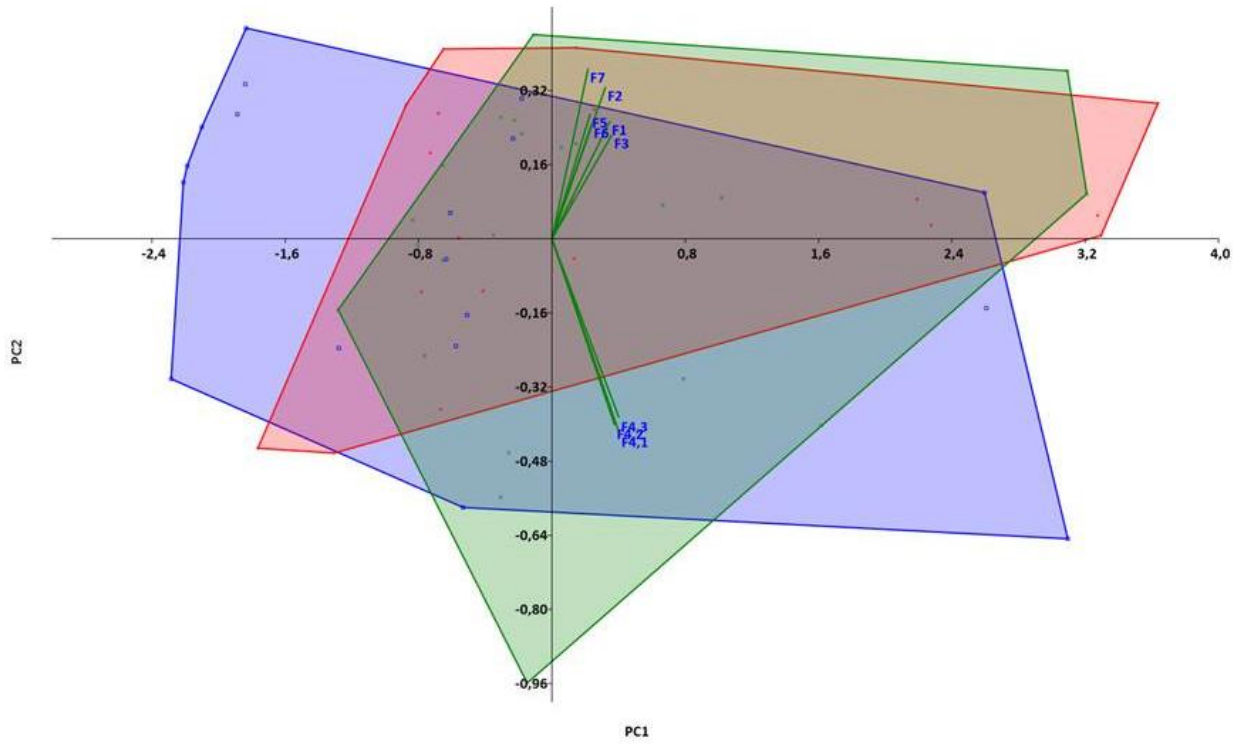

Figure 27: PCA for the femur bone mineral density. Bone mineral density landmarks for the femur bone: F1: Proximal medial border, F2: Proximal lateral border, F3: Metaphyseal surface of the lesser trochanteric facet, 4.1: Medial midshaft, 4.2: Midshaft centre, 4.3: Lateral centre, F5: Distal medial, F6: Distal centre, F7: Distal Lateral. PC1: Represents changes in size and shape. PC2: Represents changes in shape only. Early prenatal (blue), prenatal (red) and postnatal (green).

3.3 Molecular approaches to perinatal growth and age assessment

3.3.1 Postmortem RNA for gene expression analysis

Prior to examining gene expression levels from the human fetal samples, experiments were set up to ascertain if intact postmortem RNA could be isolated from bone. To test this, a preliminary investigation was done using fresh and frozen tissue samples from commercially bought chicken (*Gallus Gallus*). As fetal and perinatal bones are often mistaken for faunal (small mammals, birds or primates) (Baker *et al.,* 2005), the chicken model was selected as a proxy for the human perinate. Bone samples produced a higher concentration (ng/µl) of RNA and better purity from protein and organic compound

contamination (A260/280 ratios) than muscle derived RNA (data not shown). Following this, the effect of decomposition on RNA levels was evaluated.

Assessment of RNA stability and purity during Gallus gallus decomposition

Biological replicates of chicken (*Gallus Gallus)* were placed in a caged area on elevated trays exposed to climatic change and oviposition by the local insect activity. Cadavers were set up in this manner to imitate the circumstance (dumped on street corners and dustbins) that many human fetal and perinatal remains were found in as per the police documentation accompanying the body to the mortuary. Table 6 below details the weather conditions and insect activity recorded during the various stages of decomposition for the chicken replicates.

Table 6: Insect activity and weather conditions during chicken decomposition

Taphonomic conditions	**1. Fresh**	**2. Bloat**	**3. Active decay**	**4. Advanced decay**	**5. Dry remains**
Insect activity	Blowflies present	Blowfly eggs hatched	Maggot Masses	Beetles present	Pupae present
Minimum air temperature °C (mean)	11.5	11.3	12	13	15
Maximum air temperature °C (mean)	21.2	22.2	21.6	24.5	23.3
Humidity % (mean)	58.8	66.6	49.1	61.5	54

RNA was isolated from bone samples of the three biological replicate chickens at different stages of decomposition. Samples stored at both -80 °C and in RNA*later* (RT) were included to assess the potential difference between these preservation methods. Figure 28A represents the purity absorbance ratios at the different stages of decomposition. Pure RNA should give an A260:A280 ratio of 2. The average A260:A280 ratio for the RNA samples was below 2 for all stages of decomposition suggesting the presence of protein contaminants. The A260/A230 ratio gives an indication of contamination with phenolic compounds. This value should be higher than the A260/A280 ratio for high quality RNA. In all cases, the A260/230 ratio was lower than the A260/A230 ratio suggesting the presence of phenolic contaminants.

The effect of decomposition was found to be statistically significant as the ratio value for the A260/280 and A260/230 decreased as decomposition advanced for post mortem RNA ($p \leq 0.001$). After it was estimated that RNA could be successfully isolated from bone, the quality of RNA was tested by RT-PCR. Primers were designed and optimized to amplify a region of the chicken beta actin cDNA (data not shown). The PCR amplification of a region of the beta actin mRNA is represented by Figure 28B. Controls lacking reverse transcriptase in the cDNA reaction were included to test for genomic DNA contamination. For the three replicates, RNA isolated from stage 1 was the most stable and intact, resulting in successful amplification in the PCR. Bands were present at stage 1 for the three replicates (Figure 28B). However, bands were also present for the negative control reactions, which could indicate contamination with genomic DNA. The other stages of decomposition did not result in consistent amplification in the PCR. Individual one was selected for RT-qPCR assays to estimate if the RNA was of sufficient quality for this analysis.

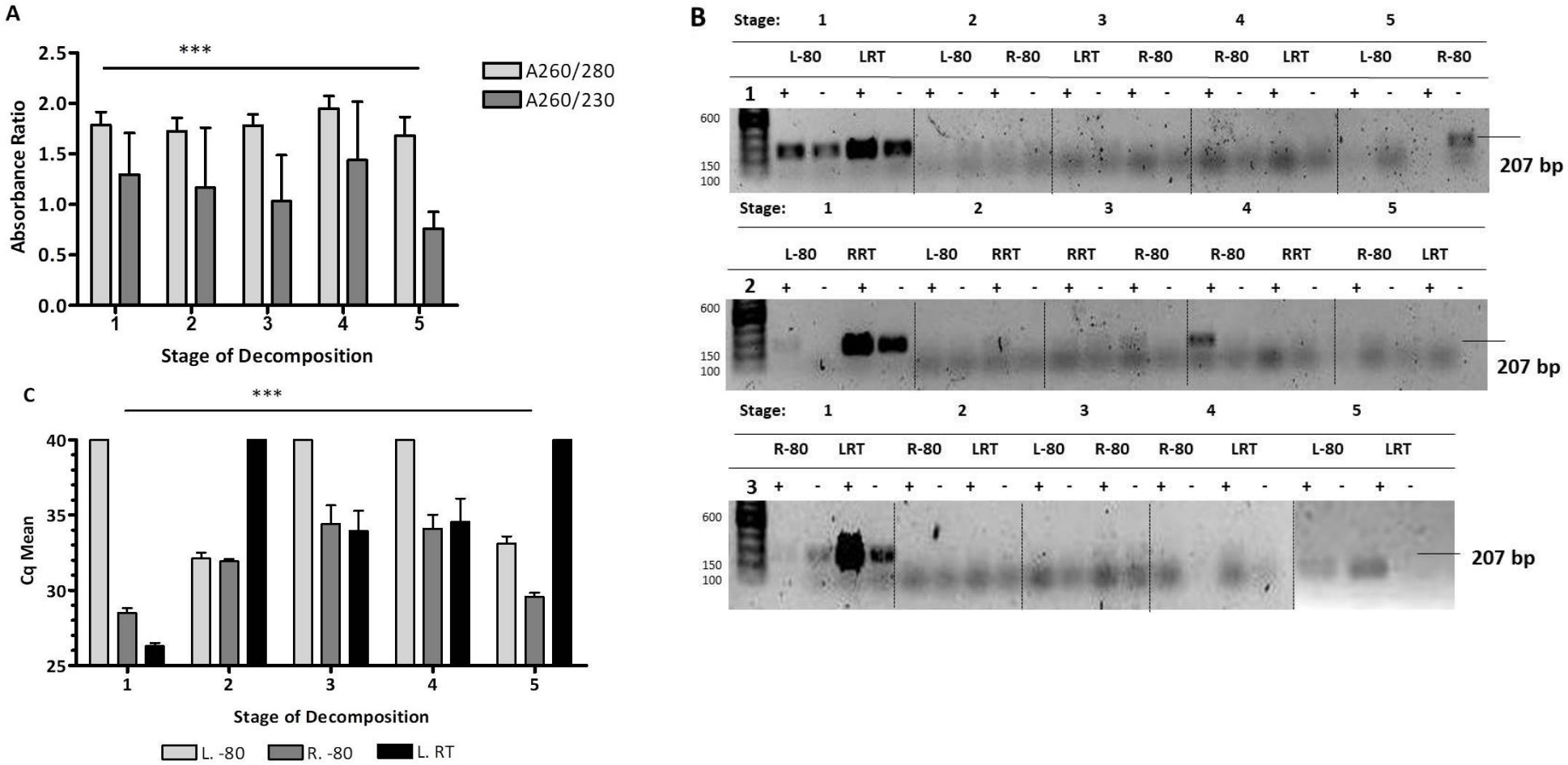

Figure 28: Assessment of changes in RNA stability and purity during chicken decomposition. A.) Mean ratio of absorbance (260/280 nm or 260/230 nm) indicating RNA purity in left and right sternal rib RNA samples from different stages of decomposition. B.) Ethidium bromide stained 0.8 % agarose gel of PCR amplification of chicken beta actin cDNA for 3 individuals at various stages of decomposition. Samples were stored in either RNA*later* (RT) or at -80 °C prior to isolation. L: Left rib sample. R: Right rib sample C.) Average Cq values from RT-qPCR analysis from the various stages of decomposition. Stages of decomposition 1-5= 1: Fresh, 2: Bloat, 3: Active decay, 4: Advanced decay, 5: Dry remains. Statistical significance was assessed using a 2-way ANOVA of absorbance ratio and stage of decomposition (A) and Cq mean and stage of decomposition (C) analysis by Graphpad Prism 4 software. *** P-value 0.001.

The average cycle threshold (Cq) quantitative PCR values obtained from the qRT-PCR are shown in Figure 28C. A lower Cq corresponds to a higher concentration of target sequence and *vice versa.* There was a significant difference between the samples stored at -80° C or in RNA*later* (RT) samples and the stages of decomposition ($p \leq 0.001$). The lowest Cq value (corresponding to the highest RNA concentration) was obtained for the stage 1 decomposition sample. Thereafter, there was no correlation between the Cq values and the stage of decomposition, although in most cases the Cq values were between 30-40, indicating very low levels of target RNA. The results of the chicken decomposition study suggested that RNA levels and quality were highly variable during decomposition and prone to contamination with genomic DNA. There were no trends identified other than the fact that PCR ready RNA (albeit with possible DNA contamination) was only obtained at early stages. There was no difference in storage at -80° C or RNA*later*.

Assessment of RNA stability and purity during Cercopithecus pygerythrus decomposition

The decomposition study was repeated using a primate species (*Cercopithecus pygerythrus*) to test for any possible differences between birds and mammals. The *Cercopithecus pygerythrus* samples were obtained as remains from the Department of Zoology (Rhodes University). Table 7 below details the weather conditions and insect activity present during the decomposition process of the monkey replicates.

The RNA from the monkey replicates was assessed by absorbance and is represented in Figure 29A. As with the chicken study, the A260/230 absorbance ratio was lower than the A260/280 ratio, indicating contamination of the RNA preparations with phenolic compounds. The significance of the decomposition effect on the purity of RNA is evident by the $p \leq 0.001$ (Figure 29A). The ability to use this mRNA in RT-PCR was estimated using primers against a region of the *Cercopithecus pygerythrus* CD4 gene. Figure 29B illustrates

the PCR amplification of a region of the CD4 gene for the samples taken from various stages of decomposition and stored in either RNA*later* (RT) samples or at -80° C.

Table 7: Insect activity and weather conditions during Monkey decomposition

Taphonomic conditions	**1. Fresh**	**2. Bloat**	**3. Active decay**	**4. Advanced decay**	**5. Dry remains**
Insect activity	Blowflies present	Blowfly eggs hatched	Maggot masses	Beetles present	Pupae present
Minimum air temperature °C (mean)	14.7	12.5	10	11.5	13.7
Maximum air temperature °C (mean)	27.2	19	18.6	21.5	22.2
Humidity % (mean)	46.5	79.5	67	56.8	61.2

A region from the CD4 mRNA isolated from the left and right rib samples was PCR amplified and visualized by agarose gel electrophoresis. Samples stored at both -80° C and in RNA*later* (RT) were included to assess the potential difference between these preservation methods. As with the chicken individuals (Figure 28B), stage 1 decomposition showed successful amplification of the CD4 region as indicated by the presence of bands at the predicted size of 128 bp on the agarose gel (Figure 29B). There was however, also the presence of genomic DNA contamination in the negative controls. However, there was amplification of the CD4 mRNA at the different stages of decomposition (particularly in individuals 1 and 2) (Figure 29B), when compared with the results of the chicken study (Figure 29B).

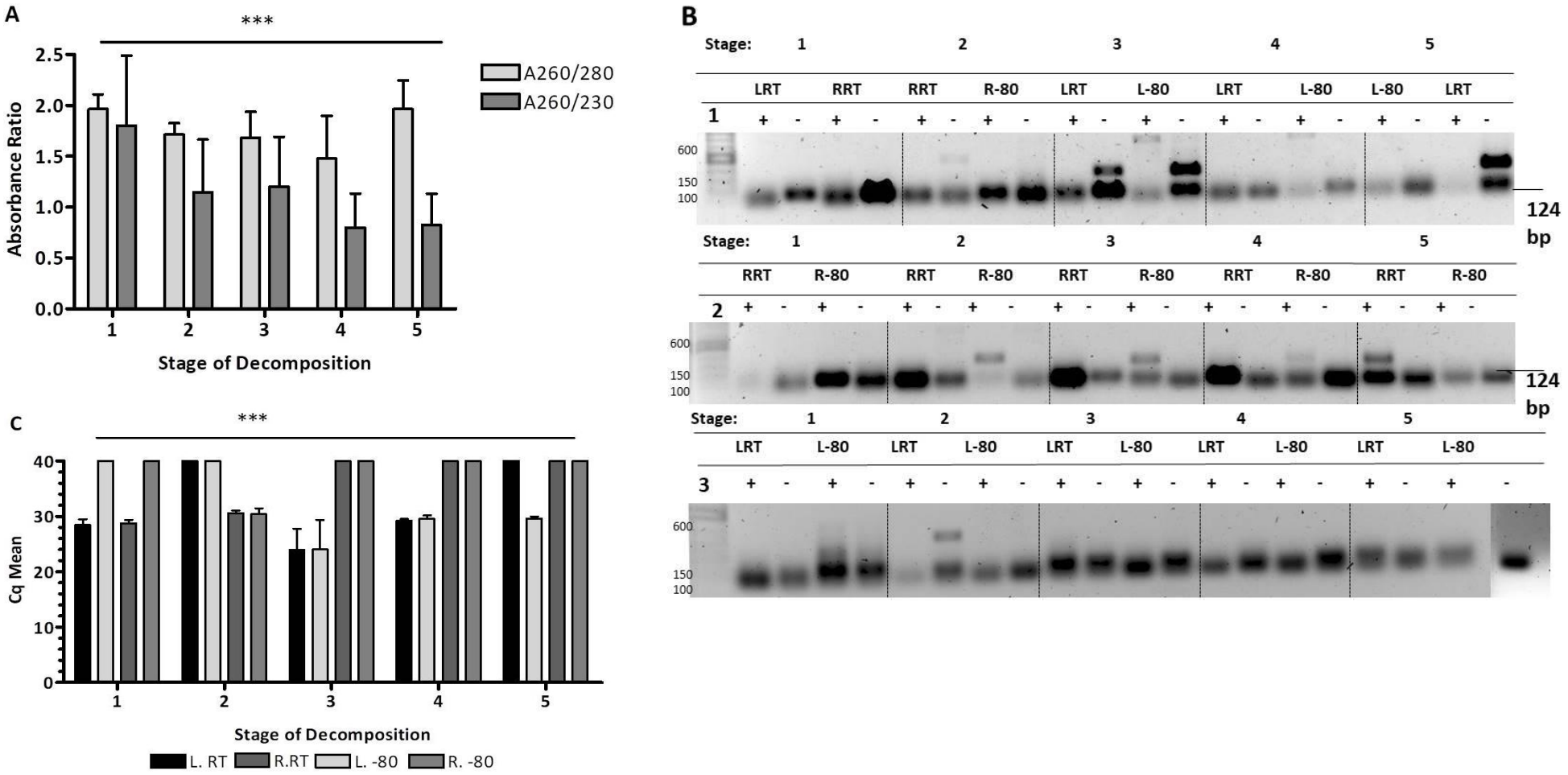

Figure 29: Assessment of changes in RNA stability and purity during monkey decomposition study. A.) Mean ratio of absorbance (260/280 nm or 260/230 nm) indicating RNA purity in left and right sternal rib RNA samples from different stages of decomposition. B.)Ethidium bromide stained 0.8 % agarose gel of PCR amplification of monkey CD4 mRNA for 3 individuals at various stages of decomposition. Samples were stored in either RNAlater (RT) or at -80 °C prior to isolation. L: Left rib sample. R: Right rib sample C.) Average Cq values from RT-qPCR analysis from the various stages of decomposition. Stages of decomposition 1-5= 1: Fresh, 2: Bloat, 3: Active decay, 4: Advanced decay, 5: Dry remains. Statistical significance was assessed using a 2-way ANOVA of absorbance ratio and stage of decomposition (A) and Cq mean and stage of decomposition (C) analysis by Graphpad Prism 4 software. *** P-value 0.001.

Individual 1 was selected for the RT-qPCR assay (Figure 29C) to assess whether the mRNA was of a quality that would permit quantitative PCR analysis. Consistent with the chicken study, lower Cq values, indicating higher CD4 transcript abundance, were detected in RNA samples isolated from stage 1 of decomposition. The negative effect of the decomposition process and the integrity of samples derived from different storage methods were found to be statistically significant ($p \leq 0.001$) across the different stages of decomposition (Figure 29C). These data suggested that mRNA levels and quality were highly variable in post mortem tissues.

The results from the chicken *(Gallus gallus*) study (Figure 28) were mirrored in the assessment of RNA derived from bone in the monkey (*Cercopithecus pygerythrus)* study (Figure 29).

After examining the stability of postmortem RNA and the effect of decomposition on RNA degradation from animal models, assays using six of the individuals from the sample were tested. The bone samples were dissected from these individuals at an advanced stage of decomposition.

Assessment of RNA stability and purity of perinatal postmortem RNA

In order to conduct RT-qPCR for our gene expression studies in the human samples, we required plasmids containing the target sequences for generation of a standard curve.

An expression plasmid for human Fibronectin was already available in the laboratory, however, generation of plasmids with the RUNX2 and FGFR3 insert was necessary to analyse gene expression from the bone samples. Generation of these plasmids are outlined in Appendix A.

The standard curves for Fibronectin, FGFR3 and RUNX2 (Figure 30A, B & C), indicate the plasmid DNA dilutions (8 X tenfold dilutions) starting at 10 ng of plasmid DNA (O) as well as the

amplification and transcript abundance of reactions from plasmid dilutions(X). These curves indicate a general trend of reactions to amplify at a high cycle number. This suggests low abundance of transcript. The transcript abundance was low (femtogram) for all reactions and genes included in these assays (data not shown). The femtogram amounts were converted to nanograms and the Gene Copy Number (GCN) was calculated (Figure 30D).

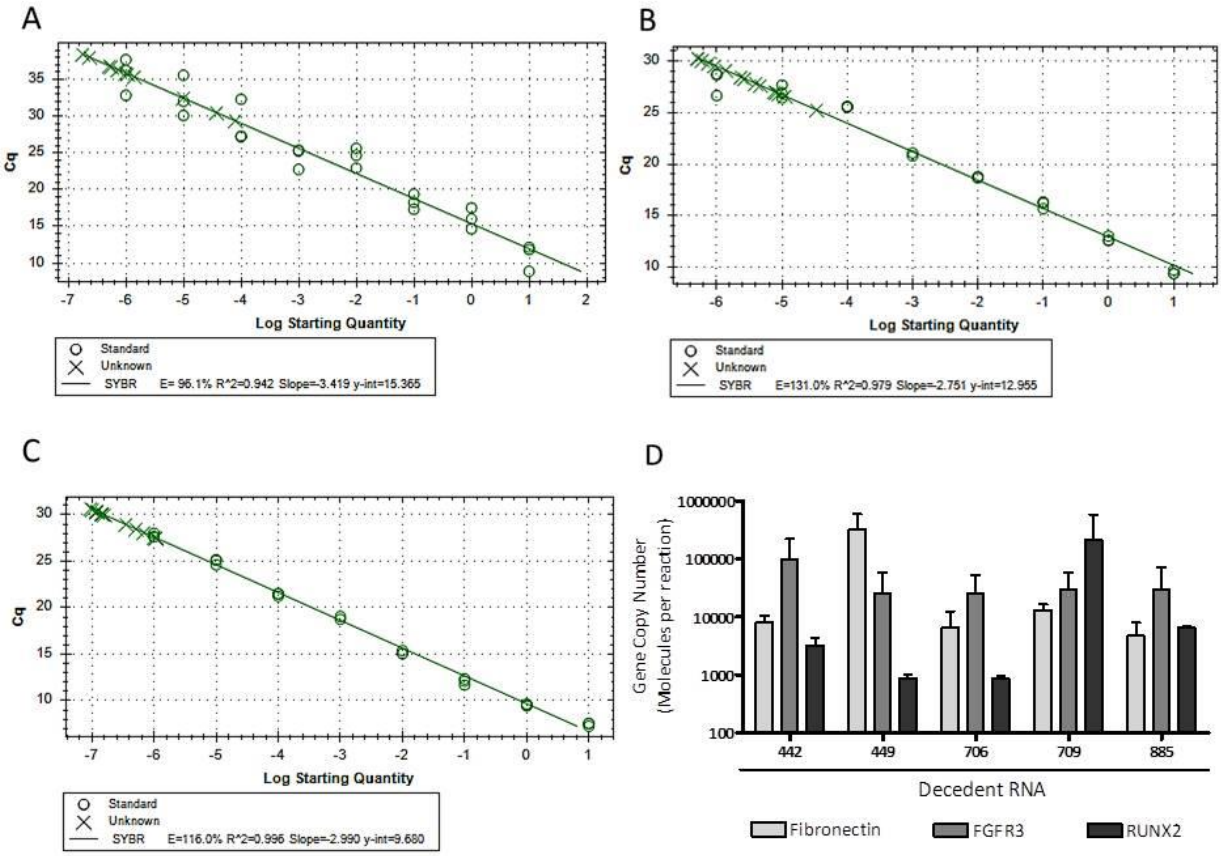

Figure 30: RT-qPCR optimisation results of gene expression analysis of perinatal RNA. A.) Fibronectin Standard curve: including plasmid dilutions and reaction starting quantity. B.)FGFR3 Standard curve: including plasmid dilutions and reaction starting quantity C.)RUNX2 Standard curve including: plasmid dilutions and reaction starting quantity. D.) Comparison of Gene Copy Number and Cq mean for gene expression analysis of perinatal RNA. Individuals included in analysis: 442, 449, 706, 709 and 885.

The molecule copy number mean and standard deviation from three technical replicates targeting the three amplicons were plotted for the individual RNA included in this assay (Figure

30D). The highest concentration of transcript molecules was found for Fibronectin in individual 449 and RUNX2 in individual 709. The abundance of FGFR3 was found to be consistently higher than Fibronectin and RUNX2 with the exception of individual 449. The standard deviation of reactions indicated a considerable amount of variability in copy number indicating possible PCR inhibitors, most likely poor RNA quality.

For the postnatal individuals of 442 and 885, aged at birth to 1.5 months, the FGFR3 was more abundant than Fibronectin and RUNX2, which were more evenly distributed at under 10 000 molecules per reaction. For the younger individual 449 (38 gestational weeks – birth), Fibronectin was considerably more abundant then FGFR3 and RUNX2. The Fibronectin gene expression from the reactions for individual aged at 30-34 gestational weeks (706) was lower when compared with the older 449 molecule number. The transcript abundance for FGFR3 and RUNX2 remained relatively similar during this perinatal period (30 gestational weeks – Birth).

The consistently low copy number for RUNX2 in the perinatal and postnatal individuals increased to a higher abundance in the individual sample for 709 (<30 gestational weeks). In these reactions, the copy number for FGFR3 and Fibronectin was lower. This suggests an active role of RUNX2 during the early stages of fetal rib development. However, these data only represent the gene expression of isolated cases representing the different dental age ranges, therefore any interpretation of results relating to bone development *in utero* and during the neonatal period should be undertaken with caution.

Taken together, the results from the post mortem RNA analysis from animal models (Figure 28 and 29) and the RT-qPCR data generated from the perinatal samples (Figure 30) indicated that the stability of RNA following death was highly sensitive to the decomposition process. The

variability of these data suggest that mRNA assessment using post mortem samples from advanced decomposition may not an viable option. For these reasons, we attempted to use DNA methylation of Fibronectin, RUNX2 and FGFR3 promoter regions as an indirect measure of gene expression. This analysis uses genomic DNA (gDNA) which could be more reliably isolated from post mortem samples. Methylation analysis of selected promoter regions of the RUNX2, FGFR3 and Fibronectin genes was incorporated into the study to assess the possible silencing of gene expression during gestation and postnatal development.

3.3.2 Analysis of methylation of selected Fibronectin, RUNX2 and FGFR3 promoter regions

Methylation of CpG (Cytosine-phosphate-Guanine) islands and sites is a dynamic form of regulation of gene expression during development (Slieker *et al*., 2015). DNA methylation is targeted to important developmental genes and is involved in tissue specific gene regulation. Methylation occurs on cytosine residues and is catalysed by DNA methyltransferases (DNMTs). The level or degree of methylation in a specific position influences the regulation and expression of tissue specific genes, with higher levels of methylation being associated with reduced gene expression (Guibert *et al*., 2009).

Restriction endonucleases cleave and degrade DNA at site specific sequences. Methylation Specific Restriction Enzymes (MSREs) are blocked from cleaving DNA at specific sites if cytosine residues are methylated. Therefore, methylation specific restriction digestion assays followed by qPCR can be used to estimate methylation of a DNA target. The difference in the Cq of amplification between an untreated and MSRE treated DNA sample can be used to calculate the percentage methylation at specific sites. In this study, this approach was used to analyse

selected sites in the promoter regions of Fibronectin, FGFR3 and RUNX2 transcripts due to their link to osteological growth and development

Once the protocols were optimized using gDNA from a cell line (Appendix A), we proceeded to analyse the methylation levels of the regions of the selected gene promoters in perinatal sample. The gDNA isolated from individuals was left untreated or subjected to MSRE digestions. These DNA samples were then used as template in qPCR assays using primers targeting regions of the Fibronectin, RUNX2 and FGFR3 promoters.

The percentage methylation at these specific sites was calculated based on the difference in Cq values for the untreated and MSRE treated DNA templates. The percentage methylation for the various regions was compared to the dental age categories for each gene and thereafter sub divided into gestational age ranges. The number of individuals included at each dental age range varied between 20 (early prenatal), 18 (prenatal) and 23 (postnatal) for Fibronectin (Figure 31A); 22(early prenatal), 16(prenatal) and 22(postnatal) for FGFR3 (Figure 31C) and 22 (early prenatal), 16 (prenatal) and 24(postnatal) for RUNX2 (Figure 31E).

The box and whiskers graphs in Figure 31 present the lower and upper 95 % CI for the methylation level means of the three genes at the different dental age categories and subcategories. The methylation level means for Fibronectin remain at 48±26.5 and 49±23 % for early prenatal and prenatal but raise slightly to 58±30.5 % for postnatal (Figure 31A). However, there was large variation in the distribution of methylation levels for the dental age categories. The range in these age groups in terms of methylation level was 21.5-74.5 % for early prenatal, 26-72 % for prenatal and 28-88 % for postnatal.

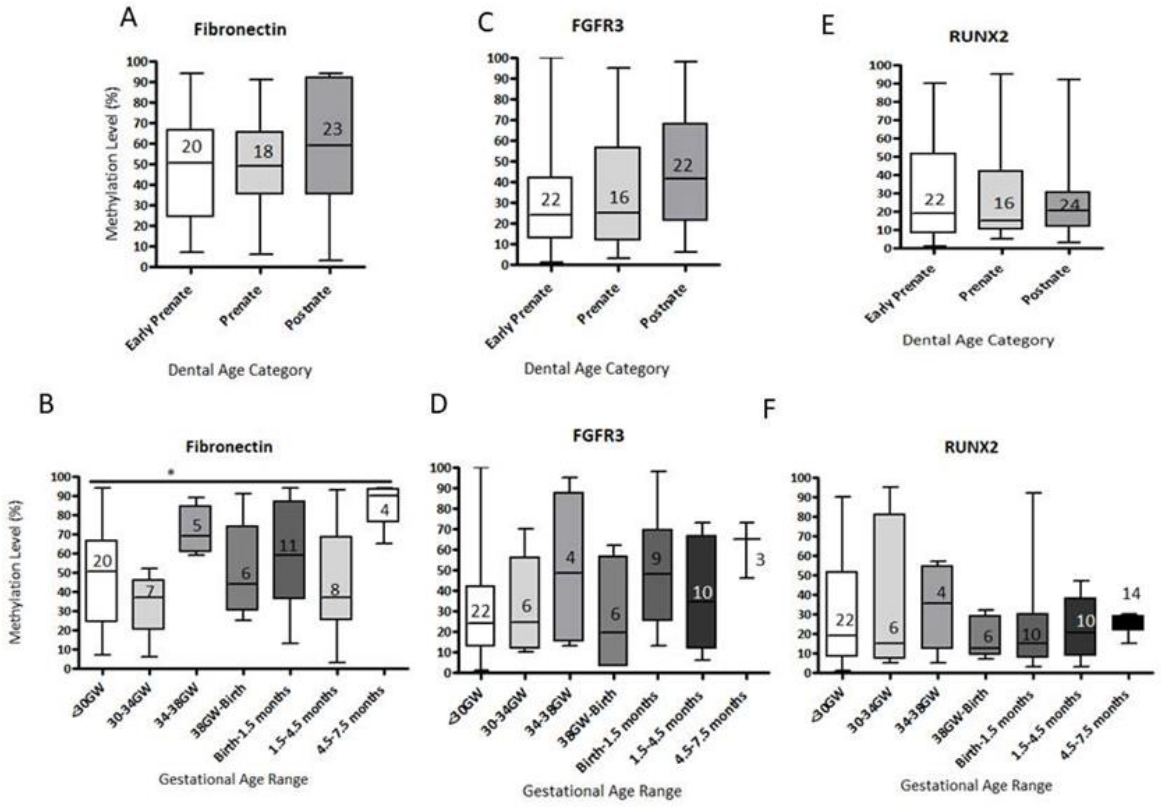

Figure 31: Methylation analysis of selected regions of the Fibronectin, FGFR3 and RUNX2 promoters in terms of dental age. A.) Fibronectin methylation levels within the dental age ranges. B.)FN1 methylation levels within the gestational age ranges. C.) FGFR3 methylation levels within the dental age ranges. D.) FGFR3 methylation levels within the gestational age ranges. E.) RUNX2 methylation levels within the dental age ranges. F.) RUNX2 methylation levels within the gestational age ranges. Statistical significance was assessed using a 1-way ANOVA analysis: * p-value < 0.05.

For the dental age subcategories in gestational age (GW) and postnatal months (Figure 31B), the Fibronectin mean values for methylation level percentage alternate from 48±26.5 % at <30GW, to 34.8±16.3 % at 30-34 GW, 71.8±12.5 % at 34-38 GW, 49.3±23.7 % around birth, 59.9 ±28.8 % during the neonatal period, 44.6±32.3 % during the 1.5 – 4.5 months and finally at 84.7±13.5 % at 4.5-7.5 months. The methylation range at gestational age was found to be 21.5-74.5 % for younger than 30 GW, 18.5-51.5 % for 30-34 GW, 59.5-84.3 % for 34-38 GW, 25.6-73 % for 38 GW-Birth, 31.51-88.7 % during the neonatal period, 12.3-76.9 % for 1.5-4.5 months and 71.2-98.2 for 4.5-7.5 months. A 2-way ANOVA was used to measure the degree of

variation between the Cq means and the dental age controls. For the Fibronectin region of interest, a significant difference was found between methylation means within the gestational age ranges (p value <0.05) (Figure 31B).

For FGFR3 mean values for methylation level percentage, the data showed 33.6±29.6 % methylation for early prenatal, 34.1±29.5 % for prenatal samples and 44.7±25.9 % for postnatal. This indicated an increase in methylation for the sites examined during the postnatal stage of development (Figure 31C). The range for FGFR3 in these age groups in terms of methylation level was 4-63.2 % for early prenatal, 4.6-63.6 % for prenatal and 18.8-76.6 % for postnatal, which demonstrated the high variation identified in the samples.

Within the dental subcategories of GW and postnatal months, mean values for methylation level percentage were more consistent at 33.6±29.6 % at <30 GW, to 30.6±22.9 % at 30-34 GW, 51.2±42.3 % at 34-38 GW, 26.3±26.3 % around birth, 49±27.8 % during the neonatal period, 35.9±25.2 % during the 1.5 – 4.5 months and finally at 61.5±13.8 % at 4.5-7.5 months (Figure 31D). The methylation range at gestational age was found to be broad at 4-63.2 % for younger than 30 GW, 7.7-53.5 % for 30-34 GW, 8.9-93.5 % for 34-38 GW, 0-52.6 % for 38 GW-Birth, 21.2-76.8 % during the neonatal period, 10.7-61.1 % for 1.5-4.5 months and 47.5-75.1 for 4.5-7.5 months (Figure 31D). No statistically significant differences were found for FGFR3 methylation within the dental age categories.

The methylation level means were similar across the dental age ranges for the master regulator for bone development (RUNX2) (Figure 31E). These were 30.3±26.3 % (early prenatal), 27.5±26.4 % (prenatal) and 23.6±18.8 % (postnatal). For dental age subcategories in

gestational age (GW) and postnatal months (Figure 31F), the RUNX2 mean values for methylation level percentage were 30.3±26.3 % at <30 GW, to 34.3±37.4 % at 30-34 GW, 33.2±25.2 % at 34-38 GW, 16.8±9.8 % around birth, 23.9±25.7 % during the neonatal period, 22.8±15.0 % during the 1.5 – 4.5 months and finally at 25.2±6.8 % at 4.5-7.5 months. However, there was variation in terms of the distribution between individual samples in the different categories. The methylation range at gestational age was found to be broad at 4-56.6 % for younger than 30 GW, 0-71.7 % for 30-34 GW, 8-58.4 % for 34-38 GW, 7-26.6 % for 38 GW-Birth, 0-49.6 % during the neonatal period, 7.7-37.8 % for 1.5-4.5 months and 18.4-32 % for 4.5-7.5 months. No statistically significant differences were found for RUNX2 methylation level and the dental age categories.

The potential variation (2-way ANOVA) between female and male individuals with respects to the methylation levels of the selected regions of the Fibronectin, FGFR3 and RUNX2 promoters was performed and no significant differences were reported (data not shown).

The methylation percentage data represented in Figure 31 were used in a comparison between the three genes at the broad dental age categories. An ANOVA was performed to test for differences in mean values between percentage methylation of regions of the Fibronectin, FGFR3 and RUNX2 promoters at early prenatal (Figure 32A), prenatal (Figure 32 B) and postnatal (Figure 32C). The lower 95 % CI of means was consistently different in these age groupings. The results produced statistically significant values ($p \leq 0.05$) for the prenatal (Figure 32 B) and postnatal age categories ($p \leq 0.001$), where Fibronectin was significantly more methylated at the specific site than FGFR3 and RUNX2 (Figure 32C).

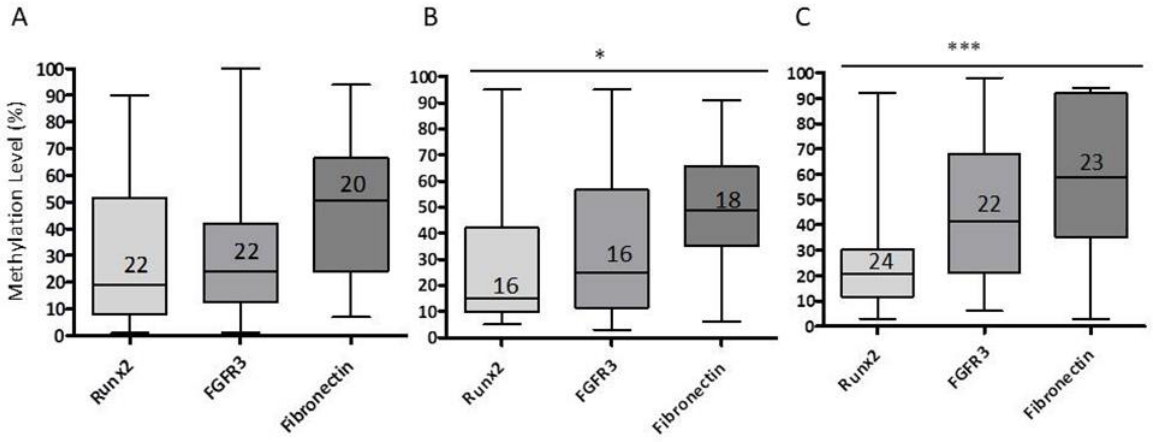

Figure 32: Comparison of gene methylation level means for RUNX2, FGFR3 and Fibronectin. A.) Early prenatal (<30 gestational weeks).B.) prenatal (30-40 gestational weeks). C.) postnatal (Birth-1.5 months). Statistical significance was assessed using ANOVA analysis. ***p-value <0.001;* p-value < 0.05.

These results indicated that regions targeted for Fibronectin, FGFR3 and RUNX2 genes don't vary in terms of methylation at the early prenatal age. The differences observed at prenatal (Figure 32B) and postnatal (Figure 32C) age categories indicate that the regions begin to differentiate after 30 weeks (Figure 32B) with respects to potential silencing of gene expression. This differentiation was more pronounced during the first year of life (Figure 32 C).

To estimate if there were any potential interactions between the genes selected in the study in individual samples, a Pearson correlation was performed for the methylation percentage for the Fibronectin, FGFR3 and RUNX2 regions. The methylation of regions of the Fibronectin, FGFR3 and RUNX2 promoters were not significantly correlated in the early prenatal and prenatal groups (data not shown). An exception to this was a positive correlation in methylation observed at the prenatal dental age range for RUNX2 and FGFR3 (Figure 33A). An increase in the RUNX2 gene methylation was coupled with a proportional increase in the methylation of FGFR3 (R=0.7119). A less significant correlation (R=0.4) was observed at the postnatal age for

the methylation of the RUNX2 and FGFR3 promoters (Figure 33B), FGFR3 and Fibronectin promoters (Figure 33C) and RUNX2 and Fibronectin promoters (Figure 33D).

These data suggested a positive relationship between the osteoblast regulator RUNX2 and the FGFR3 at the prenatal and postnatal stage of development. A potential relationship was also present between FGFR3 and Fibronectin and RUNX2 and Fibronectin genes at the postnatal age range (Figures 33C and D), however, more outliers and variation were observed between individuals for these correlations.

A correlation between the quantitative osteometric data and the methylation level percentages described in Figures 16, 18, and 20 was undertaken to estimate if any biological relationships exist between the dry bone measurements of the cranial base and the femur and the gDNA methylation levels for the Fibronectin, FGFR3 and RUNX2 promoters derived from sternal rib samples. No statistically significant relationships were identified based on the Pearson correlation co-efficient (R value) (data not shown).

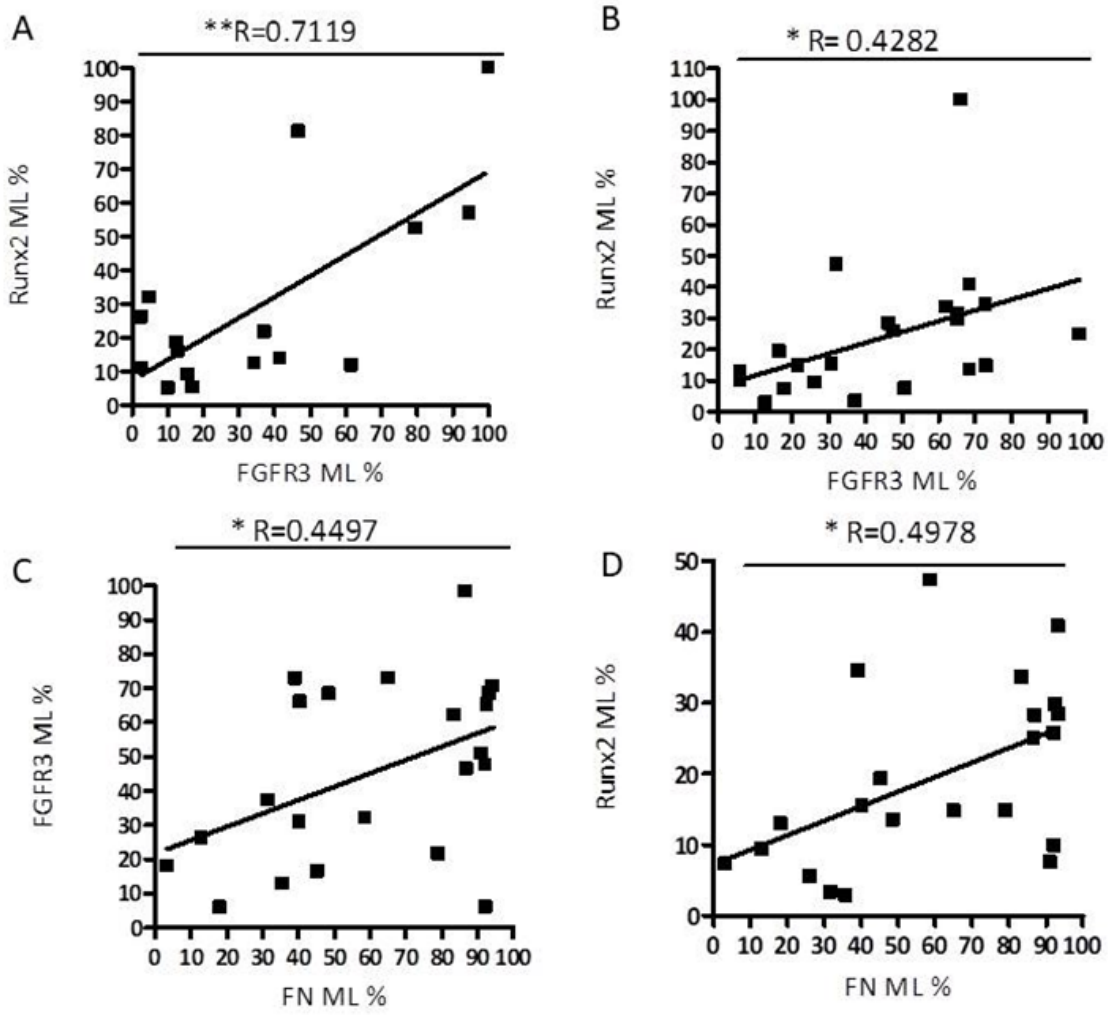

Figure 33: Correlation of methylation levels for specific sites in Fibronectin, FGFR3, RUNX2 promoters. A.) Pearson correlation between RUNX2 and FGFR3 in the prenatal dental age range. B.) Pearson correlation between RUNX2 and FGFR3 in the postnatal age range. C.) Pearson correlation between FGFR3 and Fibronectin in the postnatal age range D.) Pearson correlation between RUNX2 and Fibronectin during the postnatal age range. R = Pearson correlation coefficient. ML % = methylation level percentage.

Taken together, these data suggest that although there are possible biological relationships between the levels of methylation in the different genes studied, the methylation of the selected regions of the RUNX2, FGFR3 and Fibronectin genes was not predictive of the age for individuals in the perinatal and postnatal stage of development.

CHAPTER 4: DISCUSSION AND CONCLUSIONS

The rationale for undertaking this project relied on the prevalence of suspected concealment of birth and infanticide cases admitted to medico legal mortuaries around the country. In addition to this, the fundamental deficit of South African osteological data pertaining to the perinatal and postnatal stages of development motivated undertaking of the project. The molecular assays developed and performed on mRNA and gDNA were undertaken to provide a molecular foundation of rib bone development through the study of gene expression and methylation silencing. These data in combination with the osteological data provide a foundation for biologically profiling South African perinatal remains. Additionally, confirming and determining sex through molecular means supports the aim of providing criteria for the forensic identification of remains. The combination of three disciplines – odontology, osteology and genetics produced results, which elicit hypotheses for future study and expansion on the biological profile presented.

The novelty of this project can be found in the sample base, which is forensic and on a modern population. Similar studies incorporating dry bone measurements to examine osteological growth and development have been based on osteological material from the 18^{th} – 20^{th} century (Scheuer and Maclaughlin-Black, 1994; Scheuer and Black, 2000; Nagaoka, *et al.,* 2012; Olivares and Aguilera, 2016a). Previous studies have been represented of European populations or more recently Asian in ancestry (Scheuer and Maclaughlin-black, 1994; Scheuer and Black, 2000; Nagaoka, *et al.,* 2012; Olivares and Aguilera, 2016a). The known age of individuals included in these studies was estimated by crown heel length (Fazekas and Kosas, 1978), skeletal aging techniques (Scheuer and Maclaughlin-Black, 1994), last menstrual period (Nagaoka *et al. ,* 2012) and birth certificate information (Olivares and Aguilera, 2016a). To the best of our knowledge, this is the first study design that has used dental aging criteria by

Alqahtani *et al.,* 2010 to provide biological age when studying the skeletal elements of the South African pars basilaris, pars lateralis, sternal rib and femur of unclaimed fetal and perinatal remains. Additionally, the unique study design of combining traditional dry bone measurements, 3D imaging modalities for bone mineral density analysis and the introduction of methylation specific restriction enzyme-RT-qPCR analysis on this population group provides new insights into skeletal development.

4.1 Perinatal osteological development: growth in size and shape

The pars basilaris and pars lateralis bones were selected because of their role in stabilizing the base of the skull. The pars basilaris has forensic value as it is a robust bone and as such resists the effects of inhumation (Redfield, 1970; Fazekas and Kosa, 1978; Scheuer and Mac-Laclauglin-Black, 1994; Nagaoka *et al.,* 2012). The distinctive changes in size dimension and morphological appearance during gestation and within the first few years of life allows for the age related observations and therefore accurate age-at-death assessment (Scheuer and Black, 2000). As observed in the study, the osteometric and morphological data indicate an exponential and rapid growth rate of the basio-occipital skeletal elements during gestation and postnatal life. The pars lateralis is more fragile and subject to postmortem breakage in later gestation. The mastoid temporal part of this bone is still cartilaginous due to its proximity to the posterior mastoid fontanelle. Therefore, during early and mid-gestation, the osteology that has formed is fragile and susceptible to breakage. The femur bone was selected for the postcranial counterpart as it has been studied extensively and is widely used in juvenile, sub-adult and adult age-at-death assessment (Scheuer and Black, 2000; Dhawan *et al.*, 2014).

The main findings from the osteological analyses were the growth of the pars basilaris, pars lateralis and left femur during the age ranges observed. The significant differences observed between the different age groupings provides support for the development of diagnostic age related standards which assist in age-at-death estimations in forensic investigations when chronological or dental age are not available or possible. Of the dry bone measurements included in the methodology, maximum length and maximum width/distal width of the pars basilaris, pars lateralis and femur resulted in significant age-related differences, which have application in age-at-death estimations. Indeed, the maximum length of the pars basilaris and femur bone have been proven to be reliable age-at-death indicators in differentiating new born and late infant remains and fetal and perinatal remains (Scheuer *et al.,* 1980; Scheuer and Maclaughlin-black, 1994; Dhawan *et al.*, 2014). Our results from the osteometric data complement that of the data cited above. The maximum length was found to be the most significantly different across the age ranges. This indicates tremendous and rapid growth at these regions of the cranial and postcranial skeleton at this stage of development.

Mineralization of bone is defined by the incorporation of minerals such as calcium and phosphorus at sites of newly formed organic matrix (Land and Schoenau, 2008). The mechanostat model of bone biomechanics was first posited by Frost in 1987. The model proposed that mechanisms and stressors transform a particular bone's mechanical usage into appropriate signals. The theory's foundation relies on the hypothesis that mechanical stimuli influence the activity of bone apposition and resorption at specific locations on the bone surface (Frost, 1987). Rauch and Schoenau (2001) developed a functional model of the bone development based on the mechanostat model. Here the activity of the genome is thought to provide positional information for the blue print of the skeleton. Following this, bone cell

activity is co-ordinated by mechanical requirements of the bone. Through movement and musculoskeletal force, load is expressed on certain aspects of the bone. If the mechanical load exceeds a threshold then bone tissue is added to that specific location. This system modified and adjusted by hormones, nutrition and environmental factors. Support for this theory can be found in Hughes and Petit's (2010) perspective on the role of osteocytes in determining mechanical loading or the use of computational models to study the forces generated by fetal kicking in utero (Verbruggen *et al.,* 2016). Nonetheless, the theory of mechanical forces on bone mineral content is not widely accepted in bone research (Rauch and Schoenau, 2001) due to the dogma of the fetus passively existing within amniotic fluid. However, further study into this variable is necessary.

The hypothesis of varied bone mineral density at different regions of the pars basilaris, pars lateralis and femur was disproved as no statistically significant differences were found for any of the density points. Thus, the data reinforce the notion of the cranial base stability during growth. Bone density decreases by 30 % in the first three months after birth. The bone marrow size is bigger than the bone cortex during postnatal life (Land and Schoenau, 2008). It has been posited that a reason for these alterations in mechanical stimulation on bone mineral density is due to the impact of the intrauterine environment. An example of this is that regular fetal kicking is subject to resistance training due to the increased density of the womb environment (De Vries *et al.,* 1985; Christensen *et al.,* 1999). In addition, the density points of the pars basilaris, pars lateralis and femur were found to be higher in the female perinatal individuals when compared with the postnatal individuals. One could argue that this could be a factor of sex. However, no sexually dimorphic differences were observed for bone mineral density values were compared between males and female individuals.

A plausible explanation for the finding of little or no effect on bone mineral density is that the mineralization of osteology at the density points examined is delayed as the bone is increasing in size. The variation observed from the PCAs of bone density indicated that mineralization is being driven by the lateral angles and spheno-occipital synchondrosis metaphyseal surface (pars basilaris), the medial border for the foramen magnum, jugular foramen, metaphyseal surface of the condylar limb, primary ossification site (pars lateralis) and midshaft of the femur. These density points are situated in the same region of the maximum length and maximum width dry bone measurements. These results indicated that the ossification and expansion of the cartilaginous blueprint of developing bone is of prime importance prior to birth. The bone mass and physical density is secondary in importance. Many influences impact the bone mineral content of pre-term and newborn infants including season of birth, low weight relative to gestation, and possible diabetes in the mother, placental mineral transfer, fetal bone absorption and fetal bone resorption (Namgung and Tsang, 2000). These variables weren't included in the study design and therefore the potential influence on the sample is unknown. Certainly, Micro-CT imaging is a non-destructive and rigorous method of studying normal skeletogenesis (Nuzzo *et al.*, 2003), osteopathology and the effects of genetic and environmental manipulation using animal models (Guldberg *et al.*, 2004). An alternative method for studying the growth and development for pediatric skeletal age would be geometrics morphometrics (Braga and Treil, 2007).

In terms of anatomical development and formation of specific bone morphology, results from the study indicated that the early prenatal femur develops distinctive anatomical features and matures prior to that of the cranial bones. Cranial bones developed distinctive anatomy during the late prenatal and postnatal stages. Femoral features start maturing in sequence early in

development with the linea aspera and the appearance of the nutrient foramina for vascularization. The upper and lower shaft morphology is apparent, with the articular and metaphyseal surface morphology becoming more apparent in the late perinatal stage.

The pars basilaris and pars lateralis morphology sequence begins with the articular surface development and the rounded foramen magnum border and mastoid temporal border morphology following. The pars basilaris articulates with the pars lateralis at the condylar and jugular facets. The mastoid fontanelle aligns with the posterior mastoid border of the pars lateralis. This fontanelle in conjunction with the anterior and posterior fontanelle ossifies within the first year of life. Cranial fontanelles support the flexibility of bone plates as the brain matures and grows faster than the surrounding bone within the first year of life (Scheuer and Black, 2004). This provides explanation for the slower maturation rate of the pars basilaris and pars lateralis when compared with that of the femora. Through the use of Alzarin red staining, Noback and Robertson were able to record ossification centre appearance from embryos varying from 14-235mm (CRL). The femoral ossification centres appeared prior to the basicranial centres (Noback and Robertson, 1951) in embryos. It appears that ossification is initiated in the postcranial skeleton prior to the cranial and the rate of embryonic ossification translates to fetal growth phase. This is in agreement with Scheuer and Black (2000) as the bony collar appears at the midshaft from weeks 7 *in utero* and indicates a tendency of rapid ossification and growth in early gestation to accommodate locomotion and bipedalism.

The depression on the intracranial surface of the pars basilaris bone has not been mentioned in previous literature. A description of pitting on the concave intracranial surface for vascularization is outlined by Cunningham *et al.,* 2016. In the current study, pitting was found

in early prenatal remains. When recording data for the prenatal remains, a persistent depression was noted on the concave surface. This depression disappeared gradually as the perinate matured. At late postnatal ages, the depression was absent in the individual collection. It is hypothesized that this is evidence of a delay in ossification as the bone increases in maximum width proportions. Our morphological summaries serve as supplementary data to existing texts and provide insight into the osteological development of African fetuses, perinates and infants.

The features included in morphological summaries are based on the comprehensive text of Scheuer and Black (2000). The percentage of individuals which exhibited developing and present features at the dental age ranges were under 60 percentiles. It is prudent to note that many of the bones dissected and processed for osteological evaluation exhibited post mortem and possibly ante mortem damage to the osteology. This was predominately across regions including the right or left condyles and lateral angles of the pars basilaris. While the pars basilaris is thought to be a sturdy and robust bone that resists inhumation, these regions of the pars basilaris anatomy develop with age and therefore are mostly underdeveloped and fragile during fetal development. Damage of the pars lateralis was mostly observed on the mastoid temporal border where the bone is not as robust and undergoes tremendous growth in dimension and size during late gestation and early postnatal life. Ante/post mortem damage to the femoral elements was found on the distal end of the femur, especially on the metaphyseal surface. Despite this, the qualitative morphological observations recorded during the course of the study correlate with the fundamental descriptions regarding skeletal anatomy of the developing human for the pars basilaris and pars lateralis (Redfield, 1970; Scheuer and Maclaughlin-black, 1994; Scheuer and Black, 2000) and femur (Scheuer and Black,

2000). However, the stages of A-D for the occipital complex described by Redfield (1970) are mostly focused on the shape of the bones and the respective margins in relation to fontanelle closing. The individual features of articulation and proportional growth aren't discussed in detail for the gestational ranges and postnatal months.

The pars lateralis is not as extensively studied as the pars basilaris. There is a deficit of information regarding pars lateralis growth and development in differing populations. Despite the small sample number, our data provides dry bone measurements for African fetal, perinatal and postnatal was not which have the potential to assist in age-at-death assessment for African remains. Asymmetry of growth rate in bilateral anatomy of an individual has been reported in the literature (Bagnall *et al.,* 1977; 1982). The suggested asymmetry of this bone indicated by significant differences between the left and right components provides motivation for further study into the development of the pars lateralis. Perhaps this bone should be treated as two separate skeletal elements when evaluating growth, especially with respects to the growth towards the mastoid temporal border, as asymmetry was found in the measurement of maximum length. Based on these data, we suggest the use of the maximum length and maximum width measurement metrics to estimate age-at-death when utilising dry bone remains of the pars basilaris, pars lateralis and femur. Sagittal length of the pars basilaris was also found to be statistically significant between age ranges but was not as remarkable as the aforementioned measurements.

Our study showed differences between male and female individuals for the bones examined. However, these differences in metric and density values weren't statistically significant. Although the results of the study showed no sexually dimorphic differences in terms of dry

bone measurements and bone mineral density, the bones from male individuals were slightly larger with respect to measurement mean when compared to female individuals. In addition, the bone mineral density ratios for female individuals were higher when compared to the males. There is reason to suspect that the bones studied at this developmental stage are sexually dimorphic. Studies have shown that females advanced in terms of growth during the perinatal period and the males caught up by birth (Hill, 1939); female fetuses begin ossification earlier than males (Cope and Murdoch, 1958); females fetuses advanced in ossification after 21 weeks *in utero* (Bagnall *et al.* ,1977, 1982) and female fetuses exhibited earlier development (Burdi, 1979). There is reason to hypothesize significant sex differences in bone growth that relate to weight and length (Crelin, 1973) A discriminant function model was developed using bone lengths of fetuses (16-44 GW) by Choi and Trotter (1970). This allowed for 72 % of correct classification of sex (Weaver, 1998). For decades, researchers have used osteological craniofacial and pelvic features from adult remains to develop methods and criteria for sex typing (White and Folkens, 2005). These criteria differ according to population and aren't present in fetal and juvenile remains. A call for further studies on documented samples is needed as currently the academic consensus is that sex estimation is not reliable at the fetal or postnatal age (Ubelaker and Degaglia, 2017).

4.2 Dental versus skeletal aging: call for population criteria

Dental aging one of the most accurate methods of estimating age-at-death in juveniles. Teeth tend to survive processes of decomposition and are extremely resistant to environmental and taphonomic factors of erosion (Lewis and Garn, 1960; Demirjian, 1986; Smith, 1991; Cunningham *et al.,* 2016). Nonetheless, if dentition is unavailable, biological age is dependent

on the developing skeleton (Lewis and Flavel, 2007). The juvenile skeleton in utero is far more variable than dental development. Influences such as maternal health, socio-economic background and stresser during gestation are factors that impact variablity. These factors exist within a population or culture group (Scheuer and Black, 2000). Therefore, a degree of individual variation in growth and development of the skeleton is expected. As discussed earlier, population affinity variation has been found to exist at the fetal period of development (Lim *et al.,* 2000; Scheuer and Black, 2000; 2004, Patel *et al.,* 2004; Unterscheider *et al.,* 2013; Sletner et al. 2015). Variation between populations serves to support the undertaking of this project as is exhibited when one examines the South African osteometric data in comparison to the Hungarian (Fazekas and Kosa, 1978) and Spitalfields collections (Scheuer and Maclaughlin-Black, 1994).

The pars basilaris and femur bones have forensic value for age-at-death estimation (Weaver, 1998). The dry bone measurements of these bones have been used to estimate age of juvenile remains from a forensic and archaeological setting by Fazekas and Kosas (1978) and Scheuer and Maclaughlin-Black (1994). The standards for these estimations are based on European individuals. The most comprehensive of these is that by Fazekas and Kosas (1978). Criteria by these authors are derived from mid-twentieth century Hungarian fetal remains. The known age of this collection was taken from CHL recorded at autopsy. Individuals were categorised by gestational week (GW). The collection ranges from 12 to 40 GW. For the pars basilaris bone, standards for the maximum width and sagittal length landmarks were used. The pars lateralis metrics for gestational age are available for the maximum length and maximum width. Additionally, the femur bone was also studied by these authors and values osteometric mean and range was published for the maximum length and distal width.

The standards proposed by Scheuer and Maclaughlin-Black (1994) were based on Spitalfields and St McBride collection. Dry bone measurements of this collection derive from early eighteen century and mid nineteenth century documented European remains. Scheuer and Maclaughlin-Black criteria age the pars basilaris bone from individuals within the prenatal (26 to 40+ gestational weeks) as well as postnatal (2 weeks postpartum – 4 years) groups.

The authors used the data from Fazekas and Kosas (1978) to age individuals. Only mean values are available when using this reference as the maximum number of individuals aged at the postnatal stage of development was 3. No reference is available for the pars lateralis bone following 40 gestational weeks. Therefore, indicating a lack of reference criteria for this skeletal element. This potentially impacts the identification process in crime scene recovery and subsequent investigations.

A comparison was made between the mean values found for each point (mm) of the bones collected during the study and the established standards cited above. This comparison was made within the dental age categories. For comparative purposes, the gestational ranges were used as they coincide with that of the standards. To ascertain the level of agreement between dental age and skeletal age, a comparison was made between the dental age ranges incorporated in this study and the skeletal age ranges generated from the osteometric means of the pars basilaris, pars lateralis and femur bone values (mm) documented from this study. The skeletal age ranges were estimated from the osteological measurements and were based on Fazekas and Kosas (1978) and Scheuer and Maclaughlin-Black (1994) criteria.

The comparison of the current study osteometric means (mm) with that of Fazekas and Kosas (1978) and Scheuer and Maclaughlin-Black (1994), for the pars basilaris is detailed in table 9

(Appendix D). It should be noted that the exact age of the individuals younger than 30 gestational weeks collected in the current study is unknown. The dental aging guarantees an age no older than 30 gestational weeks. The mean value noted for the Fazekas and Kosas (1978) is the average of osteometric values from 12-30 gestational weeks. It is hypothesized that the individuals collected in this study were no younger than 20 gestational weeks.

This assumption is based on the size and development of the fetal remains at dissection. Based on this explanation, a smaller Fazekas and Kosas (1978) mean and standard deviation is understandable as the distribution was broader at this dental age range. When studying the osteometric means for the pars basilaris landmarks (mm), the majority of the current study means were consistently larger in Fazekas and Kosas (1978) and Scheuer and Maclaughlin-Black (1994) when considering the dental age ranges. Gestational and postnatal skeletal age ranges were generated for the pars basilaris ML, SL and ML osteometrics (Table 9).

For individuals younger than 30 gestational weeks, the dental and estimated skeletal age ranges positively correlated for the three measurements. After 30 gestational weeks, the dental and skeletal age estimation values begin to vary indicating potential inaccuracies in either the skeletal aging criteria, dental aging criteria or both. For the dental age range of 30-34 gestational weeks, skeletal age correlated with the dental age but underestimated age by two (MW and SL) and four gestational weeks. At 34-38 gestational weeks, skeletal age didn't correlate with that of the dental control for the three landmarks. The minimum skeletal age was 6 (MW and SL) and 8 (ML) gestational weeks younger than dental age. The maximum skeletal age for the dental age range 38 gestational weeks to birth correlated with the starting value for the dental age (38 gestational weeks) for maximum length. However, the skeletal age

was underestimated by two weeks (MW and SL) when examining the maximum value for the range (36 gestational weeks). The trend of underestimating age from skeletal criteria continued for the postnatal dental age ranges, as the skeletal age ranges calculated from the measurements in the current study did not align with the dental age ranges for any of the landmarks of the pars basilaris. The individuals were aged skeletally at the prenatal (30-40 GW) stage of development. Age estimation from the SL and ML osteometrics indicated a neonatal age (40+) for the birth – 1.5-month age range, which is in partial agreement. However, following 1.5 months to 7.5 months, the skeletal and dental age estimation differed not only in weeks but in month.

This comparison indicates that skeletal age does not correlate with dental age after 30 gestational weeks. The growth variation between populations is more evident during the third trimester and first 7 months postpartum. As stressed before, aging standards are not available for the pars lateralis following 40 gestational weeks. Therefore, the osteometric means from the Hungarian collection (Fazekas and Kosas, 1978) were used for comparative purposes with the current sample means (Table 10; Appendix D). As seen with the pars basilaris, there was a broad difference between the metric means for ML and MW for the dental age category of <30 gestational weeks (Table 10). After 30 gestational weeks, the osteometric means for the older age ranges were larger in Fazekas and Kosas (1978) when compared to the current study osteometrics. The greatest difference can be seen at the age ranges of 34-38 gestational weeks (15.4 mm versus 21.1mm) and 38 gestational weeks – birth (20.3 mm versus 24.9 mm) for the ML and to a lesser degree for the MW.

The skeletal age range based on Fazekas and Kosas (1978) for ML and MW pars lateralis osteometric ranges within the dental age ranges us outlined in Table 10. The younger than 30 gestational dental age range correlated with that of the skeletal age range for the two measurements. The skeletal age estimation of 30-34 gestational weeks (ML) and 26-34 gestational weeks (MW) falls within the dental age of 30-34 gestational weeks.

There was a 2-week difference between the skeletal age and dental age for 34-38 gestational weeks for maximum length. For the 38 gestational to birth dental measurement, the Fazekas and Kosas (1978) standards underestimated the age by 2 gestational weeks based on our measurements. For the femur osteometric means, no aging standard reference is available following 40 gestational weeks. As with the pars lateralis, osteometric means from the Hungarian collection (Fazekas and Kosas, 1978) were used for comparative purposes with the current sample means (Table 11). The trend seen for the pars basilaris and pars lateralis in terms of smaller mean values from the Fazekas and Kosas collection (Fazekas and Kosas (1978), for the <30 gestational weeks was repeated here for the femur bone (Table 11; Appendix D). There was a difference between the means for ML (42.8 mm versus 29.5 mm). However, for the distal width, the difference is not as extensive (9.1 mm versus 7.1 mm) for the dental age category of <30 gestational weeks (Table 11). This might indicate a slower growth rate for the distal part of the femur prior to 30 gestational weeks. After 30 gestational weeks, the osteometric means for the older age ranges are larger in Fazekas and Kosas (1978) when compared to the study osteometrics. The greatest difference can be seen at the age ranges of 34-38 gestational weeks (49.1 mm versus 63.7 mm) and 38 gestational weeks – birth (59 mm versus 71.6 mm) for the ML. As with the pars lateralis, the DW difference between collections is less than that observed for ML.

The skeletal age range for the ML and DW osteometric ranges within the dental age ranges (Table 11). The younger than 30 gestational dental age range correlated with that of the skeletal age range for the two measurements. The skeletal age estimation of 22-30 GW (MW) and 20-28 GW (DW), fall within the dental age range (<30 gestational weeks).

For the dental age range of 30-34 gestational weeks, Fazekas and Kosas underestimated the individual age by two weeks for ML and DW. For 34-38 gestational weeks, the skeletal age estimated did not correlate with the dental age for both the ML and DW of the femur. For the 38 gestational to birth dental age, Fazekas and Kosas (1978) underestimated the age by 2 gestational weeks for the ML and 4 weeks for the DW. When one reviews the comparisons between osteometrics from the different collections, the metric means of the landmarks studied in the current individual collection were smaller than that of Fazekas and Kosas (1978) and Scheuer and Black (1994) osteometrics. The exception to this was the findings in the younger than 30 gestational weeks group, aging modalities correlate positively during early prenatal development. The comparison between aging modalities resulted in a difference in estimation between the dental age and skeletal age estimations for all osteometrics points examined.

The skeletal age estimates for the pars basilaris of Scheuer and Maclaughlin-Black (1994) and Fazekas and Kosas (1978) were compared to chronological age of fetal remains from a Japanese population (Nagaoka et al., 2012). The measurement of maximum length and width of the pars basilaris produced values which were smaller when compared to the data of Fazekas and Kosas (1978). This difference increased with gestational age. Sagittal length of the pars basilaris was not significant in terms of difference. Maximum length of the pars basilaris

was greater in the archaeological data (Scheuer and Maclaughlin-Black, 1994) when compared to the Japanese sample. These findings are complimentary to the results in our study. The Japanese remains originated from the early to middle twentieth century during a period of socio-economic unrest and poverty. The current socio-economic situation in South Africa is one of unemployment, poverty and political unrest. As noted before, the health and nutrition of the mother affects bone turnover and compromised fetal growth *in utero* (Harrast and Kalkwarf, 1998), therefore the socio-economic environment will have an impact on growth and development. This could explain the low percentile of morphological features of the related to maturity of bones (<60 %) present at the different dental ages and the inconsistency of dental and skeletal aging standards. The aforementioned standards were recently compared to the chronological ages of the Granada collection by Olivares and Aguilera (2016a). Significant differences were found for both methods. Fazekas and Kosas (1978) were found to underestimate age and Scheuer and Maclaughlin-Black overestimated age (Olivares and Aguilera, 2016a). Therefore, the exponential skeletal growth during the fetal, perinatal and postnatal stages of development are universal, however, the size of bones and degree of maturation is population specific and subject to the influence of ancestry and historical context.

When the quantitative osteological data of the current study were compared to the widely used criteria of Fazekas and Kosas (1978) and Scheuer and Black (1994), a discrepancy between mean values was evident after 30 gestational weeks. The difference in mean values was more pronounced at the postnatal age range. While dental aging is considered more reliable and accurate than skeletal (Scheuer and Black, 2000), one could argue that the dental aging control is unreliable or not applicable to African perinates. The accuracy of the London Atlas of Tooth

Development and Eruption has been validated by the authors (Alqahtani and Liversidge, 2014) on skeletal collections from Portugal, the Netherlands, USA, Canada and France. However, application of the atlas on children from Saudi Arabia by Alshihri and colleagues (2015) and Pavlovic and colleagues (2017) on a Portuguese population, found significant differences between chronological and dental age estimates. These comparisons were performed on an age range older than two years. Therefore, these findings aren't directly related to our study and the reliability of the atlas when applied to fetal and infantile remains. We are confident in utilizing dental aging as an indicator of biological age and a control for categorizing perinatal and postnatal individuals in the study.

The reliability of dental aging stems from the genetic determinant of dental mineralization. The process of tooth mineralization *in utero* is affected by intrinsic and extrinsic conditions than skeletal mineralization (Scheuer and Black, 2000). This process is genetically estimated and therefore representative of ancestral group (Lewis and Garn 1960, Tanner 1962, Garn *et al.,* 1965; 1973). The systematic influences of nutrition, environmental and physiological conditions have been considered as minimal on the mineralization process and rate (Fanning *et al.,* 1965, Haavikko *et al.,* 1973; Brown 1978).An investigation into the extent of influences is not possible due to the forensic nature of the perinatal sample and the study design of the project. Nonetheless, advantages of dental methods over skeletal aging include less variability between and within populations (Lewis and Garn, 1960, Demirjian, 1986; Smith, 1991) and the growth of the deciduous and permanent teeth takes place from early embryonic life to late adolescence, teeth survive inhumation and aren't as susceptible to damage as other skeletal structures (Scheuer and Black, 2000). This lends support to the use of dental aging methods over skeletal as a proxy for biological age.

These results support the need for population specific standards for the pars basilaris. There is a definite need for proposed criteria and regression formulae development for the African perinatal pars lateralis and femur. The perinatal sample has the potential to satisfy this need for African perinatal standards, however, further collection is necessary as the osteometric data collected and analysed, were limited with respect to number of individuals. The data collected during this project provides a 'snapshot' of osteological development at specific periods of time. It has provided a foundation for further analysis and biological profiling of the perinatal skeleton. As such, we propose further collection and validation of these osteological findings from the postnatal dental age group in order to provide a reference for dry bone osteometrics in the investigation of suspected abandonment and infanticide.

4.3 The application of post mortem RNA to forensic sciences

Despite the difficulty of utilizing bone as a source of RNA due to the low number of cells embedded in the mineralized tissue (Carter *et al.*, 2012),Van Doorn and colleagues support the use of bone and bone marrow as a source of viable post mortem RNA through their work with skeletally mature rabbits (Van Doorn *et al.*, 2011). Putrefaction is known to be delayed in bone marrow (Cengiz *et al.*, 2006) and the survival of RNA from bone marrow was communicated by Perry and colleagues when it was found that the cell motility in bone marrow persisted 50 hours post mortem (Perry *et al.*, 1960). The use of RNA from rib samples is supported as one could suggest that RNA is protected within the structures of bone tissue during decomposition. Soft tissue such as muscle and skin display the signs of putrefaction and decomposition at stage 2 (bloat) and 3(active) which indicates tissue autolysis. Therefore, it is an attractive option

within forensic settings as obtaining intact RNA might be vital to the identification and investigative process.

A significant difference was found between the Cq (referring to the cycle in which fluorescence can be detected or quantitation cycle and gives an estimation of the quantity of target sequence) means of the samples from various stages of decomposition in the animal studies. These findings demonstrated the degrading effect of the decomposition process on RNA quality. No difference was found regarding the efficiency of traditional freezing versus that of solution based RNA*later*. This supports the findings of Mutter and colleagues (2004) when examination of preservation methods on quantitative RNA expression profiles of uterine myometrial tissue individuals resulted in no difference between traditional freezing methods and the use of RNA*later* stored samples (Mutter *et al.*, 2004). These data support the use of traditional flash freezing, -80 °C or RNA*later* for in field use preservation prior to isolation but suggest sampling from tissue when the PMI is minimal or no signs of putrefaction or decomposition are present if this is possible.

In the RT-qPCR assays, for *Gallus Gallus*, a freezer derived sample amplified under 30 cycles at stage 5 decomposition. The five individuals selected to test the assays employed in the animal studies also amplified under 30 cycles, therefore indicating successful amplification. These results suggest that it is possible to use fragmented RNA and DNA RT-qPCR because the amplicons are usually between 100-300 bp. The performance of RT-qPCR is sensitive enough to detect DNA fragments and tolerates partial RNA degradation (Kuliwaba *et al.,* 2005; Koppelkamm *et al.*, 2011). The stability of RNA and its forensic application is supported and encouraged because of its application to the investigative process (Bauer *et al.*, 2003; Bauer,

2007; Fordyce, M. Kampmann, *et al.*, 2013). In the preliminary human assays of this study, transcript abundance was detected at a femtogram amount which was converted to gene copy number that was found to be highly variable. The transcript (gene) and tissue type affects successful RT-qPCR amplification for application of gene expression profiling (Opitz *et al.*, 2010; Koppelkamm *et al.*, 2011; Sampaio-Silva *et al.*, 2013). Indeed, it has been communicated that short mRNAs and probe positions near the 5' end impact the success of profiling of tumor samples. However, the work by Sidova and colleagues (2015) found no statistically significant degradation preference of the 5' or 3' end. This suggests that preference is gene specific (Sidova *et al.*, 2015). The biological variation among patients included in assays by Opitz and colleagues (2010), resulted in more variation in gene profiles than the effect of heat induced degradation. This finding has implications for the results in our study as the biological variation of the individuals included in the RT-qPCR assays for gene expression analysis was unknown.

The fact that the rib samples were dissected at an advanced stage of decomposition could account for the variability in transcript abundance. This suggests that RNA from tissues with a PMI longer than 48 hours is unlikely to be useful in routine forensic investigations but might be useful in specific cases depending on the agonal and post mortem conditions. The police documentation detailed death scene particulars included descriptions of dumped remains in dustbins, water and wrapped in plastic. Knowledge regarding the cause of death and post mortem interval was not recorded. These factors have been described as confounding variables on the integrity of RNA (Koppelkamm *et al.*, 2011). For these reasons, it can be surmised that the RNA extracted from the individuals included in these assays was not intact and degraded prior to dissection of the rib samples.

Genomic DNA methylation assays were selected over the use of postmortem RNA for our molecular studies due to the findings of contaminated and fragmented RNA from animal studies (*Gallus Gallus* and *Cercopithecus pygerythrus)* and the sample of the individual collection. Although in some cases PCR and qPCR quality RNA could be obtained, the results were highly variable, which is unsuitable for forensic analysis. The animal assays included tissue samples from the various stages of decomposition. To the best of our knowledge, this is one of the few studies to examine the changes in mRNA quality at different stages of decomposition without the incorporation of controls such as temperature, oviposition by insects (Kuliwaba *et al.,* 2005; Heinrich *et al.*, 2007; Van Doorn *et al.*, 2011; Sampaio-Silva *et al.*, 2013; Sidova *et al.*, 2015) or no signs of putrefaction at dissection (Bahar *et al.*, 2007). In addition, no other study has reported results of RT-qPCR assays targeting the Fibronectin, FGFR3 and RUNX2 amplicon from perinatal RNA derived from advanced decomposed remains. The study design and methodology used to investigate the use of bone marrow (Van Doorn *et al.*, 2011) as a source of RNA is very similar to our studies on decomposition and RNA quality. However, the rabbits used as an animal model were isolated in glass tanks and kept at a constant room temperature. In addition, the influence of insect activity on decomposition was included in assay design. From our results, the degradation of mRNA was measured from absorbance ratios and the lack of bands from stage 2 (bloat) onwards was evident for the beta actin and CD4 gene. The increased air temperature and humidity during the stages of decomposition could have also contributed to the rate of degradation. One of the most influential factors on RNA degradation is that of heat (Koppelkamm *et al.*, 2011). This factor is reinforced as a variable on RNA integrity in the results of experimental designs set up to evaluate heat degradation on the RNA extracted from human trabecular bone, human rectal

tumor biopsies and *Xenopus Laevis* oocytes and tadpoles (Kuliwaba *et al.,* 2005; Opitz *et al.*, 2010; Van Sidova *et al.*, 2015).

The qRT-PCR data on perinatal RNA are questionable as it is not clear whether the low transcript abundance was a reflection of gene expression levels or a consequence of RNA degradation due to the post mortem interval and confounding variables discussed earlier? Given the magnitude of data available on the importance of Fibronectin, FGFR3 and RUNX2 during chondrocyte, cartilage and osteoblast development (Horton, 2003; Provot and Schipani, 2005; Goldring *et al.,* 2006; Kimura *et al.*, 2010; Michigami, 2013; McGee-Lawrence *et al.*, 2014), it is likely that the low transcript abundance was due to the decomposition process and confounding variables and not an accurate reflection of gene expression. A full understanding regarding enzymatic turnover and the RNA decay following death is unknown. Therefore, studies imitating real–world forensic scenarios which incorporate controls of different PMI, tissue type, and cause of death need to be designed and performed to provide insights into the use of RNA for forensic application (Yasojima, Mcgeer and Mcgeer, 2001; Van Doorn *et al.*, 2011; Fordyce, M. Kampmann, *et al.*, 2013).

4.4 Methylation of Fibronectin, RUNX2 and FGFR3 promoters in postmortem samples

An alternative mechanism for inferring gene expression levels of transcripts important to bone development and growth without analysis of RNA is to use the methylation level of CpG rich islands of the promoter regions. This is based on the isolation of genomic DNA, which is widely used in forensic applications. The gDNA used for these analyses derived from sternal bone tissue. Dissection of rib tissue was done at the junction of costal cartilage and ossified tissue. Only ossified tissue was collected for analyses. In younger fetuses, the proportion of cartilage

to bone was uneven. The equilibrium of cartilage and bone only becomes equal at 4 months gestation (Scheuer and Black, 2000). Therefore, in older perinates, the amount of ossified tissue at this costochondral junction was more substantial and robust. This observation supports our original hypothesis that RUNX2 and FGFR3 amplicon methylation level would be lower in older individuals. However, no statistically significant differences were found for the methylation means within the different dental age categories. The endochondral ossification process entails differentiation into chondrocytes from mesenchymal cells, proliferation of chondrocytes, hypertrophic differentiation, angiogenesis for cartilage development and then bone formation (Provot and Schipani, 2005).

When comparing the methylation means of RUNX2, FGFR3 and Fibronectin with the different dental age categories, no significant differences were found. One interpretation of these results is that during perinatal and postnatal growth, these genes are ubiquitously expressed and form a network which facilitates development. Certainly, literature has reported the roles of these genes during bone development. Fibronectin has been reported as essential to the development of the extracellular matrix and an instructor of preosteoblastic formation. Therefore, it is important during hypertrophic differentiation of chondrocytes into osteoblasts (Weiss and Reddi, 1981; Goldring *et al.,* 2006; Singh and Schwarzbauer, 2012; Kawashita *et al.*, 2016; Zollinger and Smith, 2017). Alternatively, it is possible that the CpG sites selected in our study are not involved in regulation of gene expression during development, although the fact that we observed different levels between different samples does suggest differences. There may also be individual differences that account for the differences observed.

In addition to this, the methylation of the region of the Fibronectin promoter fluctuated between the sub categories of dental aging. This suggests that the degree of methylation for CpG sites examined for Fibronectin may be involved in gene expression during gestation and the first year of life as the developing as the costal cartilage decreases in proportion as the ribs ossify and adopt an adult like morphology.

This suggestion is currently unsupported as these sites haven't been studied before and therefore aren't validated as key gene expression regulators. In order to confirm this, we will need to study the link between the methylation of these CpG sites and the levels of mRNA of the relevant genes or transcriptional activity. However, previous work supports Fibronectin as instrumental to extracellular matrix development as well as identifying the gene as a cartilage initiator. A correlation between Fibronectin, FGFR3 and RUNX2 was found in the prenatal and postnatal stages of development, the work of Ezura and colleagues (2009) found consistently low methylation levels of RUNX2 and FGFR3 before and after chondrocyte differentiation in mesenchymal stem cells (Ezura *et al.*, 2009). The amplicons targeted in the Ezura study differ from the ones designed for perinatal remains in this study. Ezura and colleagues (2009) targeted CpG sites 1000 bp upstream of the transcriptional start site (TSS) for both RUNX2 and FGFR3. The amplicons for our study started 156 bp upstream from TSS for FGFR3 and 1195 upstream of the TSS for RUNX2. Therefore, the amplicons selected for Ezura (2009) and the current studies differ. Despite the difference in study design and materials and methods, our results are complementary to those of Ezura and colleagues as low levels of RUNX2 and FGFR3 mRNA were found consistently throughout the gestational and postnatal ages. The results from future studies targeting multiple sites of the Fibronectin promoter would be interesting as we propose that Fibronectin, RUNX2 and FGFR3 operate within a network of osteogenesis

that where Fibronectin supports and facilitates the activity of RUNX2 and FGFR3, which are more active during osteoblast proliferation and differentiation (Pandit *et al.*, 2002; Mackie *et al.*, 2008; Michigami, 2013; McGee-Lawrence *et al.*, 2014; Su *et al.,* 2014; Qin *et al.*, 2015).

The murine work by Teplyuk and colleagues (2010) in part supports this hypothesis with the exception of Fibronectin which was not included in the study design. They propose that RUNX2 and FGFR3 form an ‘‘extracellular matrix (ECM)-related regulatory feed-back loop that controls osteoblast proliferation and execution of the osteogenic program” (Teplyuk *et al.*, 2010).

A limitation of this research is the sample base, number and problem with working with degraded nucleic acids. Indeed, the degrading effect of formalin preservation on tissues selected for molecular analyses has been comprehensively studied and the need for assay development has been stressed (Reid *et al.*, 2017). Some of the individuals included in this study were decomposed prior to fixation. As such, the genomic DNA was possibly damaged prior to enzymatic degradation during restriction digests. Our samples were not intact and therefore this potentially confounds some of our results regarding methylation level standards. Future studies should incorporate genomic DNA extracted at the various stages of endochondral ossification (mesenchymal – hypertrophic differentiation) from cell culture which would be subjected to the methylation protocol outlined in this study. This would provide insight into the role of these sites during development. The difference between methylation level percentages at each stage of the ossification process should be examined. Additionally the protein interaction between Fibronectin, FGFR3 and RUNX2 could be approached through the use of immunofluorescence and immunohistochemistry. The methylation percentage results from this study cannot be related to a specific age range and

therefore aren't supported as biomarkers for perinatal aging. However, from a fundamental perspective, these data support previous findings regarding gene expression analysis and encourages the investigation into the interaction of these growth and transcription factors, which have implications for perinatal molecular and clinical research.

4.6 Conclusion

When comparing the data of this research with previous work on anthropological and molecular aspects of bone development, this work provides a foundation for future inquiry into population specific biomarkers of growth and development. From the osteological perspective, new criteria have been proposed to assist in the forensic investigation of South African perinatal skeletal remains. The formation of a South African derived perinatal sample serves as a starting point for profiling the South African juvenile. As stated above, the routine use of postmortem RNA should be undertaken with caution. The development of a sex typing protocol targeting the G6PD and SRY loci provides a new PCR method for sex estimation of human remains from 25 mg of bone fragment. The efficiency of this protocol is of course reliant on the quality of genomic DNA. The results from the methylation level data can't be utilized in aging perinatal remains but fundamentally similar methylation levels across the dental age range as well as the correlation of transcripts at this developmental stage elicits questions about the nature of how these genes operate during gestation and postnatal life.

CHAPTER 5: REFERENCE LIST

Alqahtani, S.J., Hector, M.P. and Liversidge, H.M. (2010). Brief communication: The London atlas of human tooth development and eruption, *American Journal of Physical Anthropology*, 142(3), pp. 481–490.

Alqahtani, S.J., Hector, M.P. and Liversidge, H.M. (2014). Accuracy of dental age estimation charts: Schour and Massler, Ubelaker and the London Atlas, *American Journal of Physical Anthropology*, 154(1), pp. 70–78.

Alshihri, A.M., Kruger, E. and Tennant, M. (2015). Dental age assessment of Western Saudi children and adolescents, *The Saudi Dental Journal*. King Saud University, 27(3), pp. 131–136.

Antoine, D., Hillson, S. and Dean, M.C. (2009). The developmental clock of dental enamel: A test for the periodicity of prism cross-striations in modern humans and an evaluation of the most likely sources of error in histological studies of this kind, *Journal of Anatomy*, 214, pp. 45–55.

Aubin, J.E. (2008). Mesenchymal stem cells and osteoblast differentiation, in Bilezikian, J., Raisz, L., and Martin, T. J. (eds) *Principles of Bone Biology*. 3rd edn. Elsevier Science, pp. 85 - 107.

Axelsson, G. and Kiryeskari, P.(1984). Crown size of decidous teeh in Icelanders, *Acta Odontologica Scandinavica*, 42(6), pp.339-343.

Baek, J. E., Choi, J. Y. and Kim, J. E. (2014). Skeletal analysis and differential gene expression in Runx2/Osterix double heterozygous embryos, *Biochemical and Biophysical Research Communications*. Elsevier Inc., 451(3), pp. 442–448.

Bagnall, K. M., Harris, P. F. and Jones, P. R. (1977). A radiographic study of the human fetal spine, *Journal of Anatomy*, 124(3), pp. 791–802.

Bagnall, K. M., Harris, P. F. and Jones, P. R. (1982). A radiographic study of the longitudinal growth of primary ossification centers in limb long bones of the human fetus, *The Anatomical Record*, 203, pp. 293–299.

Bahar, B., Monahan, F. J., Moloney, A. P., *et al.* (2007). Long-term stability of RNA in post-mortem bovine skeletal muscle, liver and subcutaneous adipose tissues, *BMC Molecular Biology*, 8(1), p. 108.

Baker, J., Liu, J., Robertson, E.J., *et al.* (1993). Role of Insulin-like growth factors in embryonic and postnatal growth, *Cell*, 75, pp. 73–82.

Baker, B.J, Dupras, T.L. and Tocheri, M.W. (2005). *The Osteology of Infants and Children*.Texas Agricultural and Mechanical University Press, College Station, USA.

Barutcu, A. R., Tai, P.W.L., Gordon, W.H., *et al.* (2014). The bone-specific Runx2-P1 promoter displays conserved three-dimensional chromatin structure with the syntenic Supt3h

promoter, *Nucleic Acids Research*, 42(16), pp. 10360–10372.

Bauer, M., Gramlich, I., Polzin, S., *et al.* (2003). Quantification of mRNA degradation as possible indicator of postmortem interval — a pilot study, *Legal Medicine*, 5(4), pp. 220–227.

Bauer, M. (2007). RNA in forensic science', *Forensic Science International: Genetics*, 1(1), pp. 69–74.

Baylis, S. and Bassed, R. (2017). Precision and accuracy of commonly used dental age estimation charts for the New Zealand population, *Forensic Science International*, 277, pp. 223–228.

Bengston, R.G. (1935). A study of the time of eruption and root development of the permanent teeth between six and thirteen years, *Northwest University Bulletin*, 35, pp. 3–9.

Bidmos, M., Gibbon, V. and Štrkalj, G. (2010). Recent advances in sex identification of human skeletal remains in South Africa, *South African Journal of Science*, 106 (11/12), pp. 1–7.

Birth and Deaths Registration Act, 1992, No.51, s. 12, Cape Town: University of Pretoria and South African Legal Information Institute, available: http://www.chr.up.ac.za/undp/domestic/docs/legislation_55.pdf. (accessed 16 June 2018).

Black, T. K. (1978). Sexual dimorphism in the tooth-crown diameters of the deciduous teeth, *American Journal of Physical Anthropology*, 48, pp. 77-82.

Blenkin, M. and Taylor, J. (2012). Age estimation charts for a modern Austrialian population, *Forensic Science International*, 221, pp. 106-112.

Bocheva, G. and Boyadjieva, N. (2011). Epigenetic regulation of fetal bone development and placental transfer of nutrients: progress for osteoporosis, *Interdisciplinary Toxicology*, 4(4), pp. 167–172.

Boskey, A. L. (2007). Mineralization of bones and teeth, *Elements*, 3, pp. 387–393.

Braga, J. and Treil, J. (2007). Estimation of pediatric skeletal age using geometric morphometrics and three-dimensional cranial size changes, *International Journal of Legal Medicine*, 121, pp. 439–443.

Brown, T. (1978). Tooth emergence in Australian aboriginals. *Annals of Human Biology,* 5:41-54.

Brouwers, J. E. M., van Donklelaar, C.C., Sengers, B.G., *et al.* (2006). Can the growth factors PTHrP, Ihh and VEGF, together regulate the development of a long bone?, *Journal of Biomechanics*, 39, pp. 2774–2782.

Booth, T. J., Redfern, R.C. and Gowland, R. L. (2016) Immaculate conceptions: Micro-CT analysis of diagenesis in Ramano-British infant skeletons, *Journal of Archaeological Science*, pp. 1-11.

Burdi, A. R., Garn, S. M. and Miller, R. L. (1970). Developmental advancement of the male dentition in the first trimester, *Journal of Dental Research*, 49(4): pp. 889.

Cardoso, H. F. V. (2010). Testing discriminant functions for sex estimation from deciduous teeth. *Journal of Forensic Science*, 55(6), pp. 1557-1560.

Cardoso, H. F. V. Gomes, J., Campanacho, V., *et al.* (2013). Age estimation of immature human skeletal remains using the post-natal development of the occipital bone, *International Journal of Legal Medicine*, 127(5), pp. 997–1004.

Carneiro, C., Curate, F. and Cunha, E. (2016). A method for estimating gestational age of fetal remains based on long bone lengths, *International Journal of Legal Medicine*, 130(5), pp. 1333–1341.

Carter, L. E., Kilroy, G., Gimble, J.M., *et al.* (2012). An improved method for isolation of RNA from bone, *BMC Biotechnology*, 12(5), pp. 2–6.

Cazenave, M., Braga, J., Oettle, A., *et al.* (2017). Inner structural organization of the distal humerus in Paranthropus and Homo, *Comptes Rendus Palevol*, 16(5-6), pp. 521-532.

Cengiz, S., Ulukan, O., Ates, I., *et al.* (2006). Estimation of morphine in postmortem rabbit bone marrow and comparison with blood morphine concentrations, *Forensic Science International*, 156(2-3), pp. 91–94.

Christensen, F. C. and Rayburn, W. F. (1999). Fetal movement counts. *Obstetrics and Gynecology Clinics of North America*, 26, pp. 607–621.

Choi, S. C. and Trotter, M. (1970) A statistical study of the multivariate structure and race-sex differences of american white and negro fetal skeletons, *American Journal of Physical Anthropology*, 33, pp. 307–312.

Cope, I. and Murdoch, D. (1958) The estimation of foetal maturity, *International Journal of Obsetrics and Gynaecology*, 65(1), pp. 56–57.

Crelin, E.S. (1973). *Functional Anatomy of the Newborn.* New Haven, CT: Yale University Press.

Criminal Procedure Act, 1977, No. 51, s.239. Cape Town: Juta and Company, available: http://www.justice.gov.za/legislation/acts/1977-051.pdf. (accessed 16 June 2008).

Cunha, E., Baccino, E., Martrille, L., *et al.* (2009). The problem of aging human remains and living individuals: A review, *Forensic Science International*, 193(1-3), pp. 1–13.

Cunningham, C., Scheuer, L. and Black, S.(2016). *Developmental Juvenile Osteology* (2nd edn), Elsevier Academic Press.

de Andrés, M.C., Kingham, E., Imagawa, K., *et al.* (2013). Epigenetic regulation during fetal femur development: DNA methylation matters, *PLoS ONE*, 8(1), pp. e54957.

Delezoide, A. L., Benoist-Lassein, C., Legeai-Mallet, L., *et al.* (1998). Spatio-temporal

expression of FGFR 1, 2 and 3 genes during human embryo-fetal ossification, *Mechanisms of Development*, 77(1), pp. 19–30.

Demirjian, A. (1986). Dentition. In: *Human Growth,* 2nd Edition, Vol. 2. *Postnatal Growth* (E Falkner, E. and Tanner, J. M.Eds.), pp. 269-298. New York: Plenum Press.

Demirjian, A., Goldstein, H. and Tanner, J. M. (1973) A new system of dental age assessment., *Human Biology*, 45(2), pp. 211–227.

De Vries, J. I., Visser, G. H. and Prechtl, H. F. (1985). The emergence of fetal behaviour: II. Quantitative aspects, *Early Human Development*, 12, pp. 99–120.

De Vito, C. and Saunders, S. R. (1990). A discriminant function analysis of deciduous teeth to estimate sex. *Journal of Forensic Science*, 25, pp. 845-858.

Dhawan, V., Kapoor, K., Sharma, M., *et al.* (2014). Morphometry of fetal femora as an indication of gestational age, *European Journal of Anatomy*, 18(2), pp. 85–92.

Dong, X., Shen, B., Ruan, N., *et al.* (2014). Expression patterns of genes critical for BMP signaling pathway in developing human primary tooth germs, *Histochemistry and Cell Biology*, 142(6), pp. 657–665.

Duangto, P., Janhom, A, Prasitwattanaseree, S., *et al.* (2016). New prediction models for dental age estimation in Thai children and adolescents, *Forensic Science International*, 266, pp.1-5.

Ducy, P., Zhang, R., Geoffroy, V., *et al.* (1997). Osf2/Cbfa1: a transcriptional activator of osteoblast differentiation., *Cell*, 89(5), pp. 747–54.

Ducy, P., Starbuck, M., Priemel, M., *et al.* (1999). A Cbfa1-dependent genetic pathway controls bone formation beyond embryonic development, *Genes and Development*, 13, pp. 1025–1036.

Ezura, Y., Skiya, I., Koya, H., *et al. (*2009). Methylation status of CpG islands in the promoter regions of signature genes during chondrogenesis of human synovium-derived mesenchymal stem cells, *Arthritis and Rheumatism*, 60(5), pp. 1416–1426.

Faerman, M., Bar-Gal, G. K., Filon, D., *et al.* (1998). Determining the Sex of Infanticide Victims from the Late Roman Era through Ancient DNA Analysis, *Journal of Archaeological Science*, 25(9), pp. 861–865.

Fanning, E.A. (1961). A longitudinal study of tooth formation and root resorption, *New Zealand Dental Journal* 57: 202-217.

Fazekas, I.G., and Kosa, F.(1978). *Forensic Fetal Osteology,* Budapest: Akademiai Kiado, pp.1-287.

Fordyce, S. L., Kampmann, M. L., Van Doorn, N. L., *et al.* (2013). Long-term RNA persistence in post mortem contexts, *Investigative Genetics*, 4(7), pp. 1–7.

Franklin, D. (2010). Forensic age estimation in human skeletal remains: Current concepts and future directions, *Legal Medicine*, 12(1), pp. 1–7.

Franklin, D., Cardini, A., Flavel, A., *et al.* (2013). Concordance of traditional osteometric and volume-rendered MSCT interlandmark cranial measurements, *International Journal of Legal Medicine*, 127(2), pp. 505–520.

Frost, H. M. (1987). Bone "mass" and the "mechanostat": a proposal. *The Anatomical Record*, 219, pp. 1–9.

Gaballah, I. F., Shehab, A. M. and Bayoumi, K. A. (2014). Sex estimation in femurs of modern Egyptians: A comparative study between metric measurements and SRY gene detection, *Egyptian Journal of Forensic Sciences*, 4(4), pp. 109–115.

Garn, S. M. and Burdi, A. R. (1971). Prenatal ordering and postnatal sequence in dental development, *Journal of Dental Research*, 50, pp. 1407–1414.

Garn, S. M., Burdi, A. R., Babler, W. J. et al. (1975). Early prenatal attachment of adult metacarpal-phalangeal rankings and proportions, *American Journal of Physical Anthropology*, 43, pp. 367-332.

Garn, S. M., Lewis, A. B. and Polacheck, D. L. (1958) Variability of tooth formation, *Journal of Dental Research*, 38 (1), pp.135-148.

Garn, S. M., Lewis, A. B. and Blizzard, R. M. (1965a)Endocrine factors in dental development, *Journal of Dental Research*, 44, pp. 243–258.

Garn, S. M., Lewis, A. B. and Kerewsky, R. S. (1965b). Genetic, nutritional and maturational correlates of dental development, *Journal of Dental Research*, 44, pp. 228–242.

Garn, S. M., Lewis, A. B., Swindler, D. R. *et al.* (1967). Genetic control of sexual dimorphism in tooth size. *Journal of Dental Research*, 44, pp. 963-972.

Gibbon, V., Paximadis, M., Strkalj, G., *et al.* (2009). Novel methods of molecular sex identification from skeletal tissue using the amelogenin gene. , *Forensic Science International: Genetics*, 3,pp. 74-99.

Goldring, M. B., Tsuchimochi, K. and Ijiri, K. (2006). The Control of chondrogenesis, *Journal of Cellular Biochemistry*, 97, pp. 33–44.

Gorincour, G., Sarda-Quarello, L., Pierre-Eloi, L., *et al.* (2015). The future of pediatric and perinatal postmortem imaging, *Pediatric Radiology*, 45(4), pp. 509–516.

Gowland, R. L. and Chamberlain, A. T. (2002). A Bayesian approach to ageing perinatal skeletal material from archaeological Sites: Implications for the evidence for infanticide in Roman-Britain, *Journal of Archaeological Science*, 29(6), pp. 677–685.

Guibert, S., Forné, T. and Weber, M. (2009). Dynamic regulation of DNA methylation during mammalian development, *Epigenomics*, 1(1), pp. 81–98.

Guldberg, R. E., Lin, A. S., Coleman, R., *et al.* (2004).Micro-computed tomography imaging of skeletal development and growth, *Birth Defects Research*, 259(Part C), pp. 250–259.

Haavikko, K. (1973). The physiological resorption of the roots of deciduous teeth in Helsinki children, *Proceedings of the Finnish Dental Society,* 69, pp. 93-98.

Hannum, G., Guinney, J., Zhao, L., *et al.* (2013). Genome-wide methylation profiles reveal quantitative views of human aging rates, *Molecular Cell*, 49(2), pp. 359–367.

Harrast, S. D. and Kalkwarf, H. J. (1998). Effects of gestational age , maternal diabetes , and intrauterine growth retardation on markers of fetal bone turnover in amniotic fluid, *Calcified Tissue International*, 62, pp. 205–208.

Harris, E. F. and Lease, L. R. (2005). Mesiodistal tooth crown dimensions of the primary dentition: a worldwide survey, *American Journal of Physical Anthropology*, 128, pp. 593-607.

Heinrich, M., Matt, K., Lutz-Bonengel, S. and Schmidt, U. (2007). Successful RNA extraction from various human postmortem tissues, *International Journal of Legal Medicine*, 121(2), pp. 136–142.

Hess, A.E, Lewis, J.M. and Roman, B. (1932). A radiographic study of crowns of the teeth from birth to adolescence, *Dental Cosmos* 74, pp. 1053-1061.

Hill, A.H. (1939). Fetal age assessment by centres of ossification, *American Journal of Physical Anthropology*, 24, pp. 251-272.

Hjorten, R., Hansen, U., Underwood, R.A., *et al.* (2007). Type XXVII collagen at the transition of cartilage to bone during skeletogenesis, *Bone*, 148(4), pp. 825–832.

Horton, W. A. (2003). Skeletal development: insights from targeting the mouse genome, *Lancet*, 362(9383), pp. 560–569.

Hughes, J. M. and Petit, M. A. (2010). Biological underpinnings of Frost's mechanostat thresholds: the important roles of osteocytes, *Journal of Musculoskeletal Neuronal Interactions*, 10(2), pp. 128-135.

Hutchinson, E. F., Farella, M., Hoffman, J., *et al.* (2017). Variations in bone density across the body of the immature human mandible, *Journal of Anatomy*, 230(5), pp. 679–688.

Inquests Act, 1959, No. 58, Cape Town: Juta and Company, available: http://www.justice.gov.za/legislation/acts/1959-58.pdf. (accessed 16 June 2008).

Irish, J., Bratlund, B., Schild, R., *et al.*(2008). A late Magdalenian perinatal human skeleton from Wilczyce , Poland, *Journal of Human Evolution*, 55, pp. 736–740.

Iscan, M.J., and Steyn, M.(2013). *The Human Skeleton in Forensic Medicine*.3rd Edn.Charles C.Thomas, USA.

Jacobs, R., Hornsby, N. and Marais, S. (2014).Unwanted pregnancies in Gauteng and Mpumalanga provinces, South Africa: Examining mortality data on dumped aborted fetuses and babies, *South African Medical Journal*, 104 (12), pp. 864–869.

Jeffreys, A.J., Brookfield, J.F., Semeonoff, R. (1985). Positive identification of an immigration test case using human DNA fingerprints, *Nature*, 6;317(6040), pp. 818-9.

Jeffries, M. A., Donica, M., Baker, L. W., *et al.* (2014). Genome-wide DNA methylation study identifies significant epigenomic changes in osteoarthritic cartilage, *Arthritis and Rheumatology*, 66(10), pp. 2804–2815.

Johansson, N., Saarialho-Kere, U., Airola, K., *et al.* (1997). Collagenase-3 (MMP-13) is expressed by hypertropic chondrocytes, periosteal cells, and osteoblasts during human fetal bone development, *Developmental Dynamics*, 208, pp. 387–397.

Jones, M. J., Goodman, S. J. and Kobor, M. S. (2015). DNA methylation and healthy human aging, *Aging Cell*, 14(6), pp. 924–932.

Jung, M. and Pfeifer, G. P. (2015). Aging and DNA methylation, *BMC Biology*, 13(7), pp.1-7.

Kader, F. and Ghai, M. (2015). DNA methylation and application in forensic sciences, *Forensic Science International*, 249, pp. 255–265.

Karkhanis, S., Mack, P. and Franklin, D. (2015). Dental age estimation standards for a Western Australian population, *Forensic Science International*, 257, pp. 1-9.

Karsenty, G. and Wagner, E. F. (2002). Reaching a genetic and molecular understanding of skeletal development, *Developmental Cell*, 2, pp. 389–406.

Kawashita, M., Hasegawa, M., Kudo, T., *et al.* (2016). Effect of fibronectin adsorption on osteoblastic cellular responses to hydroxyapatite and alumina, *Materials Science and Engineering C*, 69, pp. 1268–1272.

Kim, H. J., Rice, D. P. C., Kettunen, P. J., *et al.* (1998). FGF-, BMP- and Shh-mediated signalling pathways in the regulation of cranial suture morphogenesis and calvarial bone development, *Development,* 125(7), pp. 1241–51.

Kimura, A., Inose, H., Yano, F., *et al.* (2010) Runx1 and Runx2 cooperate during sternal morphogenesis, *Development*, 137(7), pp. 1159–1167.

Kinaston, R. L. , Buckley, H. R., Halcrow, S. E., *et al.* (2009). Investigating foetal and perinatal mortality in prehistoric skeletal samples: a case study from a 3000-year-old Pacific Island cemetery site, *Journal of Archaeological Science*, 36(12), pp. 2780–2787.

KirIoglu, Z. and Ceyhan, D. (2012). Accuracy of different dental age estimation methods on Turkish children, *Forensic Science International*, 216, pp. 61–67.

Knight, B. and Saukko, P. (2004). *Knights Forensic Pathology*. 3rd edn. New York: Oxford University Press.

Komori, T., Yagi, H., Nomura, S., *et al.* (1997). Targeted disruption of Cbfa1 results in a complete lack of bone formation owing to maturational arrest of osteoblasts, *Cell*, 89, pp. 755–764.

Koppelkamm, A., Vennemann, B., Lutz-Bonengel, S., *et al.* (2011). RNA integrity in post-mortem samples: Influencing parameters and implications on RT-qPCR assays, *International Journal of Legal Medicine*, 125(4), pp. 573–580.

Kraus, B.S. and Jordan, R.E. (1965). *The Human Dentition before Birth.* London: Henry Kimpton.

Kristensen, L. S., Mikeska, T., Krypuy, M., *et al.* (2008). Sensitive melting analysis after real time-methylation specific PCR (SMART-MSP): High-throughput and probe-free quantitative DNA methylation detection, *Nucleic Acids Research*, 36(7), pp. 1-13.

Kristensen, L. S. and Hansen, L. L. (2009). PCR-based methods for detecting single-locus DNA methylation biomarkers in cancer diagnostics, prognostics, and response to treatment, *Clinical Chemistry*, 55(8), pp. 1471–1483.

Kronfeld, R. and Schour, I. (1939). Neonatal dental hypoplasia, *Journal of the American Dental Association*, 26, pp. 18–32.

Kuliwaba, J. S., Fazzalari, N. L. and Findlay, D. M. (2005). Stability of RNA isolated from human trabecular bone at post-mortem and surgery, *Biochimica et Biophysica Acta - Molecular Basis of Disease*, 1740(1), pp. 1–11.

Lalruatfela, B. (2013). On DNA methylation: an introductory review, *Science Vision*, 13(1), pp. 2–8.

Land, C. and Schoenau, E. (2008). Fetal and postnatal bone development: reviewing the role of mechanical stimuli and nutrition, *Best Practice and Research Clinical Endocrinology and Metabolism*, 22(1), pp. 107–118.

Lassen, C., Hummel, S. and Herrmann, B. (2015). Molecular sex identification of stillborn and neonate was not ("Traufkinder") from the burial site Aegerten, *Anthropologischer Anzeiger*, 1, pp. 1–8.

Lessard, S., Beaudoin, M., Benkirane, K., *et al.* (2015). Comparison of DNA methylation profiles in human fetal and adult red blood cell progenitors', *Genome Medicine*, 7(1), pp. 1-12.

Levanon, D. and Groner, Y. (2004). Structure and regulated expression of mammalian RUNX genes, *Oncogene*, 23(24), pp. 4211–4219.

Lewis, M. E. and Flavel, A. (2007). Age assessment of child skeletal remains in forensic contexts, in *Forensic Anthropology and Medicine: Complementary Sciences form recovery to cause of death* (Schmitt, A., Cunha, E. and Pinheiro, J. (eds), Humana Press Inc, Totowa, NJ.

Lewis, A.B, & Garn, S.M.(1960). The relationship between tooth formation and other maturation factors, *The Angle Orthodontist*, 30(2),pp. 70-77.

Lim, J. M., Hong, A. G., Raman, S., *et al.* (2000). Relationship between fetal femur diaphysis length and neonatal crown – heel length: the effect of race, *Ultrasound Obsetrics Gynaecology*, 15, pp. 131–137.

Liversidge, H. M., Lyons, F. and Hector, M. P. (2003). The accuracy of three methods of age estimation using radiographic measurements of developing teeth, *Forensic Science International*, 131, pp. 22–29.

Liversidge, H. M. and Molleson, T. (2004). Variation in crown and root formation and eruption of', *American Journal of anatomy*, 180, pp. 172–180.

Loeys, B. L., Chen, J., Neptune, E. R., *et al.* (2005). A syndrome of altered cardiovascular, craniofacial, neurocognitive and skeletal development caused by mutations in TGFBR1 or TGFBR2, *Nature genetics*, 37(3), pp. 275–81.

Logan, W. H. G. and Kronfeld, R. (1933). Development of the human jaws and surrounding structures from birth to the age of fifteen years, *The Journal of the American Dental Association*, 20(3), pp. 379–428.

Lombardi, C. M., Zambelli, V., Botta, G., et al. (2014). Postmortem micro computed tomography (micro CT) of small fetuses and hearts, *Ultrasound in Obstetrics and Gynecology*, 44, pp. 600-609.

Luke, D.A., Stack, M.V. and Hey, E.N. (1978). A comparison of morphological and gravimetric methods of estimating human foetal age from the dentition, *Development, Function and Evolution of Teeth* (Butler, P.M. and Joysey, K. A., Eds.), pp. 511-518. London: Academic Press.

Lysell, L. and Myrberg, N. (1982).Mesiodistal tooth size in the deciduous and permanent dentitions, *European Journal of Orthodontics*, 4(2), pp.113-122.

Maber, M., Liversidge, H. M. and Hector, M. P. (2006). Accuracy of age estimation of radiographic methods using developing teeth, *Forensic Science International*, 159(1), pp. 68–73.

Mackie, E. J., Ahmed, Y. A., Tatarczuch, L., *et al.* (2008). Endochondral ossification: How cartilage is converted into bone in the developing skeleton, *International Journal of Biochemistry and Cell Biology*, 40(1), pp. 46–62.

Mannucci, A., Sullivan, K. M., Pavel, L. et al. (1994). Forensic application of a rapid and quantitative DNA sex test by amplification of the X-Y homologous gene amelogenin, *International Journal of Legal Medicine*, 106, pp. 190-193.

Marini, M., Sarchielli, E., Toce, M., *et al.* (2012). Expression and localization of VEGF receptors in human fetal skeletal tissues, *Histology and histopathology*, 27(12), pp. 1579–87.

Margetts, B. and Brown, T.(1978). Crown diameters of the deciduous teeth in Australian Aboriginals, *American Journal of Physical Anthropology*, 48, pp.493-502.

Mays, S. and Eyers, J. (2011). Perinatal infant death at the Roman villa site at Hambleden , Buckinghamshire, England, *Journal of Archaeological Science*, 38(8), pp. 1931–1938.

McGee-Lawrence, M. E., Carpio, L. R., Bradley, E. W., *et al.* (2014). Runx2 is required for early stages of endochondral bone formation but delays final stages of bone repair in Axin2-deficient mice, *Bone*, 66, pp. 277–286.

Melo, M. and Ata-Ali, J. (2017). Accuracy of the estimation of dental age in comparison with chronological age in a Spanish sample of 2641 living subjects using the Demirjian and Nolla methods, *Forensic Science International*, 270, pp. 1-7.

Miao, D., Bin, H., Karaplis, A. C., *et al.* (2002). Parathyroid hormone is essential for normal fetal bone formation, *Journal of Clinical Investigation*, 109(9), pp. 1173–1182.

Michaud, C. L. and Foran, D. R. (2011). Simplified field preservation of tissues for subsequent DNA analyses, *Journal of Forensic Sciences*, 56(4), pp. 846–852.

Michigami, T. (2013). Regulatory mechanisms for the development of growth plate cartilage, *Cellular and Molecular Life Sciences*, 70, pp. 4213–4221.

Moore, G. E., Ishida, M., Demetriou, C., *et al.* (2015). The role and interaction of imprinted genes in human fetal growth, *Philosophical transactions of the Royal Society of London. Series B, Biological Sciences*, 370(1663), pp. 1-12..

Moorrees, C. F. A., Thomsen, S. O., Jensen, E. *et al.* (1957) Mesiodistal crown diameters of the deciduous and permanent teeth in individuals, Journal of Dental Research, 36, pp.39-47.

Moorrees, C. F. A., Fanning, E. A. and Hunt, E. E. (1963a). Age variation of formation stages for ten permanent teeth, *Journal of Dental Research*, 42(6), pp. 1490–1502.

Moorrees, C. F. A., Fanning, E. A. and Hunt, E. E. (1963b). Formation and Resorption of Three Deciduous Teeth in Children, *American Journal of Physical Anthropology*, 21, pp. 205–213.

Moss, M. L., Noback, Charles, R. and Robertson, G. G. (1956). Growth of Certain Human Fetal Cranial Bones, *American Journal of Anatomy*, 98(2), pp. 191–204.

Mutter, G. L. *et al.* (2004). Comparison of frozen and RNA*Later* solid tissue storage methods for use in RNA expression microarrays, *BMC Genomics*, 5(1), p. 88.

Nagaoka, T., Kawakubo, Y. and Hirata, K. (2012). Estimation of fetal age-at-death from the basilar part of the occipital bone, *International Journal of Legal Medicine*, 126(5), pp. 703–711.

Namgung, R. and Tsang, R. C. (2000). Factors affecting newborn bone mineral content : in utero effects on newborn bone mineralization, *Proceedings of Nutrition Society*, 59, pp. 55–63.

National Health Act, 2003, No.61, Cape Town: Government Gazette, available: http://www.chr.up.ac.za/undp/domestic/docs/legislation_55.pdf. (accessed 16 June 2018).

Neumann, K., Moegelin, A., Temminghoff, M., et al. (1997). 3D-computed tomography: a new method for the evaluation of fetal cranial morphology, *Journal of Craniofacial Genetics and Developmental Biology*, 17 (1), pp. 9-22.

Ngyende, A. (2012) *Statistical Release (Revised) Census 2011*. South Africa

Noback, Charles, R. (1944). The developmental anatomy of the human osseous skeleton during the embryonic fetal and circumnatal periods, *Anatomical Record*, 88, pp.99-125.

Noback, C. R. (1954). The appearance of ossification centers and the fusion of bones, *American Journal of Physical Anthropology*, 12, pp. 63–70.

Noback, C. R. and Robertson, G. G. (1951). Sequences of appearances of ossification centers in the human skeleton during the first five prenatal months, *American Journal of Anatomy*. 89, pp. 1-28.

Nolla, C. M. (1960). The development of the permanent teeth, *Journal of Dentistry for Children*, 27, pp. 254–266.

Nuzzo, S., Meneghini, C., Braillon, P., *et al.* (2003). Microarchitectural and physical changes during fetal growth in human vertebral bone, *Journal of Bone and Mineral Research*, 18(4), pp. 760–768.

Oest, M. E., Jones, J. C., Hatfield, C., et al. (2008). Micro-CT evaluation of murine fetal skeletal development yields greater morphometric precision over traditional clear staining methods, *Birth Defects Research (Part B)*, 83, pp. 582-589.

Olivares, I. J. and Aguilera, A. I. (2016a). Proposal of new regression formulae for the estimation of age in infant skeletal remains from the metric study of the pars basilaris, *International Journal of Legal Medicine*, 131(3), pp. 781–788.

Olivares, I. J. and Aguilera, A. I. (2016b). Validation of the sex estimation method elaborated by Schutkowski in the Granada osteological collection of identified infant and children: analysis of the controversy between the different ways of analyzing and interpreting the results, *International Journal of Legal Medicine*, 130, pp. 1623-1632.

Olsen, B. R., Reginato, A. M. and Wang, W. (2000). Bone Development, *Annual Review of Cell and Developmental Biology*, 16, pp. 191–220.

Opitz, L., Salinas-Riester, G., Grade, M., *et al.* (2010). Impact of RNA degradation on gene expression profiling, *BMC medical genomics*, 3, p. 36.

Ornitz, D. M. and Marie, P. J. (2002). FGF signaling pathways in endochondral and intramembranous bone development and human genetic disease, *Genes and Development*, 16, pp. 1446–1465.

Oxnard, C., Franklin, D., Cardini, A., *et al.* (2013). Morphometrics in forensic science : steps towards the development of population specific standards', *American Journal of Physical Anthropology*, 150, S56, p. 213.

Panchbhai, A. S. (2011). Dental radiographic indicators, a key to age estimation, *Dentomaxillofacial Radiology*, 40(4), pp. 199–212.

Pandit, S. G., Govinaraj, P., Sasse, J., *et al.* (2002). The fibroblast growth factor receptor, FGFR3, forms gradients of intact and degraded protein across the growth plate of developing bovine ribs, *The Biochemical Journal*, 361(Pt 2), pp. 231–41.

Pannier, S., Mugniery, E., Jonguoy, A., *et al.* (2010). Delayed bone age due to a dual effect of FGFR3 mutation in Achondroplasia, *Bone*, 47(5), pp. 905–915.

Patel, R. R., Steer, P., Doyle, P., *et al.* (2004). Does gestation vary by ethnic group? A London-based study of over 122 000 pregnancies with spontaneous onset of labour, *International Journal of Epidemiology*, 33(1), pp. 107–113.

Pavlovic, S., Pereira, C. P. and Vargas de Sousa Santos, R. F. (2017). Age estimation in Portuguese population: The application of the London atlas of tooth development and eruption', *Forensic Science International*, 272, pp. 97–103.

Perry, V. P., Stevenson, R. E., McFarland, W., *et al.* (1960). Motility studies of human postmortem bone marrow, *Blood*, 16, pp. 1020–1029.

Provot, S. and Schipani, E. (2005). Molecular mechanisms of endochondral bone development, *Biochemical and Biophysical Research Communications*, 328(3), pp. 658–665.

Pryse-Davies, J., Smitham, J. H. and Napier, K. A. (1974). Factors influencing development of secondary ossification centres in the fetus and newborn: A postmortem radiological study, *Archhives of Disease in Childhood*, 49, pp. 425–431.

Qin, X., Jiang, Q., Matsuo, Y., *et al.* (2015). Cbfb regulates bone development by stabilizing Runx family proteins, *Journal of Bone and Mineral Research*, 30(4), pp. 706–714.

Queiroz, D., Sakamoto, H. E. and Henrique, R. (2016). Dental Age Estimation Methods in Forensic Dentistry: Literature Review, *Peertechz Journal of Forensic Science and Technology*, 1, pp. 17–22.

Rauch, F. and Schoenau, E. (2001). The developing bone: slave or master of Its cells and Molecules?', *Pediatric Research*, 50(3), pp. 309–314.

Redfield, A. (1970) . A new aid to ageing immature skeltons: Development of the occipital bone', *American Journal of Physical Anthropology*, 33, pp. 207–220.

Reid, K. M., Maistry, S., Ramesar., R., *et al.* (2017). A review of the optimisation of the use of formalin fixed paraffin embedded tissue for molecular analysis in a forensic post-mortem setting, *Forensic Science International*, 280, pp. 181–187.

Regulations rendering of Forensic Pathology Service, 2007, In: National Health Act, 2003, No. 61, Cape Town: Staatskoerant (31), No. 30075.

Reppe, S., Datta, H. and Gautvik, K. M. (2015). The Influence of DNA methylation on bone cells, *Current Genomics*, 16(6), pp. 384–92.

Risnes, S. (1986). Enamel apposition rate and the prism periodicity in human teeth, *Scandinavian Journal of Dental Research*, 94, pp. 394–404.

Rissech, C. and Schaefer, M. (2008). Development of the femur — Implications for age and sex estimation, 180, pp. 1–9.

Robledo, R. F., Rajan, L., Li, X., *et al.* (2002). The Dlx5 and Dlx6 homeobox genes are essential for craniofacial, axial, and appendicular skeletal development, *Genes & Development*, 16(9), pp. 1089–1101.

Sampaio-Silva, F., Magalhaes, T., Carvalho, F., *et al.*(2013) Profiling of RNA degradation for estimation of post mortem Interval, *PLoS ONE*, 8(2).pp.1-8.

Sanders, J. E. (2009). *Age estimation of fetal skeletal remains from the forensic context*. Masters thesis: University of Montana, USA.

Schaefer, M., Black, S. and Scheuer, L. (2009) *Juvenile Osteology: A Lab and Field Manual*. San Diego, Academic Press.

Scheuer, J. L., Musgrave, J. and Evans, S. (1980). The estimation of late fetal and perinatal age from limb bone length by linear and logarithmic regression, *Annals of Human Biology*, 7(3), pp. 257–265.

Scheuer, L. and Black, S. (2004). *The Juvenile Skeleton*, London, Academic Press.

Scheuer, L. (2002). Application of osteology to forensic medicine, *Clinical Anatomy*, 15(4), pp. 297–312.

Scheuer, L. and Black, S. (2000). *Developmental Juvenile Osteology*. San Diego, Academic Press.

Scheuer, L. and Maclaughlin-black, S. (1994). Age Estimation from the pars basilaris of the fetal and juvenile occipital bone', *International Journal of Osteoarchaeology*, 4, pp. 377–80.

Schneider, E., Dittrich, M., Bock, J., *et al.* (2016). CpG sites with continuously increasing or decreasing methylation from early to late human fetal brain development, *Gene*, 592(1), pp. 110–118.

Schour, I. and Massler, M. (1941) .Development of the human dentition, *Journal of the American Dental Association*, 28, pp. 1153–1160.

Schutkowski, H. (1993). Sex estimation of infant and juvenile skeletons: Morphognostic features. *American Journal of Physical Anthropology*, 90, pp. 199–205

Sherwood, R. J., Meindl, R. S., Robinson, H. B., *et al.* (2000). Fetal age: methods of estimation and effects of pathology, *American Journal of Physical Anthropology*, 315, pp. 305–315.

Sidova, M., Tomonkova, S., Abaffy, P., *et al.* (2015). Effects of post-mortem and physical degradation on RNA integrity and quality, *Biomolecular Detection and Quantification*, 5, pp. 3–9.

Singh, P. and Schwarzbauer, J. E. (2012). Fibronectin and stem cell differentiation - lessons from chondrogenesis, *Journal of Cell Science*, 125(16), pp. 3703–3712.

Sinha, K. M. and Zhou, X. (2013). Genetic and molecular control of osterix in skeletal formation, *Journal of Cellular Biochemistry*, 114(5), pp.975-984.

Sletner, L., Rasmussen, S., Jennum, A. K., *et al.* (2015). Ethnic differences in fetal size and growth in a multi-ethnic population, *Early Human Development*, 91(9), pp. 547–554.

Slieker, R. C., Roost, M. S., Van Iperen, L., *et al.* (2015). DNA methylation landscapes of human fetal development, *PLoS Genetics*, 11(10), pp. 1–19.

Smith, H. B. (1991). Standards of tooth formation and dental age assessment, In *Advances in Dental Anthropology* (Kelley, M. A. and Larsen, C. S., Eds.), pp. 143–168.New York: Wiley-Liss.

St Jacques, B. and Helms, J. (2003). Prenatal Bone Development: Ontogeny and Regulation, in *Pediatric Bone: Biology and Diseases* (Glorieux, F. H., Pettifor, J. F., and Jüppne, H., eds.) , pp. 77–117. Academic Press.

Stone, A. C., Milner, G. R., Paabo, S., et al. (1996). Sex estimation of ancient human skeletons using DNA, *American Journal of Physical Anthropology*, 99, pp. 231-238.

Stroud, J. L., Buschang, P. H., Goaz, P. W. (1994). Sexual dimorphism in mesiodistal dentin and enamel thickness, *Dentomaxillofacial Radiology*, 23, pp. 169- 171.

Su, N., Jin, M. and Chen, L. (2014). Role of FGF/FGFR signaling in skeletal development and homeostasis: learning from mouse models, *Bone Research*, 2, pp. 14003.

Sunderland, E. P., Smith, C. J. and Svnderlasd, R. (1987). A histological study of the chronology of initial mineralization in the human deciduous dentition, *Archives in Oral Biology*, 32(3), pp. 167–174.

Tanner, J.M. (1962). *Growth at Adolescence,* 2nd edn. Oxford: Blackwell Scientific.

Teplyuk, N. M., Haupt, L. M., Ling, L., *et al.* (2010). The osteogenic transcription factor Runx2 regulates components of the fibroblast growth factor/proteoglycan signaling axis in osteoblasts, *Journal of cell Biochemistry*, 107(1), pp. 144–154.

Thamamongood, T.A., Furuya, R., Fukuba,S., et al.(2012). Expression of osteoblastic and osteoclastic genes during spontaneous regeneration and autotransplantation of gold fish scale: A new tool to study intramembranous bone regeneration, *Bone*., 50(6), pp. 1240–1249.

du Toit-Prinsloo, L., Dempers, J. J., Wadee, S. A., *et al.* (2016). The medico-legal investigation of abandoned fetuses and newborns—a review of cases admitted to the Pretoria Medico-Legal Laboratory, South Africa, *International Journal of Legal Medicine*, 130(2), pp. 569–574.

Tost, J. (2010). DNA methylation: An introduction to the biology and the disease-associated changes of a promising biomarker, *Molecular Biotechnology,* 44(1), pp. 71–81.

Turp, C. and Alt, K. W. (1998). Anatomy and morphology of human teeth', In *Dental Anthropology* (Alt K.W., Rosing F.W., Teschler-Nicola M.(eds). Springer, Vienna.

Ubelaker, D.H. (1978). *Human Skeletal Remains: Excavation, Analysis and Interpretation.* Washington, DC: Smithsonian Institute Press.

Ubelaker, D.H. (1989). The estimation of age-at-death from immature human bone, *Age markers in the Human Skeleton*, pp.55-70, Charles C. Thomas: Springfield, Ill.

Ubelaker, D. (2005). Estimating age-at-death , in *Forensic Medicine of the Lower Extremity: Human Identification and Trauma Analysis* (Rich, J., Dean, D.E., Powers, R. H. (eds.), pp. 99–112. Totowa, NJ: The Humana Press inc.

Ubelaker, D. H. and Degaglia, C. M. (2017). Population variation in skeletal sexual dimorphism, *Forensic Science International*, 278, p. 407.e1-407.e7.

Unterscheider, J., Geary, M. P., Daly, S., *et al.* (2013).The customized fetal growth potential: A standard for Ireland, *European Journal of Obstetrics Gynecology and Reproductive Biology*, 166(1), pp. 14–17.

Van Doorn, N. L., Wilson, A. S., Willerslev, E., Gilbert, T. P. (2011). Bone marrow and bone as a source for postmortem RNA, *Journal of Forensic Sciences*, 56(3), pp. 720–725.

Verbruggen, S. W., Loo, J. H. W, Hayat, T. T. A., et al. (2016). Modeling the biomechanics of fetal movements, *Biomechanics and Modeling in Mechanobiology*, 15, pp. 995-1004.

Vidisdottir, S. R. and Richter, S. (2015). Age estimation by dental developmental stages in children and adolescents in Iceland, *Forensic Science International*, 257(1), pp. 518.e1-518.e7.

Vimalraj, S., Arumugam, B., Miranda, P.J., *et al.* (2015). Runx2: Structure, function, and phosphorylation in osteoblast differentiation, *International Journal of Biological Macromolecules*, 78, pp. 202–208.

Vlak, D., Roksandic, M., Schillaci, M. A. (2008). Greater sciatic notch as a sex indicator in juveniles. *American Journal of Physical Anthropology*, 137, pp. 309–315.

Wagner, E. F. and Karsenty, G. (2001). Genetic control of skeletal development, *Current Opinion in Genetics & Development*, 11(5), pp. 527–32.

Wang, L., Lin, S., Zhang, J., *et al.* (2017). Fetal DNA hypermethylation in tight junction pathway is associated with neural tube defects: A genome-wide DNA methylation analysis, *Epigenetics*. Taylor & Francis, 12(2), pp. 157–165.

Wang, R. N., Green, J., Wang, Z., *et al.* (2014). Bone morphogenetic protein (BMP) signaling in development and human diseases', *Genes & Diseases*. Elsevier Ltd, 1(1), pp. 87–105.

Weaver, D. (1998). Forensic aspects of foetal and neonatal skeletons, in *Forensic Osteology: Advances in the identification of human remains*, 2nd edn (Reichs, K. J., (eds), pp. 187–195. Charles C Thomas.

Weiss, R. E. and Reddi, A. H. (1981). Appearance of fibronectin during the differentiation of cartilage, bone, and bone marrow, *Journal of Cell Biology*, 88(3), pp. 630–636.

White,T.D., and Folkens, P.A.(2005). *The Human Bone Manual*, Academic Press.

Willems, G., Van Olmen, A., Spiessens, B., et al. (2001). Dental age estimation in Belgian children: Demirjian techniques revisited, *Journal of Forensic Science*, 46(4), 893-895.

Wilson, L. A., Macleod, N. and Humphrey, L. T. (2008). Morphometric criteria of sexing juvenile human skeletons using the ilium, *Journal of Forensic Science*, 53 (2), pp. 269-276.

Wigglesworth, J.S and Singer, D.B (1991). *Textbook of Fetal and Perinatal pathology.* Blackwell Scientific Publications.

Winkelmann, C. T. and Wise, L. D. (2009). High-throughput micro-computed tomography imaging as a method to evaluate rat and rabbit fetal skeletal abnormalities for developmental toxicity studies, *Journal of Pharmacological and Toxicological Methods*, 59, pp. 156-165.

Yang, J., Andre, P., Ye, L., *et al.* (2015). The Hedgehog signalling pathway in bone formation, *International Journal of Oral Science*, 7(2), pp. 73–79.

Yasojima, K., Mcgeer, E. G. and Mcgeer, P. L. (2001). High stability of mRNAs postmortem and protocols for their assessment by RT-PCR, *Brain Research Protocols,* 8, pp. 212–218.

Yi, S., Xu, L. C., Mei, K., *et al.* (2014). Isolation and identification of age-related DNA methylation markers for forensic age-prediction, *Forensic Science International: Genetics*, 11(1), pp. 117–125.

Zadzinska, E., Karasinska, M., Jedrychowska-Danska, K., *et al.* (2008). Sex diagnosis of subadult individuals from medieval polish archaeological sites: metric analysis of deciduous dentition, *Homo-Journal of Comparative Human Biology*, 59(3), pp. 175-187.

Zollinger, A. J. and Smith, M. L. (2017). Fibronectin, the extracellular glue, *Matrix Biology*. International Society of Matrix Biology, 60–61, pp. 27–37.

Zubakov, D., Liu, F., Kokmeijer, I., *et al.* (2016). Human age estimation from blood using mRNA, DNA methylation, DNA rearrangement, and telomere length', *Forensic Science International: Genetics*, 24, pp. 33–43.

Zumpano, M. P. and Richtsmeier, J. T. (2003). Growth-related shape changes in the fetal craniofacial complex of humans (*Homo sapiens*) and pigtailed macaques (*Macaca nemestrina*): a 3D-CT comparative analysis, *American Journal Physical Anthropology*, 120, pp. 339–351.

Appendix A: Method optimization and development

Materials

General and specialized reagents

General reagents and consumables were purchased from Saarchem (Merck, South Africa) or Sigma Aldrich or from Lasec (South Africa). The SW480 male colon cancer cell line (ATTC CCL-228C) was obtained from the European Collection of Authenticated Cell Cultures (ECACC), while JM109 and DH5α competent cells were from the laboratory stocks of the Biomedical Biotechnology Research Unit at Rhodes University. Tri Reagent (# T9424), Dimethyl sulfoxide (DMSO #D8418) and Ethidium bromide (#E8751-1G) were purchased from Sigma Aldrich.

The Direct-Zol mini prep kit (Zymo Research #R2050), Zymoclean DNA recovery kit (Zymo Research #ZR D4008), Quick-gDNA miniprep kit (Zymo Research #D3006), Zyppy miniprep plasmid kit (Zymo Research #D4020), Genejet Gel extraction kit (Inqaba Biotec #FE K0692), DNA clean and concentrator kit (Zymo #D4003) and *Hin*dIII and *Eco*RI restriction enzymes (NEB #R0104S & R0101S) were purchased from Inqaba Biotec (South Africa). Methylation Specific Restriction Enzymes (*Hpych4*IV #R06195, *Hpa*II #R01715, *Scrf*I #R0110S, *Aci*I #R0551S) and Cutsmart Buffer (#B72045) were purchased from New England Biolabs. Nuclease free water for molecular biology (ThermoScientific #R0581), InsTAclone PCR cloning kit (ThermoScientific #K1213), 6x DNA Loading Dye (ThermoScientific #R0611), 100 bp ladder (Invitrogen #15628-019), Revert Aid H Minus First Strand cDNA synthesis kit (#k1651), RNAlater (ThermoScientific #AM7020) and Buffer R 10x (ThermoScientific #BR5) were purchased from Life Technologies (South Africa). The GoTaq green mastermix (Promega #M7122) and Bovine Serum Albumin (BSA) (Promega #R396D) were purchased through Anatech (South Africa). Seakem agarose

(Lonza #50004) and RNAse Away (#MBP-7000) were purchased from Whitesci Scientific (South Africa). Kapa universal marker (Kapa Biosystems # KL6303) and Kapa SYBR Fast qPCR mastermix (Kapa Biosystems #D4003) were purchased through Lasec or Sigma-Aldrich (South Africa). Liquid nitrogen was procured through the Department of Chemistry, Rhodes University. A sample kit of the Isolate II DNA/RNA/Protein kit (Bioline) was supplied by Celtic Molecular Diagnostics (South Africa).

Primer design

Glyceraldehyde 3-phosphate dehydrogenase (GAPDH), Actin, Glyceraldehyde 3-phosphate dehydrogenase (G6PD), sex-determining region Y (SRY), Beta Actin, CD4, Runt regulated transcription factor 2 (RUNX2), Fibroblast Growth Factor Regulator 3 (FGFR3) and Fibronectin (FN1) primers and qPCR primers were purchased from Integrated DNA technologies (IDT). For custom primers, these were designed in house using the mRNA transcript (for expression analysis) or genomic DNA (for methylation analysis) of the genes selected. Sequences were acquired from the NCBI database (www.ncbi.nlm.nih.gov) and confounding variables such as temperature hairpins, homodimers and compatibility of forward and reverse amplicons were validated using the IDT Oligoanalyser (www.idtdna.com/calc/analyzer). Table 8 details information regarding primer sequences and amplicons.

Table 8: Primers designed and used in the study

Species	Gene	Direction	Sequence of Primers 5' to 3'	Product Length (bp)	Genbank accession#	Application
Homo Sapiens (Human)	G6PD	Forward	GCAACAGATACAAGAACGTGAAGCT	191	NM_001042351.2	Sex Typing
		Reverse	GCCTCGGCTGCCATAAATATAGG			
	SRY	Forward	CTGGCACCTTTCAATTTTGTCG	556	NM_003140.2	Sex Typing
		Reverse	GTGTGGCTTTCGTACAGTCATC			
	RUNX2	Forward	CTTCACAAATCCTCCCAAGT	129	NM_001015051	Gene Expression Analysis
		Reverse	AGGCGGTCAGAGAACAAAC			
	FGFR3	Forward	GTACTGTGCCACTTCAGTGT	145	NM_022965	Gene Expression Analysis
		Reverse	CCAGCAGCTTCTTCTCCATC			
	FN1	Forward	CCTCAGAAGTGCAATCAGTGT	120	NM_212482	Gene Expression Analysis
		Reverse	TATGAGCAGGACCAGAAATACTC			
	RUNX2_1	Forward	TACTAACATGTCCCCAGAGAGG	311	NM_001015051	Methylation Patterning
		Reverse	CCTGCATGTAATTTTTGGACCAGG			
	RUNX2_2	Forward	CCTAGCCCTTACCTCCCTGCAC	227	NM_001015051	Methylation Patterning
		Reverse	GTTTTCATCAGTTGGGAGCGATGG			
	FGFR3_1	Forward	CATGTCCTCACCCCTTGCAGCCCTCTG	286	NM_022965	Methylation Patterning
		Reverse	AAGGCTCCAGGGAAGATC			
	FGFR3_2	Forward	GGAATGCCGTCCTGCCCTC	420	NM_022965	Methylation Patterning
		Reverse	CAGCCAGTGGGGGACGGTC			
	FN1_1	Forward	GATAATGCAGGTCCTAGGGAAAG	187	NM_212482	Methylation Patterning
		Reverse	CTTCCTCTAGATCGTTCTGCCTTGC			
	FN1_2	Forward	GTGCATGCATGTAAGCAGTGCC	343	NM_212482	Methylation Patterning
		Reverse	GGTTCATGCCTGTAATCCCAGCAC			

Gallus Gallus (Chicken)	Beta Actin	Forward Reverse	GATGGACTCTGGTGATGGTGTTAC GTGGCCATCTCCTGCTCGAAATC	207	NM_205818.1	RNA Stability
Cercopithecus pygerythrus (Monkey)	CD4	Forward Reverse	GAATTGCTGGTGTTCGGATTG CCCTTGGACTCCTACATTTCAC	124	NM_AF001227.1	RNA Stability

Methods

Generation of Plasmids for sex typing controls

The molecular sex typing assay was developed to use specific amplification of regions from genes on the X (glucose-6-phosphate dehydrogenase/G6PD) and Y (sex-determining region Y/SRY) chromosomes. Plasmids containing a portion of the coding regions of the X-linked G6PD and Y-linked SRY genes were generated to function as positive controls in these assays. To generate plasmids for positive controls in sex typing, RNA and gDNA were isolated from the SW480 (male) cell line and used as the template for PCR-based amplification of the sex-specific amplicons. The G6PD primers were designed to amplify a 198 bp fragment, while the SRY primers amplified a 556 bp fragment (see primer design).

A confluent T25 flask of SW480 colon cancer cells were lysed in 500 µl of Tri Reagent prior to RNA purification, gDNA isolation and cDNA synthesis (see First strand synthesis of cDNA). Amplicons using primers designed against the G6PD (X chromosome amplicon) and SRY (Y chromosome amplicon) genes were amplified with PCR. The cDNA mixture (2 µl) or genomic DNA (100 ng) was used as a template for PCR amplification. PCR reactions consisted of 10 µM forward and reverse primers (Table 8) and GoTaq mastermix in 25 µl volumes and were subject to an initial denaturation of 2 minutes at 95°C, and 30 cycles of 95 °C denaturation for 30s, a gradient annealing for 30s at 52°C, 55.1°C, 56.9 °C and 60 °C followed by a 72 °C extension for 1 minutes and a final extension of 72 °C for 5 minutes. PCR products were visualized by ethidium bromide (10 µg/ml) staining on 0.8 % w/v agarose gel in TAE (40 mM Tris base, 20 mM Acetic acid and 1 mM Ethylenediaminutesetetraacetic acid [pH 8.0]). Optimisation of amplification of the SRY locus required addition of stabilization agents in PCR reactions (0.5 µg/µl of BSA or DMSO) with a concentration of template gDNA of 200 ng. A final gradient PCR at the annealing

temperatures of 55°C, 56.9°C, 61 °C and 65 °C was conducted. These SRY PCR reactions (100 ng template DNA, 10 µM primers, GoTaq mastermix containing 1x reaction buffer (pH 8.5), 400 µM dATP, 400 µM dGTP, 400 µM dCTP, 400 µM dTTP and 3 mM $MgCl_2$) were conducted in 50 µl reactions with BSA (0.5mg) for an initial denaturation of 2 minutes at 95 °C and 40 cycles of 95 °C denaturing for 30s, annealing for 30s at the different temperatures and a 72 °C extension for 1 minutes followed with a final extension of 72 °C for 5 minutes. Results were visualized by an ethidium bromide (10 µg/ml) stained 0.8 % w/v agarose gel in TAE.

DNA gel extractions of the G6PD and SRY PCR amplicons were performed using the Zymoclean DNA gel recovery kit as per the manufacturer's instructions. DNA purity and quality was confirmed via absorbance at 260, 280 and 230 nm using the Nanodrop 2000 spectrophotometer and stored at -20 °C until used. The isolated PCR product from the gel extraction was ligated into the pTZ57R vector by TA cloning following the manufacturer's instructions for the InsTAclone PCR cloning kit. The ligation was left to incubate overnight at 22 °C before transformation into *E.coli* JM109 or DH5α competent cells. 2xYT agar plates (1.6 % w/v Tryptone, 1 % w/v yeast extract, 0.5 % w/v NaCl, 1.5 % w/v agar) inoculated with ampicillin (100 µg/ml) were spread with diluted and concentrated volumes of transformation and incubated overnight at 37 °C. A single colony was used to inoculate liquid cultures in 2xYT broth (50ml - 0.5g Tryptone, 0.25g yeast extract, 0.5g NaCl) and plasmids were extracted using the Zyppy miniprep plasmid extraction kit according to manufacturer's instructions and screened by PCR for the presence of the SRY and G6PD inserts. A total of 50 µl PCR reactions (100 ng template DNA, 10 µM primers, GoTaq mastermix containing 1x reaction buffer pH 8.5, 400 µM dATP, 400 µM dGTP, 400 µM dCTP, 400 µM dTTP and 3 mM $MgCl_2$) were run at an initial denaturation of 2 minutes at 95° C

and 30 cycles of 95° C denaturing for 30 s, annealing for 30 s at 56.9° C and a 72° C extension for 1 minutes followed with a final extension of 72° C for 5 minutes. BSA (0.5mg) was included for the SRY reactions. Results were visualized by an ethidium bromide (10 µg/ml) stained 0.8 % w/v agarose gel in TAE.

A double restriction digestion was conducted to confirm the presence of the inserts. Enzymes *Hin*dIII and *Eco*R1 (10 U) were used in 10 µl reactions with 1x RE buffer, nuclease free water and 100 ng of plasmid DNA. Each reaction was incubated at 37° C for 3 hours. Reactions were stopped with loading dye (6x) (10 mM Tris-HCl pH 7.6 0.03 % w/v bromophenol blue, 0.03 % w/v xylene cyanol FF, 60 % v/v glycerol, 60 mM EDTA) and stored at 4° C until analysis by ethidium bromide staining on an 0.8 % (w/v) agarose gel in TAE. Plasmids were confirmed by Sanger sequencing (Inqaba Biotec).

Generation of plasmids for gene expression assay controls

For RUNX2 and FGFR3 and FN1 plasmid standards for qPCR, cDNA for TA cloning was obtained from RNA isolated from HEK293T cell line or using the FN1 plasmid (FN-YPet) which was a kind gift of Harold Erickson. Amplicons of human RUNX2 AND FGFR3 transcripts were produced using qPCR Primers (IDT) in a gradient PCR. A total of 100 ng of the cDNA derived from HEK293T cell line RNA was used as the template. PCR reactions (100 ng template DNA, 10 µM primers, GoTaq mastermix containing 1x reaction buffer pH 8.5, 400 µM dATP, 400 µM dGTP, 400 µM dCTP, 400 µM dTTP and 3mM $MgCl_2$) in 25 µl volumes were subject to an initial denaturation of 2 minutes at 95° C, and 30 cycles of 95° C denaturing for 30 s, a gradient annealing for 30 s at 60° C, 58° C, 53° C and 50° C followed by a 72° C extension for 1 minutes and a final extension of 72 ° C for 5 minutes. PCR products were visualized by an ethidium bromide (10 µg/ml) stained 0.8 % w/v agarose gel in TAE.

To clone the amplicons of RUNX2 and FGFR3, PCR fragments were cleaned using the DNA clean and concentrator kit (Zymo) according to manufacturer's instructions. The PCR products were ligated into the pTZ57R vector by TA cloning following the manufacturer's instructions for the InsTAclone PCR cloning kit. The ligation was left to incubate overnight at 22° C before transformation into *E. coli* JM109 competent cells. 2xYT agar plates containing ampicillin (100µg/ml) were spread with diluted and concentrated amounts of the DNA transformation and incubated overnight at 37° C. Single colonies were used to inoculate liquid 2xYT broth cultures and plasmids were extracted using the Zyppy miniprep plasmid extraction kit according to manufacturer's instructions and screened by double restriction digest for the presence of the RUNX2 and FGFR3 inserts. Enzymes *Hin*dIII and *Eco*R1 (10 U) were used in 10 µl reactions with 1x Cutsmart buffer, nuclease free water and 100 ng of plasmid DNA. Each reaction was incubated at 37° C for 3 hours. Reactions were stopped with loading dye (6 xs) and stored at 4° C until analysis by ethidium bromide staining (10 µg/ml) on a 0.8 % (w/v) agarose gel in TAE.

Sex typing protocol optimization

For protocol optimization using G6PD (X chromosome linked) and SRY (Y chromosome linked) primers a concentration of 300 ng of perinatal RNA was used in cDNA reactions. A volume of 2µl of this was added as a template in the optimized PCR of 50 µl. Troubleshooting and optimization included separate PCR reactions which were set up with cDNA template volumes of either 1 (from 60 ng RNA) or 4 µl (from 15 ng RNA), number of cycles gradient (38, 36, 34 and 32), addition of BSA (0.5 mg) and $MgCl_2$ (1 mM) for both primer sets, primer concentration gradient of 100 µM, 50 µM or 10 µM and gDNA (100 ng) instead of cDNA as template.

The sex typing PCR protocol was optimized using genomic DNA. Reactions were set up with a 100 ng gDNA template, 100 µM primers, GoTaq mastermix containing 1x reaction Buffer pH 8.5, 400 µM dATP, 400 µM dGTP, 400 µM dCTP, 400 µM dTTP and 4 mM $MgCl_2$) in 50 µl reactions with parameters of initial denaturation for 2 minutes at 95 °C, followed by 32 cycles of 95 °C for 30 s, 56.9 °C for 30 s and 72 °C extension for 1 minutes, and then a final extension of 72 °C for 5 minutes. Results were visualized by an ethidium bromide (10 µg/ml) stained 0.8 % w/v agarose gel in TAE (data not shown).

Region specific methylation protocol optimization

Primers were designed to amplify selected regions containing putative CpG sites in the promoter regions of the genes included in the study. The schematic of enzyme degradation at CpG sites included in amplicons (Figure 34) details the two sites per gene which were targeted by RT-qPCR. Degradation is only possible if the CpG sites are unmethylated. The representation in Figure A1 shows the CpG sites in the selected regions that overlap the MSREs target sequences in the FN1, RUNX2 and FGFR3 promoters during restriction digest incubation. The MSREs *Aci*I and *Hpa*II degrade gDNA for the selected region of the Fibronectin promoter. For FGFR3 and RUNX2 the MSRE *Hpych4*IV and *Scrf*I target CpG sites within the selected amplicons. Primers were designed upstream of the Transcriptional Start Site (TSS +1) starting at -156 bp (FGFR3_1), -24 bp (FN1_1) and -1195 bp (RUNX2_1). The amplicons at the predicted molecular weight selected for RT-qPCR amplification were 286 bp (FGFR3_1), 187 bp (FN1_1) and 311 bp (RUNX2_1).

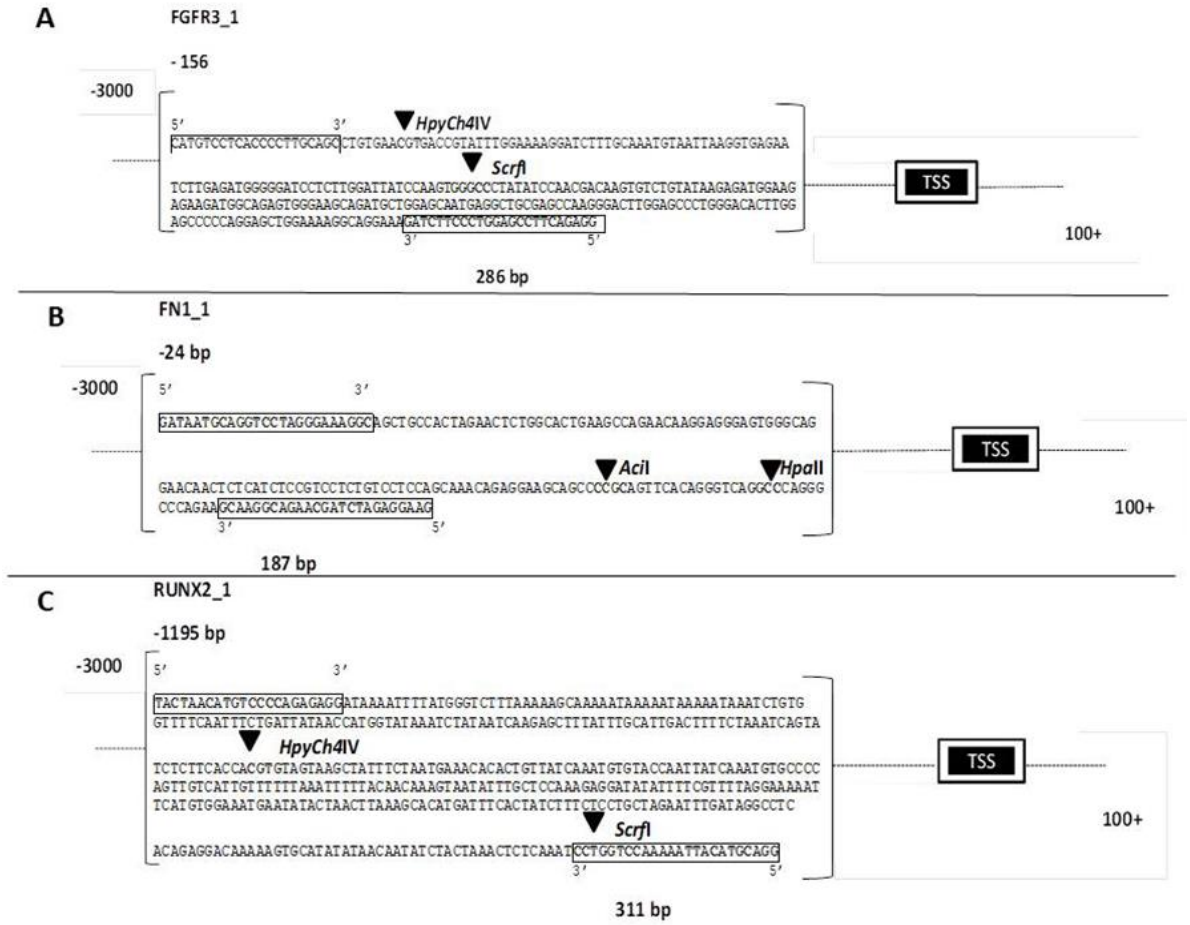

Figure 34: Schematic presentation of CpG sites within the amplicons of FGFR3_1, FN1_1 and RUNX2_1. Promoter regions encompassing -3000 and +100 relative to the Transcriptional Start Site (TSS, +1) of the FN1, FGFR3 and RUNX2 genes were analysed for CpG sites and methylation sensitive restriction enzyme (MSRE) sites. Primer binding sites for amplification of regions containing MSRE are indicated in brackets. Two CpG sites were included per amplicon. The target sequences for MSRE (HpaCh4IV, ScrfI, AciI and HpaII) in the selected regions are shown with black arrowheads.

A gradient PCR was set up to establish the optimal annealing temperature for the methylation specific primers. SW480 cell line derived cDNA from 100 ng of RNA was used as a template. Reactions (25 µl) were set up with GoTaq mastermix (12.5 µl), forward and reverse primers (10 µM) and nuclease free water (8.5 µl). Reactions were subject to an initial denaturation of 2 minutes at 95 °C and 30 cycles of 95 °C denaturing for 30 s, gradient annealing for 30 s at 60 °C, 58 °C, 53.8 °C and 50 °C, followed by a 72 °C extension for 1 minute with a final extension of 72 °C for 5 minutes. Results were visualized by an ethidium bromide (10 µg/ml) stained 0.8 % w/v agarose gel in TAE.

Results

Plasmid controls

Sex Typing

Figures 35 and 36 represent the generation of plasmids for positive controls for sex typing of perinatal remains with the X-linked G6PD and Y-linked SRY genes.

For the X chromosome, a PCR product at approximately 200 bp, corresponding to the predicted size of the X-linked G6PD amplicon, was detected in lanes which contained samples from the test reactions (Figure 35A). The lanes containing control reactions lacking template did not show any bands, suggesting specific amplification of the PCR product. The PCR reactions using the primers designed from the X-linked G6PD gene produced a product (191 bp) at all four annealing temperatures (60, 56.9, 55.1, 52 °C) tested (Figure 35A). The PCR products were ligated into the pTZ57R plasmid by TA cloning and the resultant clones screened for the presence of the insert by PCR (Figure 35B) and restriction digestion (Figure 35C), followed by agarose gel electrophoresis. Plasmid DNA in reactions (1.1, 1.2, 2.1 and 3.1) produced an amplicon with the G6PD primers indicating the presence of the G6PD insert in these clones (Figure 35B). Single and double restriction digestion (*Hind*III and *EcoR*I enzymes) reactions also confirmed the presence of G6PD insert at 191 bp in selected plasmids (Figure A2 C). Plasmid 3.1 which resulted in a positive signal in the PCR assay (Figure 35B) was excluded from restriction digests due to low DNA concentration. Plasmid 2.1 was not included in a double digest (Figure 35C) due to low DNA concentration. Plasmids 1.1 and 1.2 were selected and further confirmed by sequencing. A plasmid map of the plasmid was generated to illustrate the presence of the amplicon in the PTZ57R vector (Figure 35D).

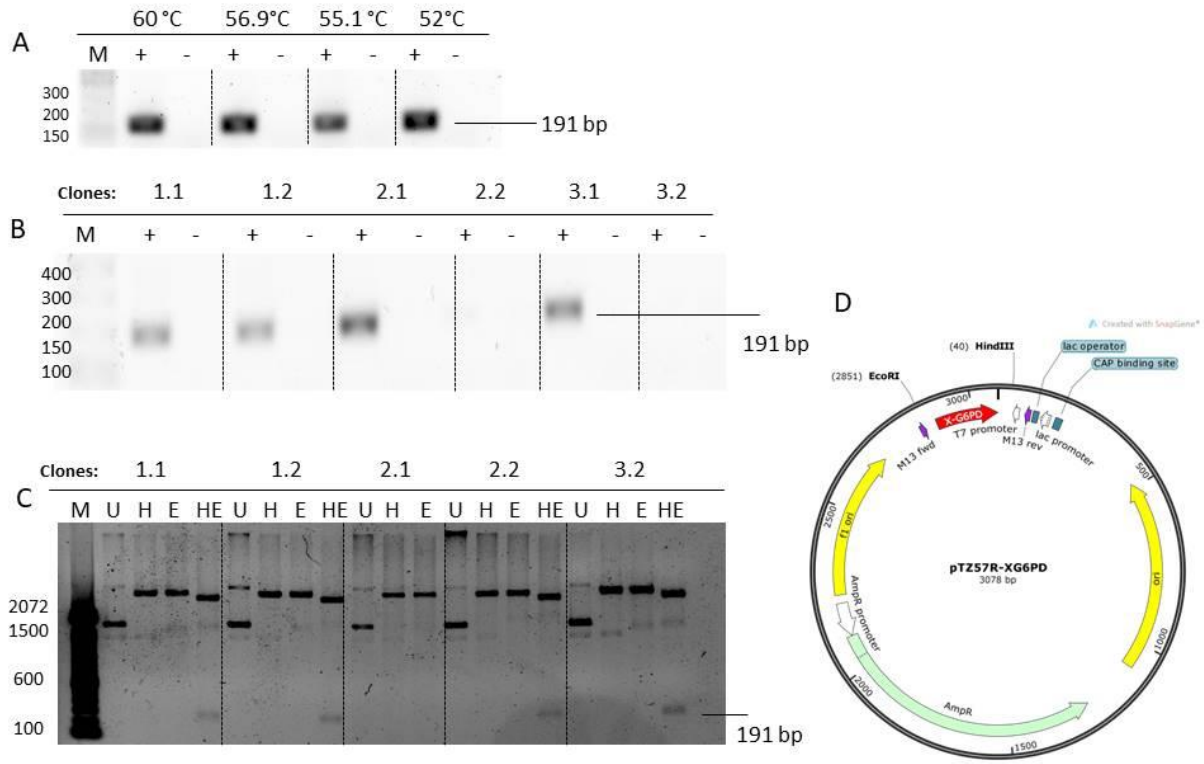

Figure 35: Confirmation of insertion of G6PD X-linked amplicon insert into pTZ57R vector for plasmid controls. A.) Ethidium bromide stained 0.8 % agarose gel of gradient PCR of G6PD primers using annealing temperatures of 60, 56.9, 55.1 and 52 °C and SW480 cell line cDNA as template. +: reaction prepared with template, -: reaction prepared without template. B.) Ethidium bromide stained 0.8 % agarose gel of PCR using putative pTZ57R-XG6PD containing plasmids as template. pTZ57R-XG6PD clones: 1.1, 1.2, 2.1, 2.2, 3.1 and 3.2 C.) Double restriction digestion of putative pTZ57R-XG6PD plasmids with EcoRI and HindIII enzymes. U: Uncut reactions; H: HindIII cut reactions E: EcoRI cut reactions; HE: Double digestion reactions. D.) Plasmid map of pTZ57R-XG6PD plasmid.

It was not possible to PCR amplify the SRY sequence from SW480 cell line cDNA (data not shown) and therefore genomic DNA was used as the template to amplify the Y-linked SRY gene. Figure 36A shows the results of the gradient PCR amplification for SRY. A PCR product, corresponding to the predicted size of the SRY amplicon (556 bp) was obtained at an annealing temperature of 56.9° C (Figure 36A). The PCR product from the SRY gene was cloned into the pTZ57R plasmid by TA cloning. The plasmid clones obtained were screened using PCR (Figure 36B) and restriction digestion (Figure 36C), followed by agarose gel electrophoresis. Plasmids 1.1, 1.2 and 2.1 showed bands at 556 bp after PCR using SRY specific primers suggesting the presence of the SRY amplicon in these clones.

The presence of the SRY amplicon in the plasmids 1.1, 1.2, 2.1 and 2.2 was further confirmed by double restriction digestions (*Hin*dIII and *Eco*RI enzymes) in Figure 36C. All of the plasmids generated an insert of ~556 bp, including plasmid 2.2 which did not produce a product in the PCR reaction. Plasmids 1.1, 1.2 and 2.1 were further confirmed by sequencing. The plasmid map illustrates the insert from the SRY gene in the PTZ57R vector (Figure 36D).

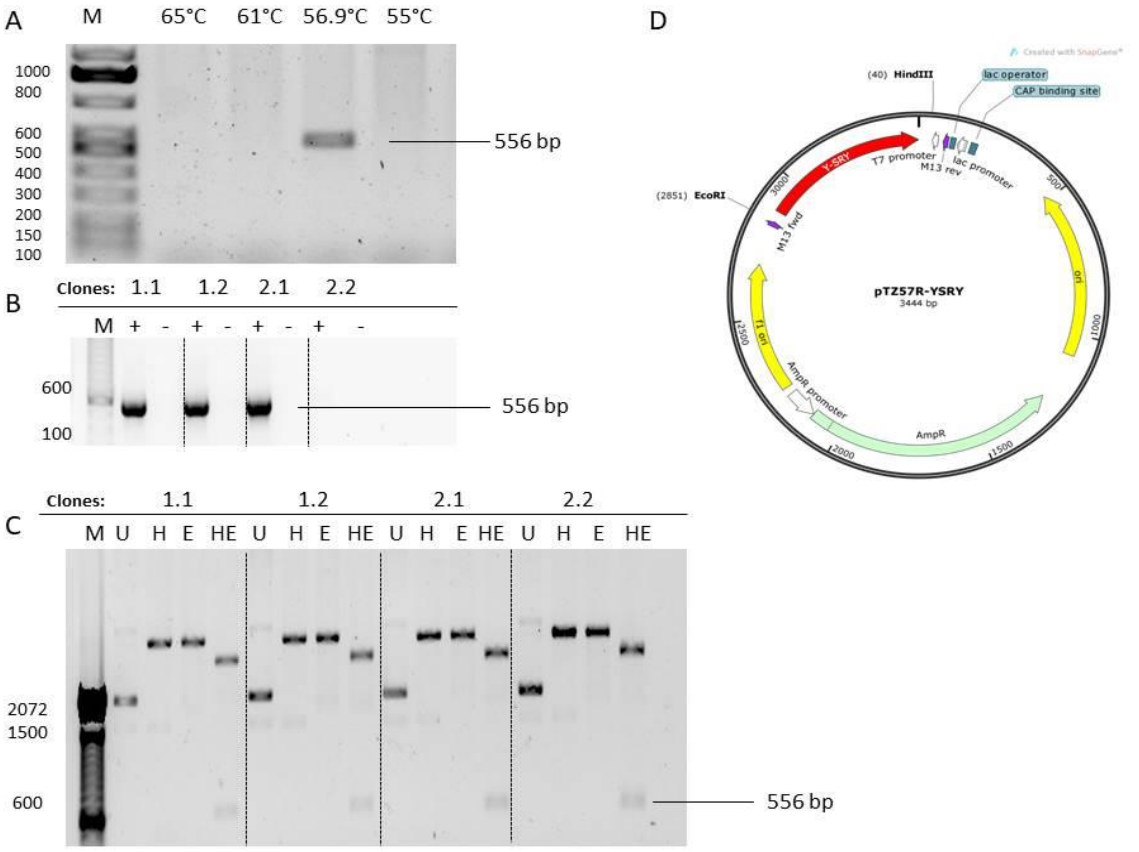

Figure 36: Confirmation of insertion of the SRY Y-linked amplicon into the pTZ57R vector for plasmid controls. A.) Ethidium bromide stained 0.8 % agarose gel of gradient PCR with primers designed to amplify a region of the SRY gene using a range of annealing temperatures (65, 61, 56.9 and 55°C) from SW480 cell line gDNA. +: reaction prepared with template, -: reaction prepared without template. B.) Ethidium bromide stained 0.8 % agarose gel of PCR using putative pTZ57R-YSRY plasmids using SRY primers. pTZ57R-YSRY clones: 1.1, 1.2, 2.1 and 2.2. C.) Double Restriction digestions of putative pTZ57R-YSRY plasmids with EcoRI and HindIII enzymes. U: Uncut reactions; H: HindIII cut reactions E: EcoR1 cut reactions; HE: Double digestion reactions. D.) Plasmid map of pTZ57R-YSRY plasmid.

Gene Expression Analysis

Figure 37 presents the process of generating the RUNX2 and FGFR3 standard curve plasmids. The PCR amplification of the RUNX2 and FGFR3 regions from cDNA from the HEK293T cell line using the qPCR primer sets is illustrated in Figure 37A.

Both transcripts were amplified at 50 °C. PCR products at approximately 129 bp and 145 bp, corresponding to the predicted sizes of the RUNX2 and FGFR3 amplicons respectively, were detected in the test reactions (Figure 37A).

The negative control reactions lacking reverse transcriptase showed no amplification. The PCR products for RUNX2 and FGFR3 were ligated into the pTZ57R plasmid by TA cloning and used to transform chemically competent *E. coli* cells. The clones obtained were subject to restriction digestions and agarose gel electrophoresis to screen for incorporation of the RUNX2 and FGFR3 bands. The presence of insert bands at 129 bp (RUNX2) and 145 bp (FGFR3) upon digestion of plasmids (RUNX2, FGFR3 1, FGFR3 2 and FGFR3 3) with *Eco*RI and *Hin*dIII enzymes was visualized in overexposed image in Figure 37B. Figure 37C & D illustrates the plasmid maps for the RUNX2 and FGFR3 plasmids.

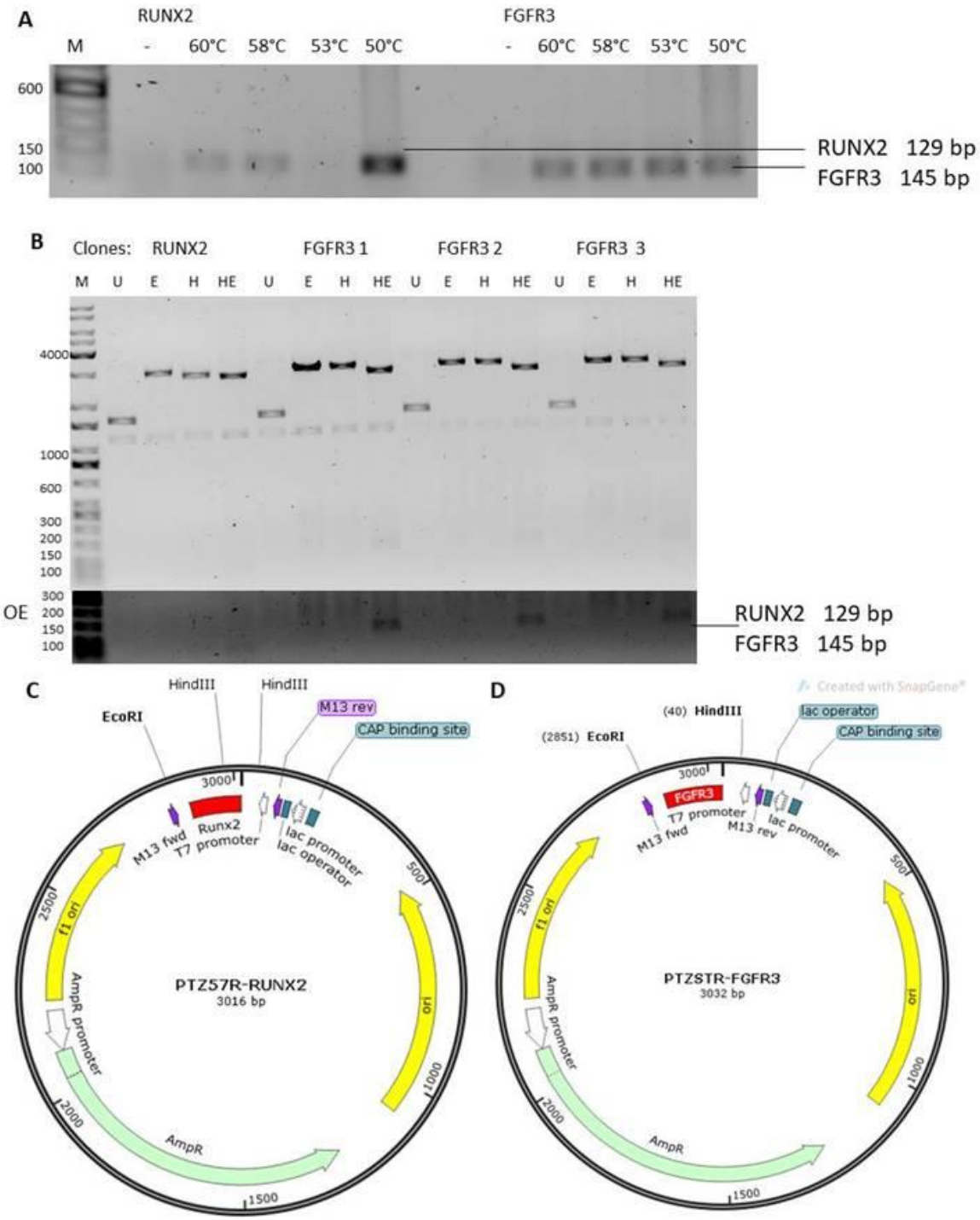

Figure 37: Confirmation of insertion of RUNX2 and FGFR3 amplicons into the pTZ57R vector. A.) Ethidium bromide stained 0.8 % agarose gel of gradient PCR using RUNX2 or FGFR3 primers and a range of annealing temperatures (60, 58, 53 and 50°C) using HEK293T cDNA. +: reaction prepared with template, -: reaction prepared without template. B.) Double Restriction digestion of putative pTZ57R-RUNX2 and pTZ57R-FGFR3 plasmids with EcoRI and HindIII enzymes. U: Uncut reactions; H: HindIII cut reactions E: EcoRI cut reactions; HE: Double digestion reactions. OE: overexposed image. C.) Plasmid map of pTZ57R-RUNX2 plasmid. D.) Plasmid map of pTZ57R-FGFR3 plasmid

Methylation Level Analysis

To optimize the primers selected for methylation analysis, the annealing temperature for PCR amplification was optimized using gradient PCR and visualized using agarose gel electrophoresis. PCR amplicons at the predicted molecular weight for FN1 (187 bp), FGFR3 (286 bp) and RUNX2 (311 bp) were obtained at annealing temperatures ranging from 60 °C to 50 °C (Figure 38A).

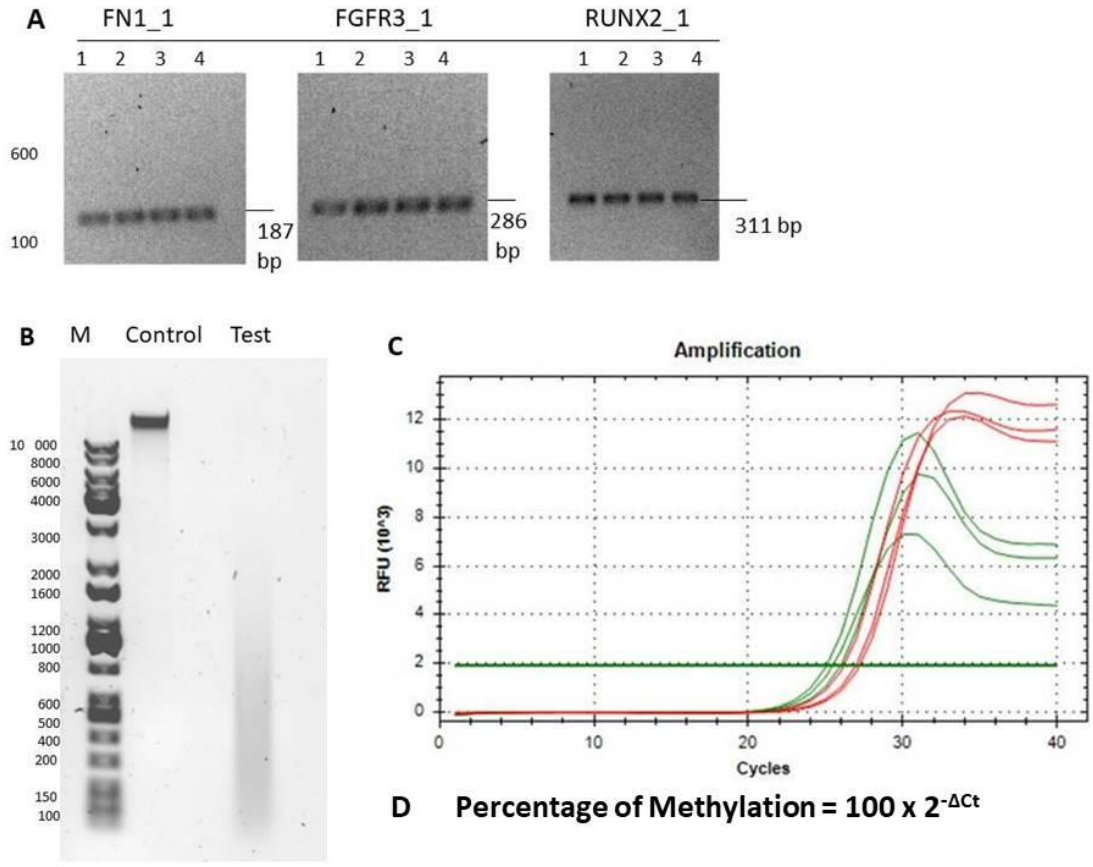

Figure 38: Methylation specific enzyme and primer optimization. A.) Ethidium bromide stained 0.8 % agarose gel confirmation of TM optimization for methylation specific primers for Fibronectin, FGFR3 and RUNX2. Lanes: 1=60 °C 2=58 °C 3= 53.8°C, 4=50°C. Amplicons – FN1_1:187bp, FGFR3_1: 286bp and RUNX2_1: 311bp. B.) Ethidium bromide strained 0.8 % agarose gel confirmation of Methylation specific restriction enzyme (MSRE) (HpaCh4IV, ScrfI, AciI and HpaII) activity after digestion of MDA-MB-436 gDNA. Control: No enzymes; Test: MSRE included in reaction. C.) Amplification RT-qPCR data of MDA-MB-436 control and test restriction digest mixture. Reactions tested with FN1_1 primers. Experiment performed in triplicate. Red = Control reactions, Green = Test reactions. D.) Equation to calculate methylation percentage from Cq means.

The efficiency of the Methylation Specific Restriction Enzymes (MSREs) was confirmed using genomic DNA isolated from the MDA-MB-436 cell line. The restriction digestion mixtures containing genomic DNA and lacking enzymes or including the *HpCHV4*IV, *Hpa*II, *Scrf*I and *Aci*I MSRE were visualized by agarose gel electrophoresis (Figure 38B).

As expected, control reactions lacking MSREs produced a high molecular band indicating intact gDNA. The smearing for the test reaction indicated that the MSREs degraded the gDNA. The restriction endonuclease digest was further validated by qPCR using the undigested and digested gDNA and primers targeting FN1 (Figure 38C). Amplification of the FN1 locus for both the untreated (red; control) and MSRE digested (green; test) gDNA template occurred before 30 cycles. However, the control reaction amplified earlier (lower Cq value) as the gDNA was intact (Figure 38C). The test reactions amplified 2 cycles after the control due to the degradation of non-methylated gDNA. The difference been cycle means for control and test reactions resulted in a methylation level of 41 % for FN in this gDNA sample. Figure 38D displays the equation used to calculate methylation percentage of that region.

Appendix B: Ethics certificates

RHODES UNIVERSITY
Where leaders learn

Rhodes University Ethical Standards Committee, Rhodes University, P O Box 94, Grahamstown, 6140
Tel: +27 46 603 7366 . Fax: +27 46 603 8934 . Email: ethics-committee@ru.ac.za

23-Jun-2015

Dear Roxanne Thornton

Ethics Clearance: Towards a biological profile for South African perinatal remains: Osteological and Genetic perspectives

Principal Investigator: Roxanne Thornton

This letter confirms that a research proposal with tracking number: RU-HSD-15-05-0004 and title: **Towards a biological profile for South African perinatal remains: Osteological and Genetic perspectives** was given ethics clearance by the Rhodes University Ethical Standards Committee.

There is one detail aspect that the researcher may consider: In a table that appears directly before the Aims and Objectives, the candidate offers evidence supporting the suggestion that ancestry can influence the reliability of age determination of the foetus. In one of her objectives she writes: "Compare the measurements and gene expression levels within the categories of male and female perinates at each GW observed." However, she does not have a similar objective relating to comparing foetuses having different ancestry.

Please ensure that the ethical standards committee is notified should any substantive change(s) be made, for whatever reason, during the research process. This includes changes in investigators. Please also ensure that a brief report is submitted to the ethics committee on completion of the research. The purpose of this report is to indicate whether or not the research was conducted successfully, if any aspects could not be completed, or if any problems arose that the ethical standards committee should be aware of. If a thesis or dissertation arising from this research is submitted to the library's electronic theses and dissertations (ETD) repository, please notify the committee of the date of submission and/or any reference or cataloguing number allocated.

Yours Sincerely,

Professor M. Goebel: Chairperson RUESC.

Note:
1. This clearance is valid from the date on this letter to the time of completion of data collection.
2. The ethics committee cannot grant retrospective ethics clearance.
3. Progress reports should be submitted annually unless otherwise specified.

R14/49 Roxanne Thornton

HUMAN RESEARCH ETHICS COMMITTEE (MEDICAL)

CLEARANCE CERTIFICATE NO. M160280

NAME: (Principal Investigator)	Roxanne Thornton
DEPARTMENT:	Forensic Medicine and Pathology University of the Witwatersrand Rhodes University
PROJECT TITLE:	Towards a Biological Profile for South African Perinatal Remains: Osteological and Genetic Perspectives
DATE CONSIDERED:	Adhoc
DECISION:	Approved unconditionally
CONDITIONS:	
SUPERVISOR:	Prof Adrienne Edkins
APPROVED BY:	Professor P. Cleaton-Jones, Chairperson, HREC (Medical)
DATE OF APPROVAL:	30/03/2016

This clearance certificate is valid for 5 years from date of approval. Extension may be applied for.

DECLARATION OF INVESTIGATORS

To be completed in duplicate and **ONE COPY** returned to the Research Office Secretary in Room 10004, 10th floor, Senate House/2nd Floor, Phillip Tobias Building, Parktown, University of the Witwatersrand. I/we fully understand the conditions under which I am/we are authorized to carry out the above-mentioned research and I/we undertake to ensure compliance with these conditions. Should any departure be contemplated, from the research protocol as approved, I/we undertake to resubmit the application to the Committee. **I agree to submit a yearly progress report.**

Principal Investigator Signature

Date 11th of April 2016

PLEASE QUOTE THE PROTOCOL NUMBER IN ALL ENQUIRIES

Appendix C: Micro-CT: Reference plane points for the occipital and femoral skeletal elements

OCCIPITAL pars basilaris	
1.	Edge of Right anterior border (near articular facet of condylar limb)
2.	Edge of Left anterior border (near articular facet of condylar limb)
3.	Anterior border of Spheno-occipital synchondrosis
OCCIPITAL pars lateralis	
1.	Midline point of Foramen Magnum border
2.	Border aspect part for the mastoid temporal articulation
3.	Border of Jugular foramen
4.	Intersection of jugular and condylar limb
FEMUR	
1. Proximal	Points made at the anterior, lateral, medial and lateral aspects of the proximal end above lesser trochanteric surface
2. Midshaft	Points made above nutrient foramen (posterior surface) at the lateral, medial and anterior aspects of the midshaft.
3. Distal	Points made at the anterior, lateral, medial and lateral aspects of the distal end above the metaphyseal surface.

Appendix D: Dental and skeletal aging comparisons

Table 9: Comparison of pars basilaris osteometrics (mm) with established standards within the dental age categories

	Pars basilaris Bone measurement (mm)						
Dental Age Estimation	**Mean** Current Study	***±***	***n***	**Mean** Fazekas &Kosa(1978); Scheuer &Maclaughlin-Black(1994)	***±***	***n***	**Skeletal Age Range** Fazekas &Kosa(1978); Scheuer &Maclaughlin-Black(1994)
Maximum Width							
<30 GW	8.2	1.2	20	5.7	2.4	89	22-28 GW
30-34 GW	9.7	1.0	9	10.9	0.8	27	28-32 GW
34-38 GW	9.5	1.4	6	12.5	0.5	9	28-32 GW
38 GW-Birth	11.0	1.5	6	14.2	0.7	17	32-36 GW
Birth – 1.5 Mths	12.6	1.5	12	15.5	0.7	10	34-38 GW
1.5 – 4.5 Mths	12.9	1.2	14	16.1	1.2	3	34-38 GW
4.5 – 7.5 Mths	13.3	0.9	4	19.2	1.2	3	36-40 GW
Sagittal Length							
<30 GW	8.9	0.9	21	6.9	2.2	89	24-26 GW
30-34 GW	9.6	0.6	9	10.5	0.3	27	28-32 GW
34-38 GW	9.6	0.5	6	11.7	0.5	9	28-32 GW
38 GW-Birth	11.1	0.9	6	12.7	0.3	17	32-36 GW
Birth – 1.5 Mths	11.5	1.0	14	12.2	0.6	10	34-38 GW
1.5 – 4.5 Mths	11.5	0.6	10	12.9	0.9	3	34-38 GW
4.5 – 7.5 Mths	12.2	0.8	4	13.6	0.1	3	34-40 GW
Maximum Length							
<30 GW	10.3	1.2	21	11.7	0.3	2	<26 -26 GW
30-34 GW	11.7	0.8	9	12.8	-	1	<26-<30 GW
34-38 GW	11.3	1.2	6	15.3	-	2	<26-<30 GW
38 GW-Birth	13.2	1.0	6	15.9	0.6	7	<30-<38 GW
Birth – 1.5 Mths	14.4	1.2	14	16.3	0.5	10	<38-<40 GW
1.5 – 4.5 Mths	14.7	1.0	10	16.9	0.9	3	<38-<40GW
4.5 – 7.5 Mths	16.1	0.3	3	19.3	1.2	3	40-40+ GW

GW-gestational weeks; Mths-postnatal months

Table 10: Comparison of pars lateralis osteometrics (mm) with established standards within the dental age categories

GW-gestational weeks; Mths-postnatal months

Pars lateralis Bone Measurement (mm)							
Dental Age Estimation	**Mean** Current study	***±***	***N***	**Mean** Fazekas &Kosa(1978)	***±***	***n***	**Skeletal Age Range**
Maximum Length							
<30 GW	13	2.4	23	8.8	3.7	89	22-30 GW
30-34 GW	16.1	2.1	9	17	1.8	27	30-34 GW
34-38 GW	15.4	1.9	6	21.1	1.6	9	30-32 GW
38 GW-Birth	20.3	3.6	7	24.9	1.5	17	32-38 GW
Maximum Width							
<30 GW	6.7	1.3	24	4.7	2.2	89	24-28 GW
30-34 GW	8.3	1.3	9	9.4	1.0	27	26-34 GW
34-38 GW	8.0	1.3	6	11.9	0.9	9	24-34 GW
38 GW-Birth	11.2	1.9	7	13.6	0.4	17	34-38 GW

Table 11: Comparison of femur osteometrics (mm) with established standards within the dental age categories.

Femur Bone Measurement (mm)							
Dental Age Estimation	**Mean** Current Study	***±***	***n***	**Mean** Fazekas &Kosa(1978)	***±***	***n***	**Skeletal Age Range** Fazekas &Kosa(1978)
Maximum Length							
<30 GW	42.8	6.9	24	29.5	12.6	89	22-30 GW
30-34 GW	51.1	6.2	9	54.6	4.5	27	28-32 GW
34-38 GW	49.1	3.7	5	63.7	3.8	9	28-32 GW
38 GW-Birth	61.5	7.2	7	71.6	2.7	17	32-38 GW
Distal Width							
<30 GW	9.5	2.0	24	7.1	3.3	89	20-28 GW
30-34 GW	12.1	1.6	9	13.9	1.2	27	26-32 GW
34-38 GW	10.9	1.1	5	16.8	1.4	9	24-30 GW
38 GW-Birth	15.2	2.2	7	19.3	0.6	17	32-38 GW

GW-gestational weeks; Mths-postnatal months